Industrial Crops & Products 194 (2023) 116275

Contents lists available at ScienceDirect

Industrial Crops & Products

journal homepage: www.elsevier.com/locate/indcrop

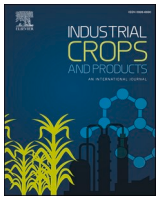

Kinetic and thermodynamic compensation phenomena in C3 and C4 energy crops pyrolysis: Implications on reaction mechanisms and product distributions

Bojan Janković [a,*,1], Nebojša Manić [b], Mina Popović [c], Slobodan Cvetković [c], Željko Dželetović [d], Dragoslava Stojiljković [b]

[a] University of Belgrade, Department of Physical Chemistry, "Vinča" Institute of Nuclear Sciences - National Institute of the Republic of Serbia, Mike Petrovića Alasa 12–14, P.O. Box 522, 11001 Belgrade, Serbia
[b] University of Belgrade, Fuel and Combustion Laboratory, Faculty of Mechanical Engineering, Kraljice Marije 16, P.O. Box 35, 11120 Belgrade, Serbia
[c] University of Belgrade, Institute of Chemistry, Technology and Metallurgy (ICTM), Njegoševa 12, 11000 Belgrade, Serbia
[d] INEP Institute for the Application of Nuclear Energy, University of Belgrade, Banatska 31-b, 11080 Zemun-Belgrade, Serbia

ARTICLE INFO

Keywords:
Energy crops
Slow pyrolysis
Thermodynamic compensation
Isokinetic temperature
Catalytic activity
Bio-fuels

ABSTRACT

This work provides insight into possibilities of maximum utilization of C3-C4 energy crops for thermo-chemical conversion (slow pyrolysis) into high value biochemicals, platform chemicals, drop-in fuels and combustible gases, using coupled kinetic and thermodynamic analyses. In order to examine the kinetics of decomposition of lignocellulosic components, model-free and model-based methods faded from thermal analysis data were used. Thermodynamic compensation was used for explicatory of entropy controlled process, where conformational changes and chemical exchange directly affect the type and distribution of obtained pyrolytic products. It was shown that external variable (*i.e.* the heating rate/temperature) does not change either an entire reaction mechanism (mechanistic nature of MG and AD pyrolyses) or transition state, but it changes activation enthalpy and activation entropy which lead to differences in terms of heat energy consumption, pyrolysis favorability and thus rates of generation of activated complex among feedstocks. To investigate the interplay of catalysts (present in feedstocks as minerals) and reactants, selective energy transfer (SET) model was applied. The model showed an activity of catalyst with different outputs towards two reactants, lignin part of the structure in MG and 1,8-cineole in AD. It was shown that AD is more convenient for thermal conversion than MG, regarding to lower transformation energy requirement, higher reactivity, as well as much faster accumulation of products.

1. Introduction

Biomass in energy production is very important as broad term that includes, among other things, all forms of organic matter such as wood, organic matter herbaceous plants, agricultural crops, agricultural residues, aquatic vegetation, fertilizers of animal origin and municipal solid waste. There are many plants which have the ability to convert solar energy into biomass with high efficiency, including herbaceous crops, fast-growing woody crops, forage crops (alfalfa, clover, switchgrass, and miscanthus), sugar crops (sugar cane, sugar beet, fiber, and sweet sorghum), grains (corn, barley, and wheat), and oilseeds (soybean, canola, sunflower, safflower, oilseed rape and cotton). Annual production *per* hectare of arable land is equivalent values of 400 GJ for C4 crops, 250 GJ for cereals, and 70 GJ for oilseeds (biodiesel) (Dželetović et al., 2007). C4 perennial crops represent suitable bioenergy crops because efficiently use available resources, retain carbon in the land, have a high degree of water use efficiency for bioproduction, they are not invasive species and have small feeding requirements (Gupta and Demirbas, 2010). Additionally, grassy biomass occupies a significant place in the view of remediation of pollutants from waste-water/soil, where dried biomass after phytoremediation can be used as a fuel feedstock as it contains high carbon and volatile matter content (Thakur et al., 2018). More recently, it was announced that because of amorphous nature, some specific grass biomasses show serious potential to produce more

* Corresponding author.
E-mail addresses: bojan.jankovic@vinca.rs (B. Janković), nmanic@mas.bg.ac.rs (N. Manić), mina.popovic@ihtm.bg.ac.rs (M. Popović), slobodan.cvetkovic@ihtm.bg.ac.rs (S. Cvetković), zdzeletovic@inep.co.rs (Ž. Dželetović), dstojiljkovic@mas.bg.ac.rs (D. Stojiljković).
[1] https://orcid.org/0000–0001-5232–4160

https://doi.org/10.1016/j.indcrop.2023.116275
Received 16 November 2022; Received in revised form 5 January 2023; Accepted 10 January 2023

pyro-gas and biochar (Kumar et al., 2023). A grass that possesses some of the above characteristics, and that produces a large amount of biomass, is *Miscanthus* × *giganteus* (Figala et al., 2015). *Miscanthus* plantation is based on rhizome planting or plants produced by micropropagation on the previously prepared land on which it remains productive in the course of 15 – 20 years. The yield potential of this bioenergy crop, which is characterized by an annual harvest, has proven to be very significant, but due to the high costs of establishing plantations, there remain some limitations for its wider cultivation. On the other hand, significant agronomic investments (annual ploughing, planting and fertilizing) have been reduced, since it was shown that *Miscanthus* × *giganteus* does not require the application of fertilizers to the extent required, for the annual production of cereals such as maize (Lewandowski et al., 2000; Dražić et al., 2010). In the Republic of Serbia, experiments with *Miscanthus* × *giganteus* were first started in 2007. Although, it is necessary to carry out long-term monitoring of growth parameters (primarily yield) as a function of environmental parameters, as well as genetic and physiological characteristics of the plant with the aim of obtaining relevant data, the results so far have shown that in the Republic of Serbia, a fairly high production of *Miscanthus* biomass is possible. On the other hand, comparing the potentials for *Arundo donax* L. C3 energy crop cultivation in an area with a moderate climate (such as the Republic of Serbia), with other types of plants for biomass production, we come to the conclusion, that in the case of planting a plantation with *Arundo donax*, significantly less herbicides, pesticides and fertilizers are needed, and that even on non-irrigated lands, 20 – 40 tons of the dry matter can be planned. Based on past experience in planting areas with *Arundo donax* plantations, the life cycle of plants is about 20 years, and during that time significant financial expenses are only in a preparing the land and the planting. During other years, *Arundo donax* does not require additional costs, because the land planted with *Arundo donax* also does not require an subsequent processing (Corno et al., 2014; Tauler and Baraza, 2015).

Lignocellulosic biomass has a great potential for the production of bio-fuels and bio-materials, energy crops such as *Arundo donax* L. (giant cane) or *Miscanthus* × *giganteus* (*Miscanthus*) with high yields, low production costs are reliable and sustainable raw material for the biomass. However, several aspects must be taken into account when selecting suitable plants for energy crops, such as soil quality, technologies available in the area and other environmental influences. Although, both cultures have promising characteristics, where multiple trials and research efforts by the company "ARUNDO Bioenergy" (ArundoBioEnergy (2022)) have shown that *Arundo donax* L. has greater potential in all significant aspects. A comparative study of *Miscanthus* and *Arundo donax* conducted by the Ohio Agricultural Research and Development Center (Ge et al., 2016) highlights that giant cane has a higher biomass yield ranging up to 15 – 45 dry tons per hectare, while *Miscanthus* has only 10 – 30 dry tons. It is also emphasized that *Arundo donax* is able to adapt to the wider environment. Although both energy crops, have the ability to thrive on marginal soils, and it is stated that *Arundo donax* is more resistant to poor soils (salty, flooded, contaminated, alkaline) with a lifespan of 25 – 30 years. According to the research of University of California (Mann et al., 2013), *Arundo donax* has been shown to be more adaptable to drought and the moisture stress and tolerates a wider pH range (5.00 – 10.00 pH) than *Miscanthus giganteus*. Namely, the cultivation of *Arundo donax* is already being implemented in Italy, Portugal, France, Greece, China, Australia and USA. Also in Serbia, planting of *Arundo donax* is implemented, but, *Miscanthus* is currently more often studied (Brosse et al., 2012), and, it is widely known that giant reed has a higher biomass yield and has the potential to be competitive with *Miscanthus* in all aspects, gaining increasing importance in the bioenergy/renewable energy sector, as a new source for biomass production. Formerly, both C3 and C4 (types of CO_2 fixation metabolism) grasses are studied from the aspect of their productive characteristics and energy balance (Angelini et al., 2009). Namely, the main interest in growing plants with high biomass is to replace fossil energy sources in order to reduce greenhouses gas emissions, primarily CO_2 originating from the fossil fuels. Drying, pyrolysis and gasification are the initial steps in the burning of solid fuels. The advantage of burning woody and herbaceous biomass is reflected in the neutrality of CO_2 emissions, considering that the burning biomass, releases the amount of CO_2 that the plant assimilated during growth (Lewandowski et al., 1995; Felten et al., 2013). This assumption can be considered correctly, if one observes the burning of biomass from herbaceous, fast-growing crops that are cut once a year, but it cannot be applied to the slow-growing biomass of trees. Considering that trees need up to a hundred years to grow, the system can be marked as CO_2 neutral, only at the end of the appropriate time limits, while in the case of fast-growing energy crops, CO_2 neutrality is achieved in a much shorter period of time. In addition to CO_2 emissions, burning of biomass also releases nitrogen oxides (NO_x) that arise from nitrogen (N) contained in a plant tissues, and the ash is also obtained (potassium and chlorine as sources of KCl). Energy crops offer the possibility of complete use in the production of heat and electricity through direct combustion, or indirectly through various processes of thermo-chemical conversion into other forms of energy, such as bio-fuels. The most important properties of lignocellulosic biomass are very good strength, flammability, biodegradability and reactivity (Putro et al., 2016). Lignocellulose represents one of the most common polymers in nature and the bulk of the structure of lignocellulosic biomass contains 40% — 50% cellulose, 25% — 35% hemicelluloses and 15% — 20% lignin (Bajpai, 2016). The ratio of the mentioned components (often called biomass "*pseudo-components*") depends on the type of the culture (Gray et al., 2006), and it also contains other compounds such as proteins, terpene oils, fatty acids/esters and inorganic substances, mainly based on the nitrogen, phosphorus and potassium. The conversion of biomass into energy includes a wide range of different sources and types of biomass, conversion possibilities, methods of the use and technological possibilities. Biomass can be converted into energy by various processes depending on the type and quality of raw material. There are three basic pathways of converting biomass, such as: *a*) thermo-chemical, *b*) bio-chemical and *c*) mechanical extraction with esterification. Bio-chemical transformations include anaerobic digestion and alcoholic fermentation, while the thermo-chemical transformations include combustion, pyrolysis, gasification and liquefaction (Chandraratne and Daful, 2021). Among the mentioned pathways of converting the biomass into the energy, *pyrolysis* as a thermo-chemical route of converting biomass into liquid fuel attracted, and continues to attract the most interest due to its advantages in terms of storage, transportation and adaptability, for the use in boilers, gas turbines, *etc.* The pyrolysis process involves the thermal decomposition of biomass in the absence of oxygen, where the final products represent an following: 1) pyrolytic bio-oil (liquid fraction), 2) bio-char (*char*-solid fraction) and 3) non-condensable gases (such as CH_4, CO, CO_2 and H_2) (Rajpoot et al., 2022). Depending on the reaction temperature, heating rate and residence time, there are three types of pyrolysis as: slow (conventional), fast and flash pyrolysis. Detailed differences between all three types of pyrolysis can be seen elsewhere (Demirbas and Arin, 2002). The fast pyrolysis is desirable to produce bio-oil, since it uses very 'high' heating rates (10 – 200 ^{o}C/s), reaction temperatures (600 ^{o}C – 1000 ^{o}C), short residence times (0.5 – 10 s), and small particle sizes (< 1 mm). The opposite, the slow pyrolysis operates at much lower heating rate magnitudes (0.1 – 1 ^{o}C/s), using prolonged residence times (300 – 550 s) with primary target of obtaining the solid product *viz* bio-char (~ 35%) and gases (~ 35%) (Escalante et al., 2022). With this kind of long-term activity, the vapor remains too long and the components in the vapor system continue to react with each other; the result is the formation of solid carbon and other liquids. However, the conditions of slow pyrolysis are generally applied for laboratory tests, which were adapted for the use of analyzers based on the thermal analysis techniques (Raza Naqvi et al., 2021) (thermogravimetric analysis (TGA) / derivative thermogravimetry (DTG) and/or differential thermal analysis (DTA) / differential scanning calorimetry (DSC))

coupled with spectroscopic techniques such as mass spectrometry (MS) with evolved gas analysis (MS-EGA) and Fourier transform infrared spectroscopy (FTIR), as well as GS-MS (Gas Chromatography — Mass Spectrometry) analysis. Accumulation of experimental data from mentioned techniques, especially an thermo-analytical (TA) measurements, enable the implementation of chemical kinetics models (Raza Naqvi et al., 2021; Kirti et al., 2022). This is strictly related to the phenomena related to the consequences of the thermal decomposition of pseudo-components of biomass (cellulose, hemicelluloses and lignin) and their reaction paths to specific products such as gaseous, liquid and solid fractions, excluding the setup of comprehensive models (referring to the description of pyrolysis by reaction rates, which are calculated based on the local temperature, using the Computational Fluid Dynamics (CFD)) (Rogaume, 2019). The computational pattern approach based on qualitative and quantitative analysis of CFD results has found the significant application in fluidized bed gasification, for converting various biomass feedstocks into useful energy (Raza et al., 2021). The microscopic kinetic models are based on physico-geometrical models (Khawam and Flanagan, 2006) which determine kinetic behavior of the reaction as much as the microscopic chemical reactions. The actual situation becomes even more complex, if the initial reactant ('*biomass*' feedstock) is a mixture of different compounds, and if multiple reactions occur as a combination of consecutive and concurrent sequences. The described case actually represents a thermo-chemical conversion of energy crops through slow pyrolysis process, reflecting endothermic structural transformations. Encompassing all of the above, thermogravimetric techniques (measurements usually carried out under non-isothermal (dynamic) conditions) were used for reactivity testing, evaluation of the physical and chemical properties, and to predict optimal conditions for these types of biomass, that can be applied as bio-fuels (Raza Naqvi et al., 2021). Table 1 shows imminent studies related to kinetics, thermodynamics and mechanistic models obtained for the pyrolysis process of *Arundo donax* L. and *Miscanthus* × *giganteus*, with the main goals of these studies.

Most of the recent research related to the investigation of the kinetics and thermodynamics of slow pyrolysis of *Arundo donax* L. and *Miscanthus* × *giganteus* are related to the application of model-fitting and isoconversional methods (Verma et al., 2022) as well as derivation of thermodynamic parameters (entropy (ΔS^{o}), enthalpy (ΔH^{o}) and Gibbs free energy (ΔG^{o})) *via* Eyring theory (Kirti et al., 2022) to predict feasibility of thermo-chemical conversion (Table 1). The most characteristic kinetic mechanism for describing a complex set of reactions is independent parallel reaction (IPR) model in order to describe the decomposition of the main components of biomass, with non-integer reaction orders. There are significant differences in the ranges of variation of the activation energy (E_a) in the pyrolysis of both energy crops, as a result of the influence of various factors such as: *a*) type of soil, environment and climate where the crops were grown *b*) particle size of samples, *c*) the applied range and symmetry of heating rates used, *d*) reliability and accuracy of selected kinetic methods, and *e*) evaluations of the proposed reaction mechanism, whether it realistically describes the given process of interest.

The isokinetic relationship (IKR) (sometimes called kinetic compensation effect – KCE; however, KCE is related to, but *distinct* from the IKR, where IKR is obeyed, if the rate constants for a family of chemical reactions become identical at a particular temperature - termed the *isokinetic temperature*, T_{iso}) is a well-known phenomenon that occurs in pyrolysis of lignocellulosic materials and bio-fuels (Xu et al., 2018; Zhang et al., 2020; Janković et al., 2021). For a complex processes (parallel reactions, successive reactions, *etc.*), it is characteristic that activation energy (E_a) and pre-exponential factor (A) depend on the degree of conversion. Thus any increase in activation energy is compensated by an increase in the pre-exponential factor beyond their linear relationship *via* IKP. There is an assertion: "The appearance of IKR shows that only one mechanism is present and that all reactions have analogous reaction profiles, whereas the existence of parameters that do not agree with the IKR implies, which there are multiple reaction mechanisms" (Vyazovkin and Linert, 1995). However, the application of this relationship is usually carried out through kinetic complexity of the process and which is closely related to detected changes in reaction pathways during system transformation. The mutual variation among kinetic parameters (E_a and log$A$ (logarithmic form of the pre-exponential factor)) for the same type of reaction system can be caused by distinct kinetic models, in which the studied samples were decomposed. On the other hand, the thermodynamic compensation (or enthalpy-entropy compensation (EEC)) can similarly to be found for an equilibrium situations, when enthalpy variation (ΔH^{o}) realizes a linear dependence on the entropy variation (ΔS^{o}) (Moulik et al., 2019). The isokinetic temperature (T_{iso}) (this temperature corresponds to separate lines on the Arrhenius plot, intersecting at a single point) and isoequilibrium temperature (T_{isoeq}) are quantities related to the phenomena described above, and which are attributed to the temperature at which the kinetic constant is approximately the same for the same set of reactions, *apropos* to the temperature at which the equilibrium constant is approximately the same for the same set of reactions, respectively (Liu and Guo, 2001). However, only when the transition state theory can be applied, if one kind of compensation happens, it can be concluded that the other also occurs, and therefore, both, isokinetic and isoequilibrium temperatures have to be approximately the same (Ibarz et al., 2017). It should be emphasized that appearance of the kinetic compensation effect does not entail the obligatory appearance of a thermodynamic compensation and *vice versa*. There are rigorous mathematical procedures in connection with checking whether there is an appearance of the real enthalpy-entropy compensation (EEC), or is it a consequence of propagation of experimental errors, which have a tendency to distribute an estimates of kinetic compensation (log$A$ and E_a, both received from ordinary linear regression of the Arrhenius equation), following a linear relation, which is called an statistical compensation (Barrie, 2012).

The main goal of this study is to provide an accurate and detailed description of the reaction mechanism of slow pyrolysis of C3 (*Arundo donax* L.) and C4 (*Miscanthus* × *giganteus*) energy crops, through application of kinetic modeling and process optimization using model-free and model-based methods (Moukhina, 2012), which are accommodated in a computational package of highly sophisticated software NETZSCH Kinetics Neo (product version: 2.6.0.1, build date: 2/16/2022). Based on the obtained results, the appearance of both, KCE and EEC compensations were discussed against the background of highly complex reaction pathways that are realized during the non-isothermal conversion of the studied samples in an inert atmosphere, through the application of thermal analysis methods. In addition, based on spectroscopic results from FTIR measurements of the raw samples, as a consequence of the calculated compensation parameters, the specific vibrational resonances are extracted, and they were associated with parts of the lignocellulosic structure that most affect the change in the type of pyrolysis reaction mechanism. The obtained results are then discussed in the light of the possible energy dissipation in a excited macromolecules, which can lead to differences in the reaction stages of biomass decomposition, and therefore to differences in the distribution of possible pyrolytic products. This can be summarized through the framework of catalytic upgrading (Raza Naqvi et al., 2015) of investigated energy crops over existed 'mineral-host' catalysts. Results presented in this study can significantly contribute to a much better understanding of reaction mechanisms (mechanistic features) and thermodynamic changes during pyrolysis processes of perennial crops.

2. Materials and methods

2.1. Materials

Miscanthus × *giganteus* Greef et Deu. and *Arundo donax* L. were grown on the experimental plot of INEP (Institute for the Application of Nuclear Energy), Zemun, Serbia (44°51 ´N, 20°22 E, 82 m a.s.l.), in the high

Table 1
Kinetic and thermodynamic results related to pyrolysis of C3 (*Arundo donax* L.) and C4 (*Miscanthus* × *giganteus*) energy crops based on evaluation of physico-geometrical kinetic model functions, with the main research objectives of the last six years (2017–2022) highlighted.

Energy crop	Technique	Conditions	Kinetic methods	Kinetic results	Thermodynamics	Main goal	Reference
Miscanthus	TGA/DSC	Non-isothermal (ΔT = 25 – 750 °C (N_2)): 2.5, 10, 20, 30 °C/min	Model-fitting (ASTM-E698) and model-free (isoconversional) methods.	Advantage of isoconversional methods: variation in the activation energies (E_a): 40 – 150/ 165 kJ/mol.	(-)	Better understanding of its physicochemical combustion/pyrolysis characteristics and consequently to achieve highest benefit from combustion / pyrolysis conversion.	Osman et al. (2017)
Miscanthus	TGA	Non-isothermal (ΔT = 25 – 900 °C (N_2)): 5, 10, 20 °C/ min	Model-fitting and model-free (isoconversional) methods; optimization of kinetic parameters *via* objective function minimization.	Application of independent parallel reaction (IPR) model: Pyrolysis was modeled using three independent reactions, one for each of its main components: hemicellulose, cellulose and lignin. Kinetic parameters are found for each independent reaction, together with fractions of volatiles associated with each biomass component.	(-)	Can the decomposition of Miscanthus during pyrolysis be explained based on decomposition of their main pseudo-components and can this decomposition be predicted using IPR model?	Zabel (2018)
Miscanthus	TGA/DTG	Non-isothermal (ΔT = 30 – 600 °C (Ar)): 5, 10, 20 °C/min	Model-free (isoconversional) methods and non-linear regression.	Application of three parallel independent reactions responsible for pyrolysis of pseudo-components (hemicelluloses, cellulose and lignin) with *n*-th reaction order mechanisms; kinetics of Miscanthus pyrolysis can be described by nonlinear-regression analysis, with E_a = 92.9, 190.1 and 170 kJ/mol for hemicelluloses, cellulose, and lignin decomposition, respectively.	(-)	Compare the pyrolysis kinetics of three types of energy crops; pyrolytic potential of energy crops can be used in designing the efficient pyrolizers.	Matusiak et al. (2020)
Miscanthus	TGA, TGA/ FTIR	Non-isothermal (ΔT = 30 – 900 °C (N_2)): 10, 20, 30 °C/ min	Model-free (isoconversional) methods	Kinetic study showed that pyrolysis followed multistep decomposition steps; increasing trend of E_a is attributed to varied compositions of biomass, which is a very complex matrix of hemicelluloses, cellulose, lignin, extractives and other inorganic compounds. E_a = 164.14–231.75 kJ/mol.	(-)	The investigation was concentrated on physicochemical properties, kinetic behavior and thermal decomposition of biomass profiled in a nitrogen atmosphere, where evolution of hot vapors was investigated using TGA-FTIR analyzer.	Kumar et al. (2022)
Arundo donax	TGA	Non-isothermal (ΔT = 30 – 700 °C (N_2)): 5, 15, 25 °C/ min	Model-free (isoconversional) method	Application of three independent reactions, with each reaction corresponding to decomposition of hemicelluloses, cellulose and lignin; High degree of variation of E_a values in the range of 210.64–2093.04 kJ/mol. Decomposition of hemicelluloses, cellulose and lignin encompasses E_a values between 210.64 and 246.41 kJ/mol, while much higher E_a can be attributed to devolatilization of produced bio-char.	(-)	To determine pyrolysis characteristics of *Arundo donax* grown on marginal land and provide detailed characterization of resulting bio-char.	Oginni and Singh (2019)

(*continued on next page*)

Table 1 (*continued*)

Energy crop	Technique	Conditions	Kinetic methods	Kinetic results	Thermodynamics	Main goal	Reference
Arundo donax	TGA/DTG-IR-GC/MS	Non-isothermal (ΔT = 25 – 800 °C (N_2)): 5, 10, 15, 20, 25 °C/min	Deconvolution of DTG curves of lignin were simulated by three independent reactions; Model-free method; Application of multi-peak fitting procedure.	Kinetic analysis at 5 – 25 °C/min shown that the E_a of lignin during *Arundo donax* pyrolysis was ranged from 166 to 182 kJ/mol and ln*A* (pre-exponential factor) was ranged from 35 to 40; All fitting peaks can be described by random nucleation followed by growth mechanism.	(-)	Emphasis on the lignin utilization from direct pyrolysis pathway of *Arundo donax* to improve economic effectiveness for future bio-ethanol production and lignin valorization.	Yang et al. (2020)
Arundo donax	TGA/FTIR	Non-isothermal (ΔT = 25 – 1000 °C (N_2)): 10, 20, 30 °C/min	Multiple linear regression (MLR) method; model-fitting and model-free (isoconversional) methods; master plots method.	The average value of E_a obtained using various model-free methods are 259.1, 262.5 and 250.2 kJ/mol; It has been identified a wide variation in E_a, due to complex multistep reactions (parallel, complex and competitive). Diffusion represents the main controlling mechanism at lower conversion value due to higher cellulose content in biomass resulting in higher thermal stability and the lower degradation rate, whereas at higher conversion value, random nucleation was the main controlling mechanism.	Thermodynamic quantities ΔH^o (kJ/mol) ΔG^o (kJ/mol) ΔS^o (J/mol) are calculated at different conversions for fixed heating rate; From positive entropy changes, it was reported that for raw *Arundo donax*, the degree of unpredictability is higher than for thermally deteriorated products.	To compare the two types of biofuels obtained from HTC and torrefaction of *Arundo donax* biomass; TGA was used to pyrolyze the raw and pre-treated biomass, as well as to evaluate kinetic parameters. Thermodynamic analysis was implemented to understand the biomass decomposition behavior and spontaneity of studied process.	Nawaz and Kumar (2022)

quality luvic chernozem soil (IUSS Working Group WRB 2015) at INEP, unpolluted by heavy metals, fertilizers and pesticides (pH in water: 6.7; pH in 1 M KCl: 5.5; total organic C: 1.71%; total N: 0.14%; available P_2O_5: 6.0 mg 100 g^{-1}; available K_2O: 17.8 mg 100 g^{-1}). Serbian climate is mostly moderate continental. Average July (the hottest month of the year) temperature is $\geq$ 22 °C, and average January (the coldest month of the year) temperature values vary mostly between 0 °C and −2 °C (Dželetović et al., 2013). In the Republic of Serbia, annual precipitation curve displays the two maxima: in the late spring and in the late autumn, while winters and summers are mostly dry periods. *Miscanthus* harvesting is considered to be performed in February/March when, despite lower yields compared to the autumn harvest, better biomass combustion properties are obtained (Dželetović et al., 2014; Fournel et al., 2015). The lowest *Miscanthus* yield obtained on chernozem from spring harvest is 23 t (66.5% d.m.) for wet yield or 18 t (85% d.m.) for dry yield, while the highest *Miscanthus* yield obtained is 42 t (66.5% d.m.) for wet yield, or 33 t (85% d.m.) for dry yield (Perić et al., 2018). A photographic representation of the planted *Miscanthus* × *giganteus* in full growth is shown in Fig. 1.

Among the different perennial crops, giant reed (*Arundo donax* L.) has received a great interest in recent years due to its tolerance to many environmental stresses (contamination, pests, salts) and its beneficial effect on soil organic carbon, soil structure and water retention (Pulighe et al., 2019). It was suggested (Visconti et al., 2020) that giant reed might mitigate soil erosion by reducing water runoff and, indirectly, soil erodibility. Besides this, studies of the average yields of *Arundo donax* L. at the INEP location are ongoing and currently not available. A photographic representation of the planted *Arundo donax* L. in full growth is shown in Fig. 2.

Miscanthus × *giganteus* and *Arundo donax* L. were harvested from November until the beginning of the following vegetation cycle (March, April).

Fig. 1. *Miscanthus* × *giganteus* Greef et Deu. planted in the INEP.

2.2. Samples preparation

Biomasses (stem portions) are cut into little bits after being air dried. A mean sample for each biomass material with a weight of roughly 1 kg was prepared for further testing by dividing the total mass of the sample from each harvest period in quarters. In this manner, a sample of the provided biomass was chosen, milled, and after sieving, the r_p = 1.0 mm particle sizes were employed in this research. Currently available samples of each biomass were split into two portions: one for chemical analysis and the other for spectroscopic measurements and tests linked to thermal analysis measurements. Fig. 3 depicts the biomass samples that were prepared for experimental measurements.

Fig. 2. *Arundo donax* L. planted in the INEP.

Fig. 3. *Miscanthus* × *giganteus* (left) and *Arundo donax* L. (right) samples.

2.3. Metal content determination

Samples of *Miscanthus* × *giganteus* and *Arundo donax* L. (Fig. 3) were prepared and liquefied by a standardized microwave assisted acid dissolution procedure, for plant material (EPA Methods 3052) in a microwave digester. The concentrations of K, Mg, Ca, Na, Fe, Mn, Cu, Pb, Cd, Ni, and Zn were determined by atomic absorption spectrometry (AAS) using a Perkin Elmer PinAAcle900 T spectrometer (Perkin Elmer, Waltham, Massachusetts, USA).

In the following text, samples of *Miscanthus* × *giganteus* and *Arundo donax* L. will be abbreviated as MG and AD, respectively.

2.4. Proximate and ultimate analyses

The proximate analysis was performed in accordance with representative ASTM standards. For determination of moisture, ash (A) and volatile matter (VM), the ASTM E (2008) (ASTM E1756–08, 2015), ASTM E (2001) (ASTM E1755–01, 2010) and ASTM (1998) (ASTM E872–82, 2019) standards were used, respectively. The total carbon (C), hydrogen (H), nitrogen (N), and sulfur (S) contents were determined by Vario EL III CHNS/O Elemental Analyzer System. The content of oxygen (O) was calculated by subtracting the C, H, N, and S and ash (A) content from 100%. After obtaining the experimental data of proximate and ultimate analysis for considered raw biomass samples, the fuel ratio (FR) was evaluated using the formula $FR = FC^{(db)}/VM^{(db)}$, where superscript (*db*) denotes dry basis, FC is the fixed carbon (%), while VM represents volatile matter (total volatiles) (%).

2.5. Determination of lignocellulosic content of raw samples

Determination of cellulose, hemicelluloses and lignin content was performed by the modified ISO 5351–1:2004 standard (ISO, 2004) (original procedure: Cellulose in dilute solutions - Determination of limiting viscosity number - Part 1: Method in cupri-ethylene-diamine (CED) solution (ISO 5351–1:1981)) in a laboratory conditions. Holocellulose content was calculated from the expression: Holocellulose (%) = (Glucose (%) + Hemicelluloses (%)). The extractives content was calculated by the difference as Extractives (%) = (Hollocellulose (%) – Lignin (%)).

2.6. Fourier-transform infrared (FTIR) spectroscopy analysis of raw samples

The chemical structure of the raw materials was characterized by FTIR spectroscopy (functional groups which give surface chemistry of raw samples are usually obtained from FTIR spectroscopy), where FTIR spectra are recorded on the ATR-FTIR Nicolet iS10 (Thermo Scientific) spectrometer (Thermo Fisher Scientific, Waltham, Massachusetts, USA). The spectra were collected at 4 cm^{-1} resolutions in the spectral range between 4000 cm^{-1} and 500 cm^{-1}.

2.7. Thermogravimetric analysis (TGA) and derivative thermogravimetry (DTG)

Thermal decomposition experiments of energy crops were carried out by simultaneous thermal analysis (STA) equipment, using NETZSCH STA449F5 Jupiter thermal analyzer (NETZSCH-Gerätebau GmbH, Germany)) that provides simultaneous TGA-DTG curves scanning at each heating rate. Pyrolysis measuring was performed with sample masses of $\Delta m = 8.0 \pm 0.2$ mg which are placed in alumina crucibles without lids and heated from the room temperature (RT) to 600 ^{o}C in a non-isothermal conditions, using three different heating rates of $\beta = 5.1$, 10.6 and 22.1 K/min, under a constant supply of 99.999% purity (Class 5.0) argon (Ar) gas, with a gas flow rate of $\varphi = 40$ mL/min.

In order to avoid the buoyancy effect on thermal balance, the standard test procedure was performed before the measurement of each of the considered heating rate. This procedure includes the minimum three correction measurements with an “empty” sample crucible, which provides the correction file that could be applied (through the software for an analysis) to measurements with samples, performed in triplicate. Furthermore, the minimization of buoyancy effect was also performed during the preparation sequence for each TA measurement. Before opening the furnace, the protective gas flow was increased to 200 mL/min to reduce atmospheric air purge into the balance area. After closing the furnace, the flow of protective gas was held at 20 mL/min for three minutes before the measurement began, and with setting the purge gas flow to a desired value.

Corresponding dynamic STA tests were performed under the constant heating rate (*i.e.* normally the linear increase with time). This is important when applying kinetic methods that can be extended to variable heating rate data, since the constant heating rate is not a necessary assumption for these methods. Nevertheless, data should be analyzed as a function of time, since the time and temperature derivatives are no longer linearly related when heating rate is not constant. In addition, the sample spends longer time at a certain temperature, when the maximum decomposition rate is approached. Afterwards, the maximum in the DTG curve with respect to time may becomes broader and does not have a clear maximum. For a given requirements, a high resolution (“Hi-Res”) in TA tests is achieved by using the low linear heating rates and small sample mass, so that, the sample reacts under a near equilibrium conditions (of course, such heating strategies may cause the processes to occur over a very narrow temperature range, and leads to an increase in resolution in the temperature domain, where this can be useful when we want to perform a qualitative kinetic analysis of the process).

In order to restrict the effect of secondary reactions and heat transfer limitations during slow pyrolysis process, we have adopted a recommendation to the work with small mass samples and low heating rates (Slezak et al., 2018). TA measurements were performed in triplicate, and the arithmetic average was adopted for the data interpretation. All collected data from STA analyses are processed through analytical software Proteus® 8.0, with unique *AutoEvaluation function* which detects and evaluates present thermal effects, *i.e.*, peaks or mass changes without user intervention. NETZSCH advanced kinetic software (Kinetics Neo) is used for the advanced analysis of TA data and further predictions and simulations. Kinetics Neo software was adapted for precise kinetic analysis of TA measurements, including model-free and model-based kinetic approaches (Supplementary Material). If obtained experimental TA curve looks complex, with several maxima and seems to contain several overlapping peaks, then the OriginPro® 9.0 64 bit software was used to qualitatively separate these peaks and to analyzes each peak, separately.

2.7.1. Specific characteristic indexes

The specific characteristic indexes are used according to the results of the TGA scans as well as kinetic analysis. The main advantage of these indexes is to provide quick identification of thermal properties of investigated biomass feedstocks. Using these indices, it is possible to evaluate the efficiency of the pyrolysis process of tested enegy crops monitored by TGA. Three indices were used in this work, as: pyrolysis peak temperature (T_p), pyrolysis index (P) and pyrolysis characteristic index (D) (Paniagua et al., 2018). All the listed indices can be calculated based on the data of TGA and DTG curves, obtained for considered biomass sample. The pyrolysis peak temperature (T_p), is the temperature corresponding to the maximum mass loss rate on the DTG curve. The pyrolysis index (P) denotes the pyrolysis capacity for each particular pyrolysis stage or the peak (usually located in the active pyrolytic zone). From a physical point of view, the higher the P value, the easier it is for the biomass to pyrolyze, making it easier to identify the sample pyrolysis capacity. This index is defined through a relation in the following form:

$$P = \frac{\left(\frac{dm}{dt}\right)_{\max}}{t_p \cdot t_e}, \quad (1)$$

where $(dm/dt)_{max}$ is the maximum pyrolysis rate (%/min), t_p is the time (min) of the largest peak (maximum decomposition rate) and t_e is referred to the pyrolysis peak temperature (T_p) (Paniagua et al., 2018). Pyrolysis characteristic index or the reactivity index (D) assesses the pyrolysis performance and denotes the energy required to pyrolyze the biomass feedstock. It is inferred that a higher (D) value translates to a better pyrolysis property of the biomass. Since a several vital parameters are analyzed in the current index, it gives a reasonably comprehensive evaluation, which can be regarded as a reference for practical operations. The reactivity index can be calculated using an following relation:

$$D = \frac{\left(\frac{dm}{dt}\right)_{\max} \cdot \left(\frac{dm}{dt}\right)_{mean}}{T_p^2 \cdot T_f}, \quad (2)$$

where $(dm/dt)_{max}$ is the maximum pyrolysis rate (%/min), $(dm/dt)_{mean}$ is the mean pyrolysis rate (%/min), T_p is the pyrolysis peak temperature, and T_f is the temperature value at the end of the peak (the burn-out temperature) (Paniagua et al., 2018; Liu et al., 2020).

2.8. Kinetics modeling

Pyrolysis mechanisms of C3 and C4 energy crops were studied with a variety of computational methods by fitting data derived from TGA and DTG experiments, into appropriate mathematical expressions. A summary of kinetic methods and kinetic models as well as process optimization approaches used in this study, are presented in the theoretical section of Supplementary Material (sections I., III., IV., and sub-sections I.1., I.2., III.1.).

2.9. Thermodynamic analysis and enthalpy-entropy compensation (EEC)

Procedures for calculating the thermodynamic parameters (changes in the reaction enthalpy (ΔH^o), entropy (ΔS^o) and free Gibbs energy (ΔG^o)) for the pyrolysis processes of investigated energy crops are provided in theoretical section related to thermodynamic analysis within Supplementary Material (section V., and sub-section V.1.). Additionally, the origin of IKR (iso-kinetic relationship) and EEC (enthalpy-entropy compensation), which can provides an extra thermodynamic information about investigated processes is also described in the theoretical part of enclosed Supplementary Material (sections II., VI., and sub-sections II.1., VI.1.).

3. Results and discussion

3.1. General analysis of C3 and C4 energy crops

The results of biomass samples (MG and AD) characterization are presented in Table 2.

Considering moisture content for observed samples and appropriate harvest periods, AD has higher moisture content than MG (Table 2). Degree of moisture retention in a given energy crops largely depends on whether the harvest season was “wet” or “dry”. Considering the above-mentioned harvested periods, the moisture content may varies, where it would be understandable that typically, high moisture content in the harvested feedstocks can be measured after the “wet” growing season. However, despite this, the moisture content values (Table 2) are acceptable considering harvest periods and still represent a good precondition for safe crops storage. Therefore, in order to utilize the feedstock for energy purposes, as long as possible, the lowest value of moisture content is required (generally, the moisture content of less than 15% in the biomass sample is preferred for thermo-chemical conversion *via* pyrolysis). Obtained values of the moisture content after drying for both samples, are associated with their calorific value (Table 2). In that

Table 2
Physicochemical properties and lignocellulosic composition of MG and AD feedstocks used in this study.

MG			
Proximate analysis /wt%		Ultimate analysis[a] /wt%	
Moisture	6.75	C	43.10
Volatile matter (VM)	79.59	H	5.92
Fixed carbon (FC)	11.33	O[c]	48.18
Ash (A)	2.33	N	0.30
HHV /MJ·kg^{-1}	18.19	H/C	1.64
LHV[b] /MJ·kg^{-1}	16.81	O/C	0.84
Fuel ratio, FR	0.142		
AD			
Proximate analysis /wt%		Ultimate analysis[a] /wt%	
Moisture	10.98	C	44.20
Volatile matter (VM)	75.85	H	6.10
Fixed carbon (FC)	11.57	O[c]	47.65
Ash (A)	1.60	N	0.25
HHV /MJ·kg^{-1}	17.50	H/C	1.65
LHV[b] /MJ·kg^{-1}	16.04	O/C	0.81
Fuel ratio, FR	0.152		

Lignocellulosic composition					
Sample	Cellulose /wt%, dry basis	Hemicelluloses /wt%, dry basis	Lignin /wt%, dry basis	Holocellulose /wt%, dry basis	Extractives /wt%, dry basis[d]
MG	53.04	18.10	25.24	71.14	3.62
AD	45.40	19.20	32.31	64.60	3.09

[a] On a dry basis (*db*).
[b] Calculated according to EN ISO 18125:2017 (ISO 18125, 2017).
[c] By the difference.
[d] By the difference.

context, the higher energy potential shows MG (HHV = 18.19 MJ·kg^{-1}, LHV = 16.81 MJ·kg^{-1}) compared to AD (HHV = 17.50 MJ·kg^{-1}, LHV = 16.04 MJ·kg^{-1}). This is because the higher moisture content reduces the amount of available energy for considered feedstock. Consequently, based on HHV and LHV values, MG seems to have advantages towards energy content compared to AD. Nevertheless, both samples with high heating values and high carbon content compared with other biomass feedstocks (such as sugarcane bagasse (Munir et al., 2009), rice husk and corn cob (Titiloye et al., 2013)) indicate the potential of MG and AD as a sources of bioenergy. The heat content of the feedstock type can vary significantly, depending on the climate and soil in which the biomass is grown as well as other conditions. As the result, the energy content of biomass should be thought of as a range rather than a fixed value. Additionally, the ash (A) content of different biomasses varies broadly with agricultural residues and energy crops, typically generating a more ash content than woody biomass, partially due to harvesting techniques and partially due to inherent differences in feedstocks. Anyway, for our samples, there is no negative correlation between LHV and ash content. There is already a positive correlation. Namely, herbaceous biomass and residuals have higher levels of the A-content compared to woody biomass, and ranges should be considered in the boiler design or particulate control technology, if these feedstocks are to be used. Compared with coals, energy crops and woody biomass are characterized by higher volatile matter (VM) contents, typically in the range of 65.0–85.0 wt% (Runge et al., 2013). Both samples are characterized by high content of volatile matter (VM) (above 70 wt%), whereby MG has a slightly higher VM content (Table 2). VM is the fraction of the biomass which transforms into vapors during pyrolysis and condenses to produce a bio-oil and non-condensable gaseous products. Vapors include mainly hydrocarbons (HC), hydrogen (H_2), carbon monoxide (CO), carbon dioxide (CO_2) and tars present in considered feedstock. A higher fraction of VM in the feedstock indicates its ease of conversion and disintegration through the pyrolysis. The obtained values of VM for our samples (75.85–79.59 wt% (Table 2)) are comparable with VM values for the same types of energy crops reported elsewhere (Krička et al., 2017). Both samples in respect to VM contents seem superior to the VM content identified in some crop residues such as Peanut straw (~ 66.4 wt%) and cotton straw (~ 64.9 wt%) (Wan et al., 2019). The fixed carbon (FC) content is the fraction of biomass which usually does not decomposes during pyrolysis and contributes to the char production. Both samples have FC values in a very narrow range as 11.33–11.57 wt% (Table 2), where these feedstocks can show significant potential for higher char yields, which can be reconfirmed from VM content as well. Considering VM and FC values, the tested samples have significant potential for producing the higher yields of chars and bio-oils from the pyrolysis process.

In addition, the ultimate analysis is an important, because this analysis has a fundamental importance for the biomass investigation, before its use in thermo-chemical conversion process. The C, H and O contents are the most important regarding its fuel-value. On the other hand, the nitrogen (N) and sulfur (S) contents are the essential from an environmental emissions perspective. Both samples exhibit higher carbon (C) content, directly related to their relevant heating values. Also, a high oxygen (O) content exists in both samples (Table 2), where C, O and H are principal elements present in plant biomass as building blocks of major constituents, including cellulose, hemicelluloses and lignin. The content fractions of these elements in the feedstock are influenced by growing conditions of plants and these constituents have significant effects on the pyrolytic behaviors of given feedstock and products formed. Higher contents of H and O in feedstocks are responsible for the higher VM. Slightly higher nitrogen (N) content is present in MG than in AD (Table 2), not neglecting the formation NO_x species (may causes severe environmental pollution and require additional treatment procedures, if the concentration of this element exceeds allowable limits). Additionally, the presence of nitrogen in both samples originated from stems of a given crops can be attributed to the nitrogen-fixing capabilities of these plants which allow them to thrive in deprived soils. The formation of sulfur oxides is minimized due to the zero tolerance for the presence of sulfur in both samples.

The H/C and O/C ratios are very similar for both samples (Table 2), and their position on the Van-Krevelen diagram is typical for "*green*" solid fuel (biomass feedstock) rich with cellulose (in the Van-Krevelen diagram, carbohydrates appear at H/C ratios > 1.50 and O/C ratios > 0) (Schimmelpfennig and Glaser, 2012). Higher H/C ratio values indicate a higher biomass potential, while lower O/C ratio values (below the unity) indicate a higher heating value and the VM content in considered feedstocks (Table 2). The obtained fuel ratio (FR) for studied samples is ranged between 0.142 and 0.152 (Table 2). The FR value represents the property of solid fuel and increased FR's suggest improved conversion performance and reduced emissions of air pollutants, when the raw biomass is used in thermo-chemical transformation. Generally speaking, when FR is less than 1.5, afterwards, the solid fuel easily burns. When the biomass is subjected to elevated temperature during thermo-chemical conversion, the reaction temperature and the time strongly affect the conversion property such as FR. This is because the indicated feature is dependent on the VM and its conversion to FC.

Concerning lignocellulosic composition, Galletti et al. (2015) investigated the lignocellulosic content of AD, and they are reported an following contents: cellulose: 41.6%, hemicelluloses: 23.6%, and lignin: 24.6%. Our results (AD) (Table 2) are consistent in terms of cellulose content (45.40%), but not in terms of hemicelluloses (19.20%) and lignin (32.31%). The lignocellulosic composition of MG was studied by Wróblewska et al. (2009) and they reported results in an following manner: cellulose: 43.2%, hemicelluloses: 25.2% and lignin: 23.0%. Other authors are reported somewhat different results as: cellulose: 45.0%, hemicelluloses: 30.0% and lignin: 21.0% (Collura et al., 2005). Considering these reports, our results are partly in line (Table 2) with the aforementioned, but obviously, there are deviations between biomass constituents. Such differences in the investigated lignocellulosic biomass feedstocks can be expected, because lignocellulosic composition is influenced by the soil, location and the harvest time. Taking these data and investigation of the chemical composition of different herbaceous and oilseed crops by Abreu et al. (2022), it was clearly indicated that herbaceous crops show promising results in thermo-chemical processes, such as pyrolysis of *Miscanthus*. Additionally, results reported by the indicated authors suggest that *Arundo donax* is suitable for bioenergy production, carried out either by bio-chemical pathway or thermo-chemical conversion routes. Considering our results related to lignocellulosic composition of MG and AD (Table 2), they fit very well within the range of variation of these biomass constituents reported from different reference sources (Abreu et al., 2022). Extractives in biomass contains non-structural aromatic compounds such as alkaloids, proteins, phenolics, simple sugars, pectins, mucilages, gums, fats, oils, waxes, resins, and terpenes (Kumar et al., 2020). Extractives content is slightly higher in the case of MG sample than in the case of AD sample (Table 2). MG contains fatty acids, sterols and other aromatic compounds as extractives (Brosse et al., 2012). These extractives are of high value in terms of precursors for industrial chemicals and materials. AD is rich with lipophilic extractives which are widely used in the pulp and papermaking industry. However, extractives content in MG and AD can vary considerably in a ranges 9–17% (MG) and 12–22% (AD) (Abreu et al., 2022), while actual samples are characterized with "lower" extractives content (*note*: based on theoretical calculation, but not directly by extraction).

Results related to the main ash-forming elements (K, Mg, Ca, Na, Fe, Mn, Cu, Pb, Ni, Cd and Zn; where K, Mg, Ca, Na and Fe represent the major elements, while Mn, Cu, Pb, Ni, Cd and Zn represent the minor elements) for both samples are listed in Table S1 (Supplementary Material). Generally, the ash is formed by combusting inorganics under controlled conditions, where ashing temperature for biomass feedstock is ~ 550 °C, while for coals is higher ~ 780 °C. Namely, the chlorine, potassium and sodium are usually released during high temperature

combustion process. Major elements, such as K, Mg, Ca, Na and Fe are typically manifested in terms of their oxides and chlorides. They have a major impact on the ash melting, fouling and corrosion, whereas they have a low impact on the environment. From obtained results (Table S1), both samples are rich in K and Ca, as well as by elevated quantity of Fe. AD sample is particularly distinguished in increased quantity of K and Fe compared to MG. Calcium and magnesium increase the ash melting temperature, whereas potassium and sodium decrease it. Therefore, it should be expected that the perennial crops ashes have low melting temperatures, while much higher melting temperatures can be expected for wood feedstocks. Comparing with coals, biomass samples have higher amounts of K_2O and KCl (Kowalczyk-Juško et al., 2022). Later in this study, it will be particularly highlighted the catalytic effect of the ash components, briefly discussed through proposed model for pyrolysis process of C3 and C4 energy crops.

3.2. FTIR analysis

Fig. 4 shows FTIR spectra of MG and AD samples in the range between 4000 cm^{-1} – 500 cm^{-1}. It is shown that the most prominent bands of MG and AD are similar with those previously observed FTIR spectra of other lignocellulosic materials (Arellano et al., 2016; Carrier et al., 2011). The bands that appear at 3300 cm^{-1} are characteristic for O–H groups which are assigned to intermolecular hydrogen bonds in the cellulose (Kenkyu, 1997). Then, the peaks that are presented at 2917 cm^{-1}, 2849 cm^{-1} in AD, and the peak at 2916 cm^{-1} in MG, belong to stretching in methyl and methylene groups (C–H), that are presented in both samples (Chen et al., 2019). In both samples, there are presented peaks at 1732 cm^{-1}, that are attributed to acetyl and uronic ester groups of hemicelluloses, and also the characteristic of C═O conjugates in hemicelluloses (Oh et al., 2005). Further, the peaks at 1062 cm^{-1} in MG, 1593 cm^{-1} in AD are associated with the aromatic skeletal stretching together with —COO— stretching in the hemicelluloses, which is related to the connection of lignin and hemicelluloses (Mou et al., 2013), while the peaks at 1506 cm^{-1} that are presented in the both samples were ascribed with aromatic skeletal vibrations of lignin.

The content of lignin in the sample can be determined with the vibration band presented at 1508 cm^{-1}, which did not overlap with those

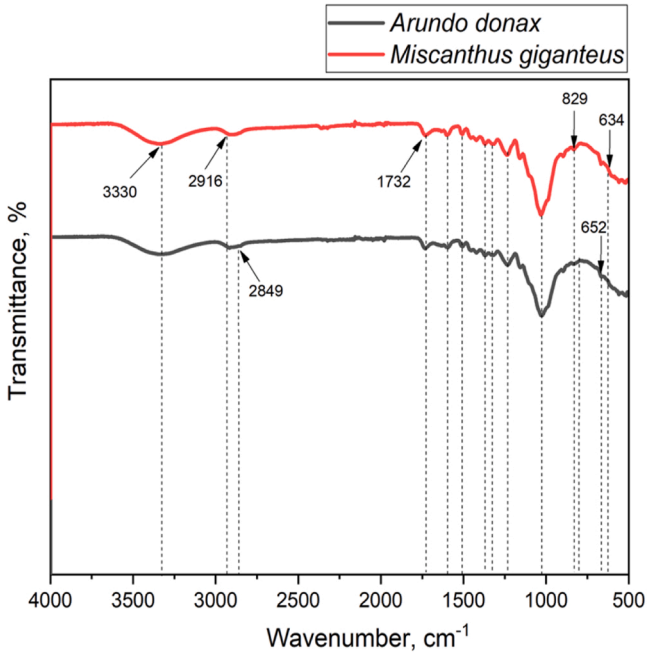

Fig. 4. FTIR spectra of *Arundo donax* L. (AD) and *Miscanthus* × *giganteus* (MG) in wavenumber range of 500–4000 cm^{-1}.

related to the polysaccharides, as shown in the study Horikawa et al. (2019). Then, the C–H bending vibration in the cellulose and hemicelluloses are attributed to the weak peaks at 1376 cm^{-1} and 1375 cm^{-1} (Chen et al., 2019). The bands that appear at 1369 cm^{-1} and 1370 cm^{-1} in AD and MG respectively, are characteristic for the vibration of benzene ring, and corresponded to C–O groups. Aromatic skeletal vibrations are around 1324 cm^{-1} in the AD sample, and 1423 cm^{-1}, 1320 cm^{-1}, 1235 cm^{-1} in the MG sample. The C–O–C vibration is appeared at 1158 cm^{-1} in the MG sample which is characteristic for the cellulose and hemicelluloses (Mosiewicki et al., 2011). Further, peaks at 1027 cm^{-1} in AD and at 1031 cm^{-1} in MG, are attributed to C–O–C and C–O starching that is characteristic for the cellulose and hemicelluloses. Likewise, the peak at 900 cm^{-1} in the MG is attributed to C–H deformation in the cellulose (Osman et al., 2017; Casillo et al., 2018). Two weak peaks at 808 cm^{-1} and 829 cm^{-1}, for AD and MG, respectively, can be attributed to C–H deformation. These bands belong to the region of aromatic C–H out of plane vibration, because of the presence of lignin (Mosiewicki et al., 2011). Table 3 provides an overview of identified chemical band assignment obtained through FTIR measurements.

Likewise, the presence of other two weak peaks at wavenumber position of 652 cm^{-1} (Schulz and Baranska, 2007) in the AD sample, and 634 cm^{-1} (Larsen and Barsberg, 2010; Agarwal, 1999) in the MG sample, are detected as, ring deformation of 1,8 cineole which belongs to the bicyclic monoterpenes (Schulz and Baranska, 2007), and the ring and skeletal deformation of the lignin (Lupoi et al., 2015), respectively. In addition, terpenes as a chemical compounds are identified in the *Arundo donax* L. (Al-Snafi, 2015).

3.3. Pyrolysis profiles derived from TG-DTG scans and thermal properties of investigated feedstocks

TG-DTG measurements were accomplished at various heating rates (5.1, 10.6 and 22.1 K/min) for both considered samples, and the effect of applied heating rates on the obtained TA curves of pyrolysis process was presented in Fig. 5a) – b). In all observed cases, the moisture evaporation stage (biomass dehydration step) (from room temperature (RT) up to $T \sim 130\ ^{o}C$) was not shown and will not be considered in the further analysis.

For both samples, the mass loss curve in Fig. 5a) shows continuous

Table 3
Summary of chemical bands assignment by FTIR.

Functional groups	Wavenumber (cm^{-1})
Hydrogen bonded stretching (O - H)	3300
Stretching in methyl and methylene groups (C – H)	2916
	2917
	2849
Acetyl and uronic ester groups of hemicellulose, conjugates in hemicellulose (C═O)	1732
	1062
Aromatic skeletal stretching together with —COO— stretching in hemicellulose	1593
	1506
Aromatic skeletal vibrations in lignin	1508
The content of lignin	1375
Bending vibration in cellulose and hemicellulose (C - H)	1376
Vibration of benzene ring (C – O)	1369
Aromatic skeletal vibrations	1370
C – O – C vibration in hemicellulose and cellulose	1324
C– O-C and C – O starching	1423
C - H deformation in cellulose	1320
C – H deformation in lignin	1235
Ring deformation - terpenes	1158
Ring and skeletal deformation of lignin	1027
	1031
	900
	808
	829
	652
	634

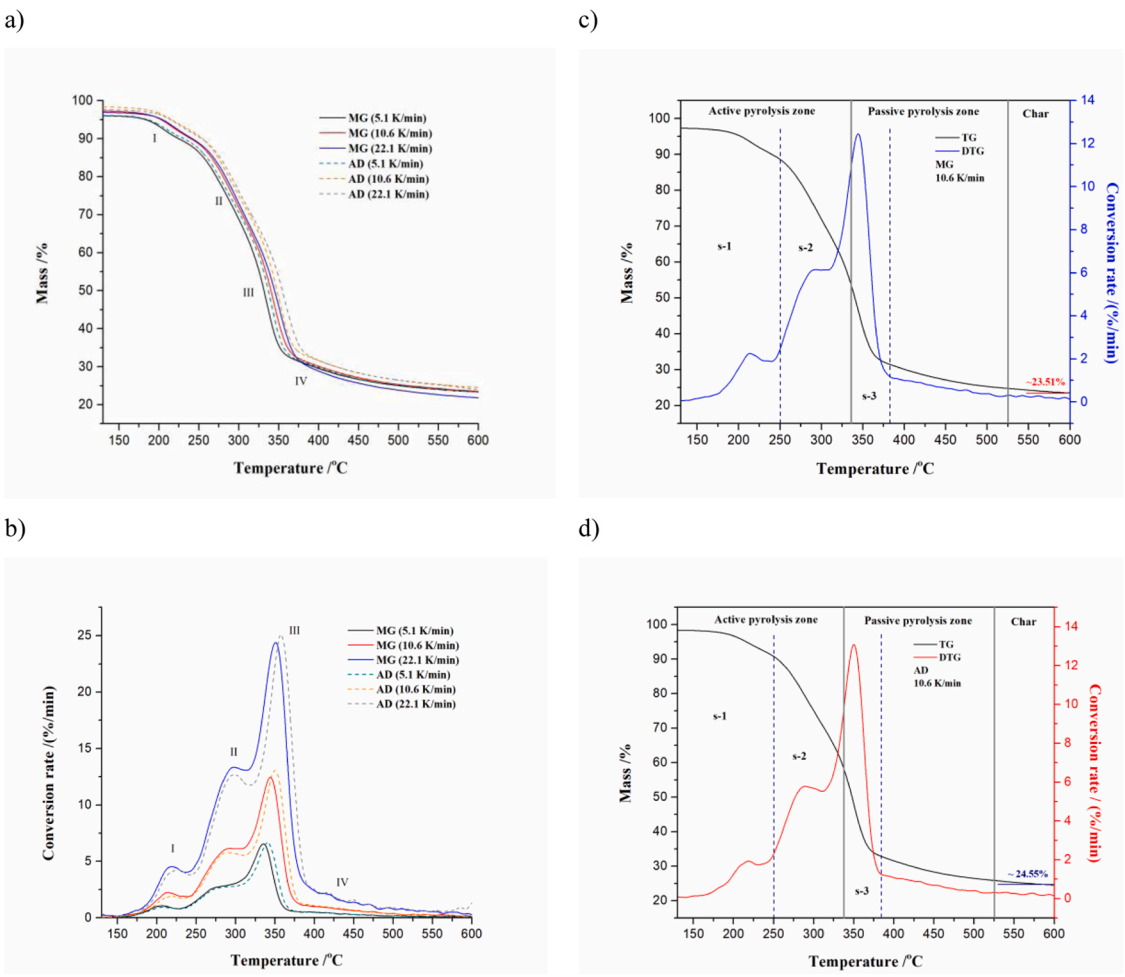

Fig. 5. Simultaneous display of TG a) and DTG b) curves (conversion rate *vs.* temperature) for the pyrolysis process of C4 (*Miscanthus* × *giganteus*: MG) and C3 (*Arundo donax* L.: AD) crops at $\beta = 5.1$, 10.6 and 22.1 K/min; Simultaneous TG-DTG curves at 10.6 K/min for pyrolysis processes of MG c) and AD d) with marked reaction zones, determined on the basis of position of inflection points in thermo-analytical curve (values of residual mass loss for both samples are also indicated).

reduction in the mass of the specimen with the increase of pyrolysis temperature at various heating rates. The heating rate represents a key operational parameter in the pyrolysis of biomass. The onset and offset temperatures as well as peak ("*max*") temperature of the *main devolatilization* stage ("III" (Fig. 5a) – b))) shift obviously toward the high temperature region as the heating rate increases. This phenomenon was attributed in previous studies to the heat and mass transfer limitations (Haykiri-Acma et al., 2006; Mani et al., 2010). Thus, the Fig. 5b) clearly shows this phenomenon which appears in the pyrolysis of both samples, so this means that temperature gradients can exist in tested sample, and the devolatilization rate is faster than volatile release. Therefore, the different devolatilization stages take place, and because of that, the small particle size of the sample with an uniform distribution is preferred for TGA tests.

Given that relatively small amounts of sample were used in TA measurements and small particle sizes were relevant, it can be noted that there are almost no differences in the appearance and distance of the TG-curves with the change of the heating rate (Fig. 5a)). Consequently, the influence of different parameters such as particle size, the initial mass of the sample and the heating rate on the devolatilization of biomass particles, can be monitored by TGA measurements. For quality obtained results from TG scans, the small mass and uniform biomass sample are preferred in order to mitigate the effects such as non-uniform temperature distribution and the product decomposition.

It was noted that there is a certain difference in pyrolysis residues (*i.e.*, the char) considering both samples (MG and AD, Fig. 5a)), especially at the highest heating rate. However, among the given samples, these differences are not large (MG: 23.36% at 5.1 K/min to 21.84% at 22.1 K/min; AD: 23.31% at 5.1 K/min to 23.93% at 22.1 K/min). However, observed changes, 1.52% (for MG) and 0.62% (AD), suggest that indicated ranges are "spread out" enough to see a measurable difference ($\sim\Delta(\Delta m_{res}) = 0.90\%$). At this difference magnitude, heating rate affects on the char yields in pyrolysis of C4 and C3 crops monitored by TG-DTG techniques. In addition to observed difference, still, for both samples, the obtained data of residues yields are very close. Consequently, the residues yields of MG and AD pyrolyses at different heating rates were found as: 10.6 K/min > 5.1 K/min > 22.1 K/min, and 10.6 K/min > 22.1 K/min > 5.1 K/min, respectively. In our cases, the influence of the heating rate is limited, since that residues yields do not increase regularly with an increasing of the heating rate (Oyedun et al., 2013).

Fig. 5a) – b) shows four regions of steep mass losses, numbered "I" to "IV". The region I, which extends from 130 °C to 250 °C, can be attributed to volatilization of the extractives with smaller contribution to the overall pyrolytic process of both samples. Regions II and III are located approximately at 275 °C and 330 °C, respectively, and represent the highest mass loss rate, as shown by one "shoulder" feature, and one peak in DTG curves (Fig. 5b)). The identified decomposition range of both regions is comparable with the decomposition temperatures of hemicelluloses and cellulose constituents of investigated feedstocks (Singh et al., 2021). The apparent differences in the decomposition rates of these components of lignocellulosic material (Fig. 5b)) originate from

their thermal stability diversities. This especially applies to the third constituent of biomass, lignin. The final thermo-analytical slope change occurs at approximately 380 °C considering both samples (region IV), which is consistent with decomposition of lignin, which occurs at much broader temperature ranges from roughly $T \sim 200$ °C to $T \sim 525$ °C. Considering biomass constituent structural components, hemicelluloses has higher reactivity in respect to thermal decomposition by virtue of its un-fixed structure, with short molecular chains and many branches. On the other hand, the cellulose is a highly linear, non-branching polymer formed by *D*-glucose, leading to a much higher thermal stability. Finally, the lignin is full of the aromatic rings and is heavily cross-linked, and therefore, it is difficult to decomposes. If we look at the pyrolysis DTG curves of MG and AD samples (Fig. 5b)), the former "shoulder" feature resulting from hemicelluloses devolatilization, while the latter, the main pyrolysis peak, resulting from the cellulose devolatilization. Lignin decomposition is not characterized by a "pure" (clearly visible) thermal decomposition peak, but it is already reflected by tailing reaction path.

The evaluated process range was split into three zones: active pyrolysis, passive pyrolysis and char formation (Fig. 5c) – d)). Considering the obvious difference in the kinetic behavior of these reaction zones, in which there is a coupled reaction complexity among the components of the biomass being decomposed, further analysis will use the recommendations set by the International Congress on Thermal Analysis and Calorimetry (ICTAC) Kinetics Committee (Vyazovkin et al., 2020). The active pyrolysis zone includes extractives removal (130 °C – 250 °C), where in this zone (step s-1), all organic compounds with lower thermal resistance undergo decomposition. Furthermore, within the same zone, in the temperature range between 250 °C and 335 °C (step s-2), hemicelluloses and partly cellulose are pyrolyzed. Several cellulose structural fragments are temporarily stable at latter temperature, so its co-products and their subsequently decomposition requires a rise in the temperature, moving into the area of passive pyrolysis (up to 380 °C) (step s-3) (Fig. 5c) – d)). From 380 °C to 525 °C, the passive pyrolysis takes place, where the mass loss is mostly generated by lignin and fixed carbon (FC). Beyond 525 °C, the residual pyrolysis process occurs and final amount of char is formed. The residual pyrolysis stage includes as well decomposition of co-products generated during the previous steps. It should be emphasized that the lignin decomposition covers a wide temperature range mixing in the active and passive pyrolytic zone, and this can lead to a serious decrease in accuracy, if we want to determine sample composition based on TG-data. Considering the strong heterogeneity of the reaction stages in which, there is clearly an effect of parallel reactions, then, it is necessary to apply the deconvolution procedure to identify and isolate these reactions, in the kinetically complex process. Hence, among available methods for the separation of parallel reactions, the most widely used is the deconvolution of conversion rate curves (Fig. 5b)), in which a fit of multiple peaks with some pre-selected function was performed. It should be pointed out that in the case of multi-component decomposition, such as the pyrolysis of energy crops, the application of the deconvolution approach with asymmetric functions (such as Lorentzian function) was applied (Ba et al., 2020).

For our monitored process, we used the best selected function for this kind of operation and that is the amplitude version of Gaussian peak function (*GaussAmp*), which is described in detail within Supplementary Material (sub-section III.1.). This function turned out to be the best choice, because it gave best fits, according to the coefficient of determination (R^2 - Adj. R-Square) (high R^2 values; $R^2 > 0.99930$). It should be mentioned that deconvolution approach was not used in this work for kinetic calculation, where kinetic parameters are determined simultaneously. It was announced that the deconvolution method gives worse results than for an example, model-fitting methods (Fonseca et al., 2022). In this sense, the deconvolution approach was used here as a tool for the efficient separation of the presence of possible parallel and overlapping reactions during decomposition of lignocellulosic components. Fig. S1 a) – f) (Supplementary Material) shows experimental results of conversion rate curves and the cumulative fit curve for considered heating rates considering both samples, in which, there are five peaks, identified as Peak 1, Peak 2, Peak 3, Peak 4 and Peak 5. It can be immediately noticed that the number of determined peaks does not correspond to the number of established stages in Fig. 5a) – b). Namely, there is obviously the presence of parallel and overlapping reactions in the pyrolysis process of both samples. The applied deconvolution function (Eq. (S23)) separates these reactions very efficiently, resulting in a very high values of R^2 in fitting procedure. As can be seen in Fig. S1 a) – f), there is considerable overlap between three lignocellulosic components due to concurrent decomposition. There are also two overlapping reactions in the cellulose decomposition region with different contributions to the pyrolysis processes of MG and AD samples (Fig. S1 a) – f)). Therefore, the observed peaks can be attributed to the following transformations: Peak 1 - volatilization of extractives, Peak 2 – thermal decomposition of hemicelluloses, Peak 3 and 4 – strong overlapping degradation reactions attached to cellulose breakage, and Peak 5 – thermal decomposition of lignin. Peak related to lignin pyrolysis is characterized by the inclusion of a very wide duration time in thermo-chemical conversion of both samples, which is in agreement with previously established facts. On the other hand, observing independently of each other, reactions related to Peak 3 and Peak 4, have shorter duration of the transformation (considering as the short range of cellulose pyrolysis) compared to the Peak 5, and this is consistent with literature report (Zhang et al., 2014). Table S2 (Supplementary Material) lists the values of deconvolution parameters for AD and MG pyrolysis processes at various heating rates, using *GaussAmp* function (Eqs. (S23) and (S24)). The values of T_c (specific temperature related to the '*maximum*' of the corresponding peak is associated to x_c value (the peak center time)) are also presented in Table S2. Comparing both samples, at all heating rates and for all peaks, T_c values for AD are higher than T_c values related to MG, suggesting a higher thermal stability of AD. The values of x_c attached to a given samples behave in accordance with the above discussion of "temporal reactivity" ranges of lignocellulosic components, such as cellulose and lignin. Achieving the maximum duration of hemicelluloses decomposition during the pyrolysis of a given samples (Table S2), approximately, corresponds to its presence in a samples, based on determined hemicellulosic composition (Table 2). Considering established errors (standard errors) related for both samples, generally, the lowest errors were found for extractives, hemicelluloses and partly cellulose (Peak 4) decompositions (Table S2). However, these errors show some variation with the heating rate change, but are essentially stable. Considering the values of fitting peak area, their percentages clearly suggest that in both samples, cellulose and lignin contribute the most to the production of the pyrolytic by-products (Table S2). However, defining the peak area contribution, it is obvious that lignin decomposition from MG pyrolysis leads to a larger contribution of the charring reaction at high temperatures, compared to the same for AD pyrolysis (Table S2). The listed results obtained by deconvolution of the complex conversion rate curves, are in very good agreement with the examination of the lignocellulosic content, as well as thermal properties of tested energy crops (Table 2 and Fig. 5).

Table 4 shows the experimental T_p values, the maximum pyrolysis rates ($(dm/dt)_{max}$), pyrolysis index (P) and reactivity index (D) values for MG and AD samples.

Considering both maximum pyrolysis rates, an increasing of the heating rates causes the material to reach the temperature in a shorter time, in turn, leading to the shift of the peak temperature towards higher values (Table 4).

This is a result of the larger temperature gradient which is developed between the inside and the outside of investigated material. Beside, the higher temperatures are less effective than a lower temperatures. Additionally, the lower heating rates allow the biomass samples to be heated gradually, giving rise to more efficient heat transfer within a given material (Biagini et al., 2006). Namely, TGA devices can use a high heating rates even with a extreme value of 500 K/min, but to minimize the effect of the temperature gradient within tested sample, most of the

Table 4
Characteristic parameters (T_p, $(dm/dt)_{max}$, P and D) related to pyrolysis process of MG and AD feedstocks at different heating rates ($\beta = 5.1$, 10.6 and 22.1 K/min).

MG				
β /K/min	T_p /°C[a]	$(dm/dt)_{max}$ /%/min[a]	P /%·min^{-3}	D /%^{2}·min^{-2}·°C^{-3}
5.1	336.0	6.600	1.51×10^{-3}	6.49×10^{-6}
10.6	345.0	12.500	5.33×10^{-3}	2.63×10^{-5}
22.1	351.0	24.400	1.90×10^{-2}	9.78×10^{-5}
AD				
β /K/min	T_p /°C[a]	$(dm/dt)_{max}$ /%/min[a]	P /%·min^{-3}	D /%^{2}·min^{-2}·°C^{-3}
5.1	340.0	6.709	1.48×10^{-3}	6.90×10^{-6}
10.6	350.0	13.152	5.41×10^{-3}	2.53×10^{-5}
22.1	357.5	25.230	1.88×10^{-2}	9.21×10^{-5}

[a] Related to the main pyrolysis peak (main devolatilization stage: "III").

laboratory-scale experiments are performed by using the lower heating rates (as in the range of 5 – 50 K/min) (Ng et al., 2018). Further, the heating rate can also influence the resolution of obtained thermo-analytical features. So that, the choosing slower heating rates usually results in a higher resolution of the curves. Our used heating rates clearly show this situation, which is very important for a precise and accurate kinetic analysis (Fig. 5). On the other hand, experimentally obtained values of T_p (Table 4) are in good agreement with the behavior of the corresponding T_c values attached to the Peak 4 (within cellulose decomposition region) in resolved conversion rate curves for MG and AD pyrolyses (the difference between these temperatures is two to three Celsius degrees) (Table S2). Based on the established P values, both samples are characterized by being easier to pyrolyze at higher values of the heating rate, β (Table 4). Comparing mutually P values among given samples, on individual β-values, very low and high heating rates in pyrolysis are more suitable for MG sample, while for the pyrolysis of AD sample, the medium heating rate is more suitable. In addition, comparing D values for both samples, the pyrolysis performance is much better for $\beta \geq 10.6$ K/min. Looking individual biomass samples, MG shows better pyrolytic performances than AD at heating rates higher than 5.1 K/min (Table 4), considering the significantly higher thermal stability of AD feedstock (see discussion above). Overall, D indexes for AD are relatively low, its thermal stability is relatively good, but it is 'difficult to decomposes' compared to the MG sample (MG has a tendency for much stronger release of volatiles). However, an interesting contrasting feature should be noted: at the heating rate higher than 5.1 K/min, MG has higher values of D in relation to AD, so it would be expected to have higher values of $(dm/dt)_{max}$ in considered process stage. However, this is not the case, because the values of $(dm/dt)_{max}$ are lower than those of AD for $\beta > 5.1$ K/min. The key point regarding this phenomenon lies in the contribution of overlapping reactions in the observed pyrolytic zone (considering the areas under the fitting peaks as Peak 3 and Peak 4 (Table S2 and Fig. S1 a) – f))). It can be observed that there are almost no variations in the percentage contribution of these reactions during pyrolysis of cellulose in the case of the AD sample, than in the case of the MG sample (Supplementary Material). A significant variation in contribution of these reactions to the overall process of cellulose degradation in the MG sample can be clearly seen at higher heating rates (10.6 K/min and 22.1 K/min), which leads to the reduction of $(dm/dt)_{max}$ values for MG compared to AD (Table 4).

3.4. Isoconversional kinetic analysis

Isoconversional (model-free) methods involve no assumption of any reaction (kinetic) model and thus are able to accurately estimate the activation energy (E_a) as a function of conversion degree, and the most frequently applied model-free methods include Friedman's (FR), Kissinger-Akahira-Sunose (KAS), Ozawa-Flynn-Wall (OFW) and Vyazovkin's (VY) methods, which were applied in this study (Supplementary Material, section I.). These methods allow recalculation of the pre-exponential factor ($logA$) based on the kinetic compensation effect (KCE), without knowing the exact reaction mechanism of the process of interest (for more details, see section I., within Supplementary Material). Consequently, the accurate determination of kinetic parameters (E_a; $logA$) for lignocellulosic biomass feedstock pyrolysis (thermal decomposition process) is necessary for material performances in a real-times, the modeling of various pyrolyzers, combustors, and gasifiers, as well as to optimize an operational parameters. Fig. S2 a) – f) shows representative non-isothermal isoconversional plots at the selected conversion values obtained by application of FR, KAS and OFW methods, for pyrolysis process of MG and AD feedstocks. From constructed isoconversional plots, the values of kinetic parameters (E_a, $logA$) at different and constant values of conversion (x), in the range of $0.01 < x < 0.99$ (with conversion step $\Delta x = 0.01$) were estimated. Fig. 6a) – d) shows distribution of activation energies (E_a) and pre-exponential factors ($logA$) as a function of conversion, for pyrolysis processes of MG and AD samples, under a slow heating conditions. The variation of activation energies with conversion in the x interval of $0.01 < x < 0.99$ for all applied isoconversional (model-free) methods, in the case of MG and AD pyrolysis processes, is shown in Table S3 (Supplementary Material).

For all samples, the E_a and $logA$ values exhibit strong variation with conversion, as the process progresses further. As observed, E_a and $logA$ profiles for MG and AD show certain differences, but with an equal number of activation energy variation stages (numbered as 1 *, 1, 2, 3, 4 and 5). On the other hand, all applied isoconversional methods are consistent with each other in the calculation of kinetic parameters, but larger errors show the values of E_a and $logA$ obtained in the case of AD pyrolysis (Fig. 6a) – d)). In regard to the variation of E_a with conversion for both samples, E_a values show the overall upward trend, but there are some fluctuations in the local manner. This indicates that chemical reactions involved in the pyrolysis process are complex, including a series of parallel, overlapping and consecutive reactions. Regardless of the small shift in terms of varying conversion ranges for both samples, there are five process stages that can be explained mechanistically through the E_a variation, which reflects the change in the strength of chemical bonds undergoing thermal cracking (Vyazovkin et al., 2011; Ba et al., 2020) in a following way:

a) Stage 1 * - represents the initial stage of pyrolysis process forming U-shape through $E_a - x$ relationship curve. This stage, which includes the beginning of the process (excluding the biomass drying stage) until reaching ~10% conversion, can be attributed to volatilization of extractives occurring below 250 °C. The E_a variation range includes values approximately between 237.99 kJ/mol and 320.80 kJ/mol for MG pyrolysis, as well between 205.97 kJ/mol and 283.68 kJ/mol for AD pyrolysis (considering FR method). Since MG is very rich with sterols, fatty acids and long-chain fatty alcohols in extractive portion (Villaverde et al., 2009), their release through degradation pathway requires higher E_a value compared to AD that contains short chain-fatty acids and phenolic compounds in larger amounts (Girotto et al., 2021). The current stage (Fig. 6a) – b)) can be responsible for obtaining the alkanes to the decomposition of extractives in MG and AD pyrolysis, particularly fatty acids, which are subjected to decarboxylation and cracking.
b) Stage 1 - this stage that builds on the stage 1 * is characterized by an increase of the activation energy (E_a) in the temperature range of approximately $\Delta T = 255$ °C – 300 °C and can be attributed to the decomposition of hemicelluloses in a given samples (Fig. 6a) – b)). For both samples, E_a values are very similar, but they are significantly larger than E_a values related to the pure biomass component pyrolysis (the respective range for hemicelluloses pyrolysis is 70 kJ/mol – 215 kJ/mol) (Anca-Couce et al., 2020). However, it was identified that the E_a values for hemicelluloses decomposition for AD sample are slightly lower than in the case of MG sample, for approximately same conversion changes. The factor leading to this

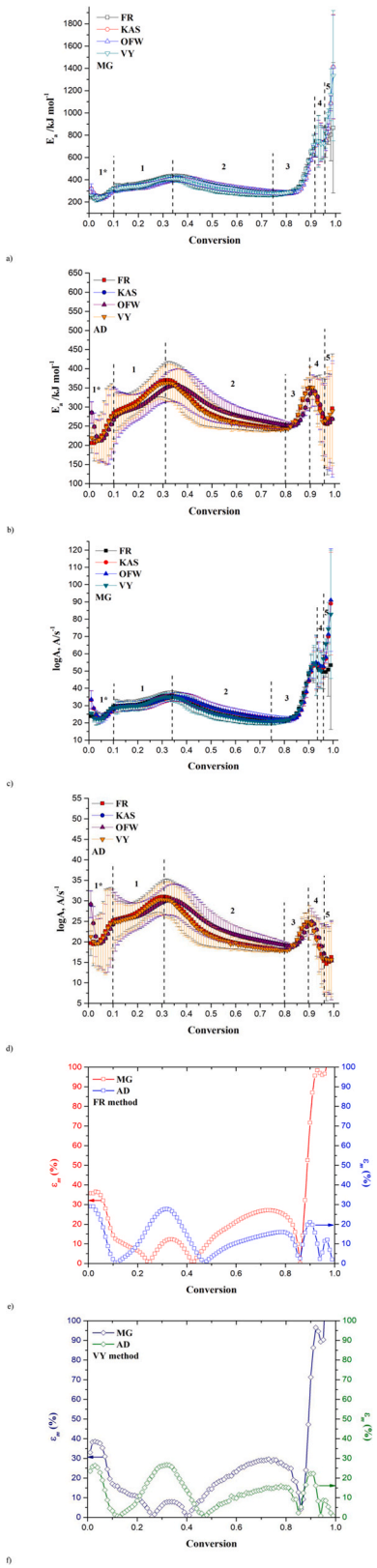

Fig. 6. E_a and *logA vs.* conversion (x) profiles estimated for C4 (MG) and C3 (AD) energy crops pyrolysis (a) – d)) using FR, KAS, OFW and VY methods. The deviation of E_a to its mean value ($E_{a(m)}$) for MG and AD pyrolyses (e) and f)) shown for FR and VY methods (mean values considering entire conversion range: $E_{a(m)}$ (FR) = 375.01 kJ/mol and $E_{a(m)}$ (VY) = 381.43 kJ/mol for MG; $E_{a(m)}$ (FR) = 289.98 kJ/mol and $E_{a(m)}$ (VY) = 286.69 kJ/mol for AD).

observation is the higher amount of lignin in the AD sample, which can increases the decomposition rate of hemicelluloses at low β's and thereby reducing E_a. Additionally, the type of hemicelluloses may differ substantially from one source to another. Namely, xylan is the only type of hemicelluloses in grasses, while hemicelluloses in hardwoods is composed mainly of xylan, with glucomannan that represents about 10% of the total hemicelluloses (Technical Bulletin (1994)). Contrary, softwoods are rich in glucomannan and relatively poor in xylan. In our case, the high E_a values observed for hemicelluloses decomposition in pyrolysis processes of MG and AD are the consequence of the cleavage of the glycosidic bond, that involves energy barriers as *mean* valuation, approximately ranging from 280 kJ/mol to 310 kJ/mol (Fig. 6a) – b)). Namely, this energy barriers correspond to depolymerization through concerted reactions involved in β-1,4-xylan degradation.

c) Stage 2 – this stage can be attributed to the cellulose decomposition, which is characterized by a gradual decrease in the E_a value in the temperature range of approximatelly $\Delta T = 310\ ^{o}C - 360\ ^{o}C$. In both considered cases (Fig. 6a) – b)), the E_a value for cellulose pyrolysis is lower than that of hemicelluloses, due to orderly crystal structure in cellulose whose decomposition pathway is relatively simple than hemicelluloses. In this case, there are two regions of E_a values associated with cellulose degradation, one with higher values and one with lower values at elevated x (Fig. 6a) – b)). These regions may suggest on existence of more than one reaction, where radicals can be formed. Namely, formed radicals require less energy to further decomposes, which is reflected in the decrease of E_a value. Then finally, as radical species have decomposed to light gases and have been depleted, only bonds left to cleave are the more stable bonds of the aromatic lignin moiety (the next stage – stage 3).

d) Stage 3 – this stage is characterized by sudden increase in the E_a value within temperature range of approximatelly $\Delta T = 360\ ^{o}C - 420\ ^{o}C$ with slightly variable movement of x values for MG and AD pyrolysis processes (Fig. 6a) – b)). This temperature segment corresponds to a clear change in the slope of the TG-curves at the entrance to the passive pyrolysis zone (Fig. 5c) – d)). In the current stage, there is a significant difference in the activation energy values, which are higher for MG than for AD. These differences in E_a values may indicate on divers initial reaction centers in the process of lignin decomposition, which can progresses *via* similar reaction network, but which requires a significantly different amount of energy, for MG *apropos* AD sample. This is also a consequence of certain compositional variability of lignin in a tested samples. One of the important facts that follows from such differences in the kinetic parameters among the samples in this stage, is the different yield of the solid residue, where a higher values of E_a (MG) (Fig. 6a) – b)) for the decomposition of the lignin structure, lead to a lower yield of the char (Fig. 5c) – d)).

e) Stage 4 – this stage is characterized with decreasing trend of E_a value for both samples, but which retains high values especially for MG (Fig. 6a) – b)). In this context, it is obvious that for MG, the thermal cracking is much slower than for the AD, resulting in aggravated char formation (in the temperature range of $\Delta T = 425\ ^{o}C - 475\ ^{o}C$).

f) Stage 5 - the subsequent increase in activation energy for both samples at the very end of the pyrolysis process, indicates the occurrence of secondary charring reaction (Anca-Couce et al., 2014), where besides H_2O which was produced together with char, additional quantities of CO_2 and H_2 gases are probably generated. This process is much slower in the MG than in the AD sample (for $T > 475\ ^{o}C$).

However, in the view of standard error bars, the confidence range of E_a values at a higher conversion of $x = 0.92 - 0.99$ was relatively higher (Fig. 6a) – b)). This means that the non-determinacy of estimated E_a in this higher conversion range is high. Namely, the non-determinacy and accuracy can be attributed to data noise at the high conversion levels.

Since they were estimated in 95% confidence limit, E_a values were credible in the observed conversion range. The deviation of E_a to its mean value, $E_{a(m)}$, can be calculated using an following relation: $\varepsilon_m(\%) = 100 \cdot \frac{|E_a - E_{a(m)}|}{E_{a(m)}}$. Fig. 6e) – f) shows that E_a varies significantly with conversion for MG sample, considering FR and VY methods, especially for $x > 0.86$ (this variation even exceeds 100% (it tends to '*infinity*')). This strongly suggests on the distinct kinetic complexity of the pyrolysis process in the considered conversion range, for the MG sample. Consequently, the kinetically complex process indicates that monitored pyrolysis may occurs *in the mechanism changes and multi-step reactions rather than a single-step reaction*. The *mechanism changes* is truly reflected *via* affirmed *variation* of E_a against conversion (Table S3, Supplementary Material).

3.5. Model-free results associated with the maximum pyrolysis rate

Among model-free methods, Kissinger's method (Supplementary Material, sub-section I.2.) represents non- isoconversional kinetic method. This method relies on the unique solution rather than finding activation energies at each successive conversion (x) point. It considers the temperature value at which the rate of the reaction (as the function of heating rate) is maximum, so the kinetic parameters can be estimated. This methodology allows to identify the E_a value from DTG peaks temperature at different heating rates. A second kinetic parameter, the pre-exponential factor (A), is usually calculated under assumption that the reaction proceeds through n-th order reaction model ($n \sim 1$). The E_a is grouped along with pre-exponential factors and resultant equation exhibits a linear behavior (Eq. (S16) – the intercept and the slope of current linear equation were used to estimate the kinetic parameters). Fig. 7 shows Kissinger's plots for MG and AD pyrolysis processes, related to the one prominent peak on DTG curves situated within main devolatilization stage ("III") (Fig. 5b)).

The calculated pair of kinetic parameters [E_a; A] from Kissinger's method (Fig. 7) do not always approximate the arithmetic average of E_a values ($E_{a(m)}$) (Fig. 6) since that E_a significantly varied with x. The arithmetic average values of activation energy (considering FR isoconversional method) related only for stage 2 where the '*maximum*' peak was placed, amount 329.63 kJ/mol for MG, and 283.79 kJ/mol for AD, respectively. The differences between the values of E_a obtained by the Kissinger method and arithmetic average E_a values are as follows: $\Delta\{E_a(\text{MG})\} = 35.46$ kJ/mol and $\Delta\{E_a(\text{AD})\} = 26.96$ kJ/mol. Since that the magnitude difference is not large, this approach seems that quite well describes deviation of conversion degree x_p with respect to sample temperature at T_p (Table 4). In addition, all regresion lines have high r-values (and relatively high R^2-values), where intercepts and slopes are located within confidence limits (Table S4, Supplementary Material). The applied regression analysis to model-free "peak" kinetics (Eq. (S16)) gives quite satisfactory fitting results of experimental data, so that, generally, an apparent *single-step* reaction model could explain the cellulose decomposition during MG and AD pyrolyses.

3.6. The kinetic compensation effect (KCE) from isoconversional methods

The *logA vs.* E_a relationship estimated for MG and AD pyrolysis processes throughout observed stages are shown in the Fig. 8a) – b). The presented relationships were obtained from FR isoconversional method.

As can be seen from Fig. 8a) – b), the both samples show a very good linear relationships between *logA* and E_a for the first three reaction branches (stages 1 *, 1, 2, and 3) ($R^2 > 0.99850$), while for the remaining two branches (stages 4 and 5), the poorer linearity was obtained. Therefore, the strong linear correlation is valid for branches 1 – 3, while for branches 4 and 5, the weak linear correlation exists. Based on the directions of changes in the slope of linear relationships between *logA* and E_a, as the temperature increases, both kinetic parameters increase first and then decrease, indicating that there is a kinetic compensation effect (KCE) between them (Supplementary Material, section II.). The linear compensation relationship between *logA* and E_a does not necessarily indicate the existence of KCE due to the influence of systematic error propagation and mass transfer caused by sample

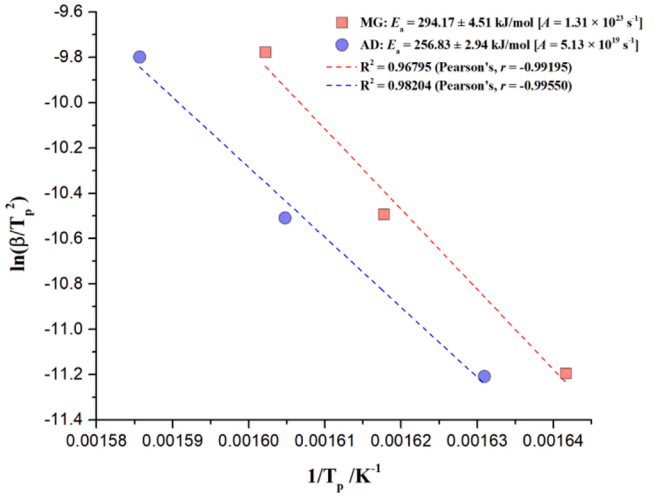

Fig. 7. Variation of kinetic parameters (E_a, A) *vs.* temperature for MG and AD pyrolysis demonstrated by Kissinger method (linear plots were obtained on the basis of 95% lower and 95% upper confidence limits (LCL and UCL) of experimental data).

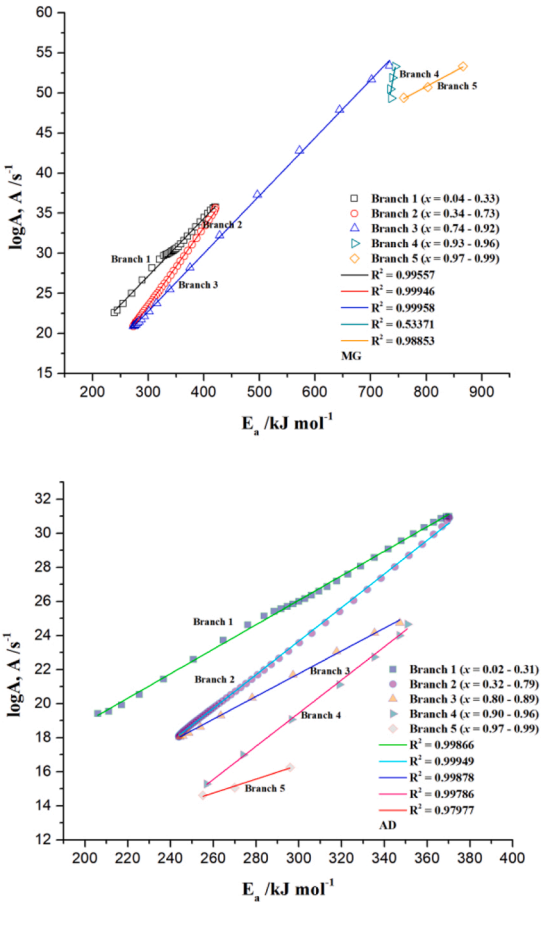

Fig. 8. The kinetic compensation effect (KCE) established from isoconversional (FR) method for MG a) and b) AD pyrolyses, including identified reaction branches (Branch 1: stages 1 * + 1, Branch 2: stage 2, Branch 3: stage 3, Branch 4: stage 4, and Branch 5: stage 5 (considered stages from Fig. 6a) –b))).

temperature deviation during the current experiment (Zhang et al., 2020). During our experiments, some problems such as experimental conditions, experimental errors, and equipment quality were avoided as much as possible. Namely, feedstock samples are placed on the top of the thermocouple (STA449F5) to ensure the accuracy of the mass loss and recorded temperatures. Further, the mass of the sample is controlled within 8.0 mg during each measurement, and the smaller sample quality ensures minimization of the mass transfer effect throughout the reaction. Therefore, both samples have different extents of KCE in different pyrolysis processes, and the extent of compensation effect varies depending on the composition of each sample. In the pyrolysis of complex multicomponent organic matter such as MG and AD energy crops, the thermal decomposition reaction becomes a more difficult as process progresses, showing higher E_a and *logA* values (Fig. 8). As shown in Fig. 8a) – b), *logA* against E_a for MG and AD pyrolysis processes ($x \sim$ 2–99% conversion) is roughly divided into five kinetic branches, where branch 1 encompasses two pyrolysis stages determined in Fig. 6a) – d) [*st*: 1 * and 1]. As stated above, for three kinetic branches there is a strong KCE, and they refer to extractives + hemicelluloses decomposition, then cellulose decomposition, and finally lignin decomposition, and in that case, at least three different mechanism types may exist. However, observing the entire pyrolysis of MG and AD samples, this complex heterogeneous process *can not* be described by *the single-step reaction*. As mentioned in "Introduction" section of this work, many researchers (Table 1) assigned that pyrolysis stages can be attributed to decomposition of C3 and C4 energy crops components (biomass "pseudo-components"), with the most common mechanism of independent parallel reactions. Such mechanisms did not delve deeper into the essence of the existence of more branched kinetic schemes and physical-geometric characteristics of the model for describing C3 – C4 energy crops pyrolysis. Based on the established KCE for considered reaction systems, the Eq. (S17) was used to find the values of T_{iso} (*isokinetic temperature*) and k_{iso} (*isokinetic rate constant*). The results of this test are shown in Table 5.

Based on presented results in Fig. 8a) – b) and Table 5, for the variable heating rate and also different and constant conversion degrees, the isoconversional kinetic compensation effect obviously exists. However, we can see that there is a scattering of isokinetic temperature values (T_{iso}) from the experimental ones, where all values of T_{iso} lie far beyond the experimental temperature range. Namely, isoconversional principle from *logA vs.* E_a relationship reveals that even slight increase in *logA* to E_a (but extreme cases appear in branches 4 and 5) can causes that the slope in Eq. (S17) is transformed into $1/RT_{iso} \rightarrow 0$, when $T_{iso} \rightarrow \infty$ (Table 5). This approach is limited by assumption that $logA = const.$, but in our investigated cases, it is not a true assertion. Namely, *logA* also shows strong variability with conversion degrees, which is directly reflected in the values of k_{iso} (Table 5). Consequently, in actual cases, there is no intersection point on the plots $logk_{iso}$ *vs.* $1/T_{iso}$ considering all kinetic branches, so, the apparent compensation effect still works, but there is no appearance of isokinetic relationship (IKR). Thus, in the application of the isoconversional methods to pyrolysis process of C3 and C4 energy crops, the isoconversional KCE values are characterized by strong variability of E_a corresponding to the weak variation of *logA*, which actually means that it is $logA = const.$ This was not fulfilled in our observed cases, so that the classical Arrhenius law (in the typical Arrhenius plot, the value of isokinetic rate constant (k_{iso}) increases [$k_{iso}\uparrow$], with an increase of temperature T_{iso} [$T_{iso}\uparrow$]) for a simple one-step reactions is not valid. For that matter, the determined isokinetic temperatures are not the compensating quantities in the isoconversional approach, and therefore have no physical meaning. Therefore, we can assume that thermodynamic principles in the form of the enthalpy-entropy compensation (EEC) related to the temperature compensation are the source of the kinetic compensation effect (KCE), where the compensation temperature can be treated as the isokinetic temperature (see later results).

Furthermore, the '*existence*' of isokinetic relationship (IKR) was checked by application of Exner criterion (Supplementary Material, subsection II.1.). The corresponding Exner plots for MG and AD pyrolysis processes are shown in Fig. 9a) – b).

It can be observed from Fig. 9a) – b) that constructed plots exhibit linear correlations with a slightly different quality of fit, which is reflected in the values of R^2 and *r*, respectively. But despite the slightly different quality of fit, for considered pairs of temperatures (Eq. (S20)), the following values of isokinetic temperature (T_{iso}) were obtained: T_{iso} = 563.29 K, 602.14 K and 609.64 K for MG; T_{iso} = 559.97 K, 600.96 K and 609.97 K for AD. It can be seen that obtained isokinetic temperature values do not lie in the experimental range of interest (Fig. 9a) – b)). This result clearly confirms that *logk vs.* $1/T$ plot does not shows the temperature at which all lines concur to a single point (see above discussion), proving the *absence* of IKR in pyrolysis processes of MG and AD.

3.7. Results of numerical optimization of pyrolysis processes

Based on the isoconversional (model-free) analysis, the numerical optimization of pyrolysis processes was performed. Numerical optimization method is model-free method using nonlinear least square

Table 5
The values of KCE coefficients (*a*, *b*) and parameters (k_{iso}, T_{iso}) along with linear regression analysis results (RSS – residual sum of squares, R^2 - Adj. R-Square, and the Pearson's coefficient - *r*) for corresponding kinetic branches of MG and AD pyrolysis processes.

MG					
Branch	**1**	**2**	**3**	**4**	**5**
Conversion	$x = 0.04 - 0.33$	$x = 0.34 - 0.73$	$x = 0.74 - 0.92$	$x = 0.93 - 0.96$	$x = 0.97 - 0.99$
a /s^{-1}	5.62 ± 0.31	-5.89 ± 0.12	1.10 ± 0.15	-227.48 ± 132.38	20.95 ± 2.30
b /mol·(kJ)$^{-1}$	0.07186 ± 0.00009	0.09785 ± 0.00004	0.07219 ± 0.00003	0.37729 ± 0.17918	0.03733 ± 0.00283
k_{iso} /s^{-1}	276.6768	0.0028	3.0088	1.6142×10^{-99}	0.1256×10^{10}
T_{iso} /°C	1400.65	956.07	1392.99	45.65	2948.90
RSS	1.672	0.478	0.942	2.756	0.046
R^2	0.99557	0.99946	0.99958	0.53371	0.98853
Pearson's *r*	0.99786	0.99974	0.99980	0.83015	0.99713
AD					
Branch	**1**	**2**	**3**	**4**	**5**
Conversion	$x = 0.02 - 0.31$	$x = 0.32 - 0.79$	$x = 0.80 - 0.89$	$x = 0.90 - 0.96$	$x = 0.97 - 0.99$
a /s^{-1}	4.50 ± 0.15	-5.92 ± 0.09	1.71 ± 0.22	-9.76 ± 0.58	4.13 ± 1.13
b /mol·(kJ)$^{-1}$	0.07190 ± 0.00005	0.09862 ± 0.00003	0.06682 ± 0.00008	0.09736 ± 0.00184	0.04086 ± 0.00413
k_{iso} /s^{-1}	89.8121	0.0027	5.5467	5.7596×10^{-5}	62.2383
T_{iso} /°C	1399.71	946.47	1526.90	962.25	2670.54
RSS	0.465	0.372	0.066	0.136	0.015
R^2	0.99866	0.99949	0.99878	0.99786	0.97977
Pearson's *r*	0.99935	0.99975	0.99946	0.99911	0.99493

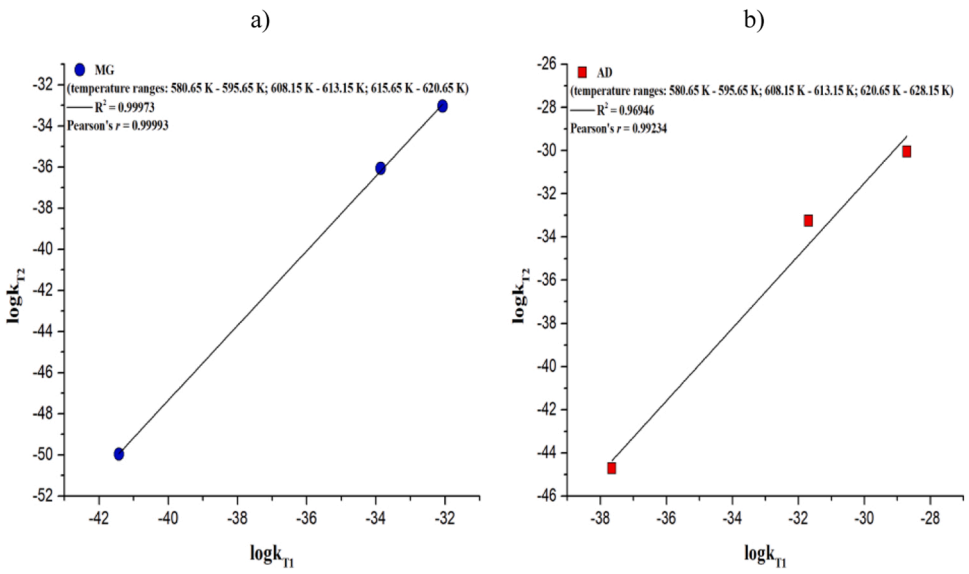

Fig. 9. Plot of $logk_{T2}$ *vs.* $logk_{T1}$ for a) MG and b) AD pyrolysis, where the strong KCE exists (Branch 2) with indicated experimental temperature ranges, which were considered in the Exner analysis.

optimization, minimizing the sum of squared residue (Eqs. (S14) – (S15), Supplementary Material). Numerical method searches optimal functions E_a *vs.* conversion and *logA vs.* conversion (Fig. 6a) – d)), in order to get best fit for experimental TG-curves. Optimization technique is a powerful tool to obtain the desired design parameters and best set of operating conditions. This would guide the experimental work and reduce the risk and cost of design and operating, if the pyrolysis process of considered energy crops would be adapted for conditions taking place in pyrolytic reactors, at the industrial (large-scale) level. The optimization refers to finding kinetic parameters values as decision variables, which correspond to, and provide maximum or minimum, of one or more desired objectives.

Fig. 10 a) – d) shows numerical optimization results toward experimental TG-curves for pyrolysis of MG and AD samples, when using the data from FR and VY model-free isoconversional methods. It can be seen from Fig. 10 a) – d) that for both samples, there is an excellent agreement between experimental and simulated data for investigated pyrolysis processes ($R^2 = 0.99997$). These results confirm that kinetic parameters obtained from model-free analysis are true (real) kinetic parameters, reflecting an reasonable physicochemical changes that occur in reaction systems. This approach does not presuppose knowledge of the exact reaction mechanism, but only detects the degree of its complexity (*i.e.*, it cannot extract the number and manner of individual reaction steps) (through parallel, consecutive and similar reaction schemes). The revealing of entire reaction mechanism allows model-based analysis (see later results).

3.8. Thermodynamic analysis and the enthalpy-entropy compensation (EEC) for MG and AD pyrolysis

Bearing all the above considerations in mind, we are ready to address another issue: given a general thermodynamic model of the process, what are the sources of occurrence of EEC during pyrolysis of tested energy crops? Namely, certain authors (Curtis and Conner, 1982) believe that the transition-state theory of heterogeneous reaction kinetics may explain appearance of the compensation effect. According to mentioned theory, the distance between atoms in a activated complex state is longer than the normal chemical bond, which results in the bond of activated complex being weaker than normal bond, but translation, rotation and limited vibration can still be performed like in a normal molecules. Pyrolysis process of MG and AD represents an typical heterogeneous process, so energy crops pyrolysis compensatory dynamics can be explained from the aspect of the transition-state theory. Before presenting the results of this analysis, we must note that the aforementioned existence of the kinetic compensation effect (KCE) (but not isokinetic relationship (IKR)) can arises from the change of reactant properties in MG and AD pyrolysis behavior and kinetics. Given that all interfering factors (experimental conditions, experimental errors and equipment errors) were minimized as much as possible, as the process progresses for MG and AD, the organic matter is continuously cracked and new active substances will also be generated and participate in a further reactions. The new active sites are generated and active sites continue to appear and consume, resulting in the KCE. Above results clearly confirm high reliability of calculated kinetic parameters, so they can help much better in a deeper understanding of the mechanism of energy crops pyrolysis, and deepen the thermodynamic study of the same process.

Using Eqs. (S25) – (S27) (Supplementary Material), thermodynamic parameters of activation, such as changes in enthalpy of activation (ΔH^o), changes in Gibb's free energy of activation (ΔG^o) and changes in entropy of activation (ΔS^o) are calculated for a given experimental temperatures (T_p has been replaced by T) and conversion degrees at different heating rates, in order to construct the Eyring plots (Eq. (S29)) for MG and AD pyrolysis, respectively. Plots were formed using FR model-free data according to the procedure described in sub-section V.1. (Supplementary Material). Fig. S3 a) – b) shows Eyring plots at different heating rates, for non-isothermal pyrolysis of MG and AD samples. The model-free approach through the FR method provides sufficient separation of Eyring plots at considered heating rates and in both cases, the process curves receive an typical W-shapes. W-shaped Eyring plots are complex and innerly divided according to previously established kinetic branches (1−5) (Fig. 8a) – b)). It is interesting to note that narrow part which is the closest to the linear Eyring plot behavior represents the reaction segment attached to the branch 2 (Fig. S3 a) – b)).

The actual reaction segment corresponds to the cellulose degradation in a given samples. Such highly non-linear Eyring plots at different heating rates suggests very complex heterogeneous process (model with single-step reaction mechanisms fails), where apparent linearity can concealed the change in the rate-limiting step during thermo-chemical conversion. This highlights the importance of confirming whether the same rate-limiting step holds throughout the experimental pyrolysis temperature range, before any interpretation of non-linear or apparently

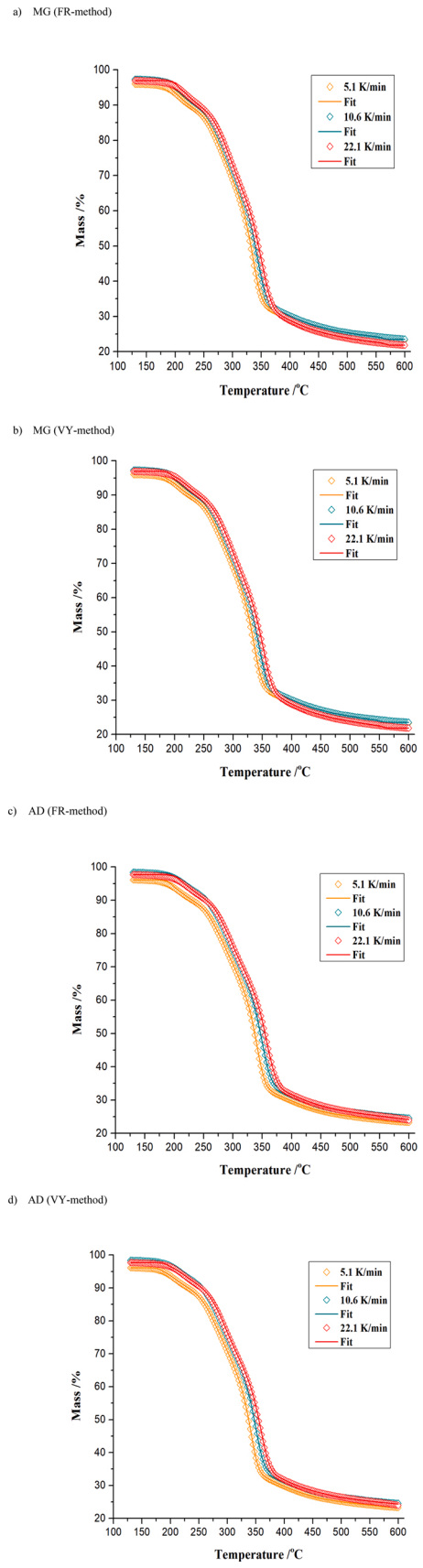

Fig. 10. Numerical optimization of experimental TG-curves at various heating rates (β = 5.1, 10.6 and 22.1 K/min), based on model-free results (FR and VY methods), for MG a) – b) and AD c) – d) pyrolysis processes (R^2 = 0.99997).

linear Eyring plots in the case of macroscopic rate constants. A more detailed analysis of this issue will be presented in sub-section related to model-based results (see later). In further considerations, thermodynamic tests will be based on the characteristic reaction temperature, T_p.

Table 6 lists the values of ΔH^o, ΔG^o and ΔS^o (Eqs. (S25) – (S27) (Supplementary Material)) at various heating rates for MG and AD pyrolysis processes, using Kissinger's kinetic results.

It can be seen from Table 6 that for both samples, the values of activation enthalpy (ΔH^o) follow the values of determined activation energies (see above), and the heat energy consumed by AD to dissociate bonds was generally less than that of MG (considering ΔH^o value at individual heating rate, AD requires smaller amount of external energy for its transformation than MG). The differences between activation energy and ΔH^o were 5.13 kJ/mol for MG and 5.17 kJ/mol for AD, respectively. Because of this small difference, it is relatively easy to overcome potential energy barrier, which was necessary to form an activated complexes. When the pyrolysis system is at the state of thermodynamic equilibrium, the difference of Gibb's free energy of activation (ΔG^o) is zero. Based on the obtained ΔG^o values (Table 6), both samples are very suitable as biomass sources used for bioenergy production (ΔG^o values are consistent and positive, where all pyrolysis processes are endergonic). However, $\Delta G^o(MG) > \Delta G^o(AD)$ (Table 6), and because of this fact, the pyrolysis favorability for MG is lower than in the case of AD. This is in excellent agreement with the results obtained from the above kinetic analysis, especially considering the pyrolysis efficiency of cellulosic material in these samples (Fig. S1, Supplementary Material). Thermodynamic analysis revealed positive values for both, ΔH^o and ΔG^o, which indicate that separated devolatilization events for pyrolysis of MG and AD are connected with introduction of heat and non-spontaneous reactions. Concerning the activation entropy change (ΔS^o), which can be interpreted as the degree of disorder in a pyrolysis reaction, the positive values (Table 6) reflect an increase in the disorder of reaction. The high values of ΔS^o for AD suggest that the reaction system has high reactivity and could generate activated complex much faster (Xu and Chen, 2013). So, AD feedstock manifests "*fast*" reactions for the devolatilization event compared to the MG feedstock. These results are in good agreement with those related to reactivity indexes (see above), considering an adaptation and influence of the heating rate, on the effective implementation of pyrolysis processes to produce precursors for bio-fuels and value-added chemicals.

Furthermore, we checked the existence of the EEC phenomenon using the Eq. (S30) (Supplementary Material), where constructed ΔH^o - ΔS^o plots for MG and AD pyrolyses are shown in Fig. 11 a) – b).

The obtained results show very strong ΔH^o — ΔS^o compensation relationships, reflected in very high regression coefficients (R^2 and r). Any pair of ΔH^o — ΔS^o values lying within the confidence ellipse gives an acceptable fit to the experimental data. By visual summary, both confidence ellipses are very elongated (tends to infinity) drastically reducing standard errors. This corresponds to "high-leverage" and "small-residual" case in the analysis of the data by statistical methods through elliptical geometry (Friendly et al., 2013). The derived T_{isoeq}

Table 6
Values of ΔH^o, ΔG^o and ΔS^o at heating rates of 5.1, 10.6 and 22.1 K/min, for MG and AD pyrolysis.

MG			
β /K/min	ΔH^o /kJ·mol^{-1}	ΔG^o /kJ·mol^{-1}	ΔS^o /J·mol^{-1}·K^{-1}
5.1	289.10	235.96	87.24
10.6	289.03	235.18	87.12
22.1	288.98	234.65	87.04
Average	289.04	235.26	87.13
AD			
β /K/min	ΔH^o /kJ·mol^{-1}	ΔG^o /kJ·mol^{-1}	ΔS^o /J·mol^{-1}·K^{-1}
5.1	251.73	179.31	118.11
10.6	251.65	178.13	117.97
22.1	251.59	177.25	117.87
Average	251.66	178.23	117.98

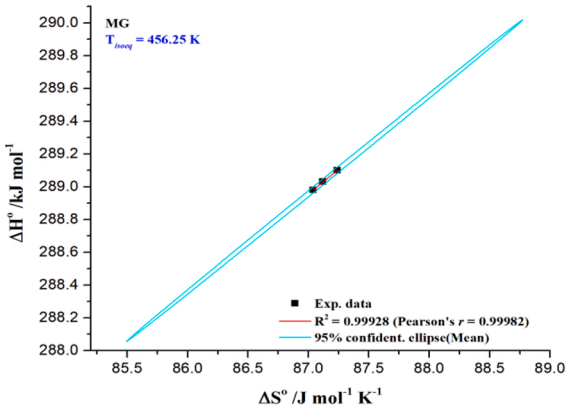

a)

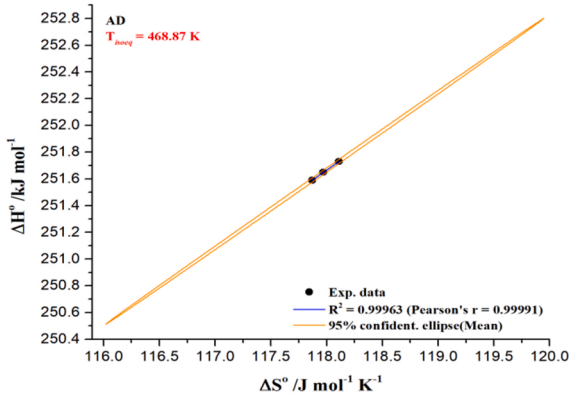

b)

Fig. 11. Plots of activation enthalpy change (ΔH^o) *vs.* activation entropy change (ΔS^o) for a) MG and b) AD pyrolysis, together with fitting line: $\Delta H^o = const. + \beta^* \cdot \Delta S^o$ (Eq. (S30)) (R^2 and r values are also shown) within the region of parameters space described by the confidence ellipse. The calculated values of isoequilibrium temperatures (T_{isoeq}) are highlighted.

values (Fig. 11 a) – b)) represents physically meaningful T_{iso}, $T_{isoeq} = T_{iso}$ (T_{iso} belongs to experimental temperature range of both, MG and AD pyrolysis processes), where using the Eq. (S31), the experimental harmonic mean temperature (T_{hm}) was estimated. In both cases, the value of $T_{hm} = 607.85$ K was obtained. Since that $T_{hm} >> 1$ and R^2 is close to the unity (Fig. 11 a) – b)), the ratio between the lengths of the principal axes of the confidence ellipse (which shows eigenvalues of the variance-covariance matrix (not shown)) expressed as: $Ratio = \sqrt{\frac{R^2(T_{hm}^2+1)}{1-R^2}}$ is quite large (22,645.11 for MG, and 31,594.81 for AD, respectively), for considered pairs of thermodynamic parameters. The orientation of confidence ellipses, and theirs aspect ratio, depend only on temperatures at which pyrolysis experiments were performed. This means that the fitted thermodynamic parameters are completely dependent on each other. The T_{hm} value which is unique for both systems, is placed inside the pyrolysis zone where the cellulose decomposition occurs. In addition, since that $T_{iso} \neq T_{hm}$ (Fig. 11 a) – b)), according to Krug et al. (1976), the compensation theory ('*chemical compensation*') exists in pyrolysis process of MG and AD feedstocks. So, for our systems, there is linear correlation between *logA* and E_a and also between enthalpies and entropies of activation, clearly indicating the presence of *true compensation effect*. Thermodynamic compensation always occurs when kinetic compensation also takes place, as long as the equilibrium and kinetic parameters are related through the transition state theory. If kinetic compensation takes place, it means that the kinetic constant k does not depend on environmental (external) variable for isokinetic temperature and, thus, from Eq. (3):

$$K_{eq}^{\neq} = \frac{h}{k_B \cdot T_p} \cdot k, \tag{3}$$

(h - Plank constant (6.626×10^{-34} J·s) and k_B - Boltzmann constant (1.381×10^{-23} J/K)) it may be concluded that $K_{eq}^{\neq}$ does not depend on the same environmental/external variable at the same temperature, which means thermodynamic compensation at the same isokinetic temperature. Then, isokinetic and isoequilibrium temperatures must coincide. Relationship between equilibrium constant and compensatory expressed by the Eq. (S30) can be represented as: $\Delta G^o = -RT_p \ln K_{eq}^{\neq} = \Delta G^o(T_{iso}) + T_{iso} \cdot \Delta S^o - T_p \cdot \Delta S^o$, showing, when the temperature is the specific T_{iso} value, $K_{eq}^{\neq}$ and ΔG^o are the same, regardless of the external variable. Table 7 lists the values of $\Delta G^o(T_{iso})$, $K_{eq}^{\neq}$ and k (specific rate constant) in relation to the heating rate change, for MG and AD pyrolysis.

At every heating rate considered, $K_{eq}^{\neq}$ for AD is almost twice as high as in MG, so very large values of $K_{eq}^{\neq}$ indicate that the concentration of the products (their accumulation) is much greater in AD than in MG pyrolysis process ($\Delta G^o(T_{iso})$[AD] < $\Delta G^o(T_{iso})$[MG]) (Table 7). On the other hand, specific rate contants (k) for both samples have the same order of magnitude ($\times 10^{14}$), but k values for AD are higher, making the process faster. In general, at established T_{iso} values (Fig. 11 a) – b)), the rate constant was given by some simple principles throughout reaction series. Considering "*solid*" values of k for investigated systems (Table 7), the specific rate constant does not depend on environmental/external variable (*i.e.*, the heating rate, β) (infinitesimal change of k with β's) for T_{iso}. Based on presented results, there is certain parallelism in the variations of Gibb's free energy of activation and entropy of activation in a reaction series leading to iso-equilibrium relationship, showing that effects of molecular *interactions* can have the considerable role in this phenomenon. This will be analyzed later.

In order to confirm an existence of real compensation in pyrolytic processes of interest, we reached for a more rigorous statistical analysis through Krug's tests (Krug et al., 1976), to obtain extra-thermodynamic properties of systems (Supplementary Material, section VI.). This approach enables a difference to be discerned between statistical and the real compensation. Table 8 shows the results of Krug test for MG and AD pyrolysis processes.

The obtained harmonic mean temperature is the outside of the isokinetic temperature range for both feedstocks, and it was different from T_{iso} (Table 8). Also, as can be seen from Table 8, the isokinetic temperatures are lower than T_{hm}, which indicates that the processes are controlled by *entropy*. Extra-thermodynamic findings addresses that observed compensation *is not caused* by the propagation of experimental errors. Therefore, the pyrolysis processes are strongly influenced by *levels* of *disorder* during feedstocks conversions. Entropy guidance obviously describes possible numbers of different arrangements of particle positions and energies, in which the disorder of the process - system is generally stated; but still, an extent of this disorder differs between MG and AD samples. One of the key reasons for this behavior is the role of the present catalysts in feedstocks, since entropy plays a pivotal role

Table 7
Values of $\Delta G^o(T_{iso})$, $K_{eq}^{\neq}$ and k (specific rate constant) at various heating rates for MG and AD pyrolysis.

Energy crop	β /K/min	ΔG^o (T_{iso}) /kJ mol^{-1}	$K_{eq}^{\neq}$	k /s^{-1}
MG	5.1	236.87	13.291	1.69×10^{14}
	10.6		14.856	1.91×10^{14}
	22.1		15.968	2.08×10^{14}
	Average		14.705	1.89×10^{14}
AD	β /K/min	$\Delta G^o(T_{iso})$ /kJ mol^{-1}		
	5.1	182.92	27.302	3.49×10^{14}
	10.6		32.385	4.21×10^{14}
	22.1		36.671	4.82×10^{14}
	Average		32.119	4.17×10^{14}

Table 8
Results of Krug's tests for MG and AD pyrolysis.

MG	
Isokinetic temperature, T_{iso} /K	456.25
Harmonic mean temperature, T_{hm} /K	607.85
Isokinetic temperature variance, $Var(T_{iso})$	0.02280
Isokinetic temperature interval /K	[456.27;456.22]
AD	
Isokinetic temperature, T_{iso} /K	468.87
Harmonic mean temperature, T_{hm} /K	607.85
Isokinetic temperature variance, $Var(T_{iso})$	0.01590
Isokinetic temperature interval /K	[468.89;468.85]

in a catalyst promoted reactions. This could also be the way to understanding an enthalpy-entropy relationship that defines the reaction pathways of the molecular species.

3.8.1. SET model results

Since that the isoequilibrium relationship employs the model of energy distribution, it provides a joint of variation of E_a and ΔS^o when either, the height of potential barrier or number of oscillators is varied (Koudriavtsev et al., 2001). In other words, the corresponding parametric sensitivities of ΔH^o and ΔS^o are non-zero in the model of energy distribution. Variations of activation energy and activation entropy (the standard internal energy and standard entropy of activation) result from variations of the potential barrier height and from variations of the number of oscillators (at a constant potential barrier height). Namely, the variation of potential barrier height at constant number of oscillators results in positive isokinetic temperatures (T_{iso} ($\equiv T_{isoeq}$)) (Fig. 11). The physical significance of the isokinetic temperature becomes more clearer, when we consider the existence of the high potential barriers. In addition, the T_{iso} actually reflects the energy *per* oscillator, which is required to pass over the average potential barrier, in a given reaction series. In this study, we applied SET (selective energy transfer) model (Supplementary Material, sub-section VI.1.) which considers an existence of vibration frequency of possible catalyst in reaction system and vibration frequency of reacting molecule, which transforms an reactant onto the 'activated state'. In the formation of model, data from FTIR analysis were used. The applied model allows determining how specific resonance is developing between a "specific vibration" within observed catalyst system and corresponding vibration within a reacting system, *transferring energy* which serves to drive the reactant molecules to *desired reaction products*.

Based on the Eq. (S36) (for known values of T_{iso} (Table 8)) (Supplementary Material), the corresponding vibration modes (ν) of reactants present in MG and AD energy crops are determined, and the following values were obtained: $\nu = 634.56\ cm^{-1}$ for MG, and $\nu = 652.11\ cm^{-1}$ for AD, respectively. The obtained frequencies are in excellent agreement with identified vibration modes from FTIR measurements at wavenumbers of 634 cm^{-1} and 652 cm^{-1}, for MG and AD, respectively (Fig. 4). These bands belong to the ring and skeletal lignin deformations and ring deformation of 1,8-cineole in MG and AD feedstocks, respectively. The recorded resonances define two different reactants, one represents the lignin biomass structure (MG) and the other arises from bicyclic monoterpenes - 1,8-cineole (eucalyptol) abundant in C3 grass (Lathière et al., 2006; Lupoi et al., 2015). The identification of possible catalyst in considered feedstocks (as energy donating system), FTIR spectra of raw MG and AD samples (Fig. 4) were used. On the presented FTIR spectra (MG and AD), it was noticed weaker vibration at wavenumber of about 538 cm^{-1}, in the far-IR radiation (Fig. 4). This vibration can be attributed to the presence of KCl (Jensen and Dam-Johansen, 1998; Manimekalai and Jayaprakash, 2021; Kalembkiewicz et al., 2018) in tested samples. Therefore, the actual vibration was flagged as catalyst signal at $\omega = 538\ cm^{-1}$. Since that $\nu \neq \omega$, the energy dissipation of an excited molecule is not a zero, so, there is some route for energy loss.

Depending on the structure of the catalyst, it will be more or less easy for catalyst entities (atoms or ions) to reach a suitable position for attacking the excited reactant molecule. If it is a difficult, an extent of distortion of catalyst-reactant unit is significant, and can lead to large activation energy values. If catalyst entity was well placed, then distortion will be small, leading to lower values of activation energy. Therefore, the E_a value of reaction will depend on the "activity" of the catalyst.

Potassium can be found in organic and inorganic form in the biomass. Inorganic potassium in a form of K^+ can creates crystallized salts as the particle starts to dry. This process, when the potassium is present in a lesser amount, can be considered through the reaction: *Inorganic*K (K^+) → ψ_1KCl, where the constant ψ_1 is calculated based on the Cl content, assuming that Cl in the biomass is mainly bonded to K (Knudsen et al., 2004). On the other hand, organic potassium is transformed into carboxyl groups, releasing atomic K into a gas phase (dedeCarvalho, 2017). The transformation and decomposition of organic potassium can be considered through reactions: *Organic*K (R–COOK) → Char-K, and *Organic*K (R–COOK) → R–COOH (*carboxyl groups*) + $CO_{2(g)}$ + $K_{(g)}$ (dedeCarvalho, 2017). The soluble K is released into gas-phase as $K_{(g)}$ and $KCl_{(g)}$ providing Cl which is available. The K releases start very early during devolatilization, as the organic structure of biomass begins to decompose at lower temperatures. It was founded that this release is associated with a decomposition of the alkaline carboxylate (~ 300 °C) and the phenol-associated potassium (~ 400 °C) (van Lith et al., 2008; Johansen et al., 2011). By using an Eq. (S35) (Supplementary Material, sub-section VI.1.), the SET T_{iso} values were calculated for both, MG and AG pyrolysis processes. Fig. 12 shows the calculated values of T_{iso} from the Eq. (S35) as a function of the frequency of the vibration of the reacting specie (ν), for assumed value of the "heat bath" frequency (for $\omega = 538\ cm^{-1}$).

For both samples, the calculated values of T_{iso} from SET (Fig. 12) are lower than experimentally obtained T_{iso} values (Table 8). This means that catalyst during thermal demineralization of biomass feedstocks (K-ions) has an 'inhibiting effect' on the thermal degradation of lignin structure (indicator parameters for this are *w* and FWHM in Table S2; *w* and FWHM values are higher for MG (delayed thermal decomposition time)). This time delay leads to a sudden increase in the activation energy (see Fig. 6a)) as well as activation enthalpies, reducing reactivity (↓ΔS^o). Nevertheless, the amount of potassium in both samples is comparable, but, the MG contains a greater amount of Ca (Table S1). This cannot be ignored, because in the lower temperature zone, Ca^{2+} ions can catalyze the cleavage of ether bonds between aromatic rings, and in short branches bonded to the aromatic structures. So, within the lignin

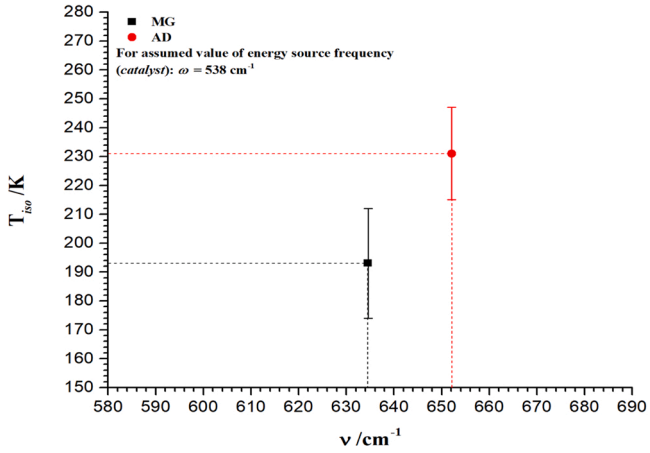

Fig. 12. Calculated values of T_{iso} for MG and AD (Eq. (S35)) as a function of the frequency of the vibration of the reacting specie, ν, for an assumed value of energy source frequency ($\omega = 538\ cm^{-1}$). The diver's positions of T_{iso} in relation to ν indicate differing in the reactivity.

structure, most likely, a synergic effect of Ca and K ions may occurs, enhanced decreases in T_c values (Table S2). Additionally, the role of the anionic counterion such as Cl^-, acting as a slight inhibitor of the catalytic effect of K and Ca ions, can not be excluded. Consequently, in the case of MG pyrolysis, the presence of KCl (K^+) has a weak effect on the initial thermal decomposition temperature of lignin (the negative coupling with high energy dissipation). Therefore, it can be concluded that presence of potassium in MG can *increases the reaction rates of hemicelluloses* and *cellulose* (the "negative" influence of the catalyst on lignin degradation is in favor of faster degradation of the remaining two biomass components) (Trendewicz et al., 2015). Therefore, it is possible that alkali metal catalyst has a weak influence on the lignin conjugate structure, since on the strong bond dissociation energy of C—O bond due to π-π conjugation. As a consequence, there is a fall in T_{iso} for MG, compared to T_{iso} for AD (the energy donated by the catalyst is not enough to attain the activated state of reacting molecule much faster) (Fig. 12). This has a strong influence on the distribution of pyrolysis products (gaseous (CH_4, CO_2, CO, H_2) and liquids) from lignin and other biomass components decomposition, during MG pyrolysis. Namely, it was reported that in the *T*-range of 300 °C – 500 °C, a small amount of K is released (Wang et al., 2017), but at higher temperatures (> 500 °C), the K releases can be increased due to the decomposition of organic K. The presence of K significantly contributes to the cellulose decomposition than for a lignin, because cellulose contains active functional groups, such as hemiacetal and exocyclic hydroxymethyl, and both groups attached on the rings (—CH_2OH) lead to Cl releasing (usually over ion-exchange reaction) (Strömberg and Zintl, 2008).

On the other hand, the influence of potassium on decomposition of bicyclic monoterpenes is significant and has a more positive effect than on the decomposition of the lignin structure. The alkali metal catalysts (such as K^+) in synergism with a transition metal catalyst (Fe) (Table S1) are effective for the ring-opening polymerization of cyclic ethers. The catalytic transformation of 1,8-cineole during AD pyrolysis is occurs faster at much lower experimental temperatures (< 250 °C; at approximately of 5% of x for $T \sim 215$ °C), associated with lower E_a and ΔH^o (E_a(AD) = 225.33 kJ/mol < E_a(MG) = 244.66 kJ/mol, $x \sim 0.05$, Fig. 6a) – b)). This transformation leads to the formation of *p*-cymene and dipentene as main products in hydrophobic phase (high value-added chemical compounds, also considered as fuels (such as dipentene)) (Leita et al., 2010; Martín et al., 2022) and H_2O, as well as CO, CO_2 and H_2 (in a higher yield), in the gaseous phase. As a consequence of these facts, the calculated value of T_{iso} for AD (Eq. (S35)) is higher (elevated) than that obtained for MG (Fig. 12) (there is much less energy dissipation than in the previously considered case). Observed deviations between calculated (SET) and experimentally obtained T_{iso} values (Table 8 and Fig. 12) for a present series of reactions can result from the unique entropy term in addition to pre-exponentrial factor, *A*, such as: *Entropy term* $= \ln A + \Delta S^o/R$. The inclusion of entropy term in the SET entropy contribution supports the active molecules interaction with the catalyst leading to desired reactions. However, this contribution is not equal in the case of MG *apropos* AD thermo-chemical conversion. Therefore, the phenomenological equation for the isokinetic effect would be in a form:

$$lnk = \ln A + \frac{\Delta H^o}{R}\left[\frac{1}{\left(T_{iso} - \frac{1}{\langle T\rangle}\right)}\right] \tag{4}$$

(where $\langle T\rangle$ represents the average value of the experimental temperature), where follows that when reaction temperature (T) is equal to T_{iso}, *lnk* is independent of activation energy value. Additionally, by introducing an enthalpy term for transition state as $S^{\#\#}$, the appropriate relation for experimental T_{iso} is as follows:

$$T_{iso}^{\exp} = \frac{1}{\left[\frac{S^{\#\#}}{\Delta H^o} + \frac{1}{T_{iso}^{calc}}\right]}, \tag{5}$$

where T_{iso}^{exp} and T_{iso}^{calc} are experimentally determined isokinetic temperature (Table 8) and calculated isokinetic temperature (Eq. (S35)) (Fig. 12), respectively. Combining known values of T_{iso}^{exp} and T_{iso}^{calc} and determined ΔH^o's, $S^{\neq\neq}$ value can be estimated for both, MG and AD samples. Using the Eq. (5), we can get the corresponding values of $S^{\neq\neq}$ for the catalytic action of alkaline/alkaline earth and/or transition metals towards reaction molecules, in pyrolyses of MG and AD feedstocks. Fig. 13 shows the values of $S^{\neq\neq}$ for MG and AD, during certain transformations of reaction molecules into valuable products, under the influence of metal catalysts.

As can be seen from Fig. 13, in both cases, we have negative values of $S^{\neq\neq}$ which suggest that entropy decreases on forming the transition state that indicates the associative mechanism, wherein two reaction species form a single activated complex. The large negative entropy (for MG) (Fig. 13) results in the reduced internal energy content of the transition state, leading to a significant increase in ΔG^o. Namely, dehydrations for mid-chain patterns of β-1,4-xylan with presence of metal catalyst is a less desirable reaction pathway that requires higher activation energies than those involved in the cleavage of the glycosidic bond. Likewise, the lowest energy barrier founded is the ring opening, resulting from the cleavage of the C_4-C_5 bond (~372.4 kJ/mol) (Goussougli et al., 2021). This activation energy is for about $E_a \sim 90.4$ kJ/mol higher than a lowest energy barrier involving in the concerted glycosidic bond fission (Goussougli et al., 2021). Therefore, forcing a ring opening *via* cleveage of the C_4-C_5 bond probably leads to unfavorable thermodynamic behavior in terms of larger negative value of $S^{\neq\neq}$ for the MG sample.

Considering AD sample, the obtained negative value of $S^{\neq\neq}$ is significantly lower than that for MG case, where dehydrogenation (and subsequently rearrangement of the double bonds) represents main reaction pathway which permits *p*-cymene (target chemical in the liquid phase) in a high yield (Aparicio et al., 2007), especially in the presence of transition metal (Fe) catalyst (a more ordered system). Probably, an initial reaction involves breakage of the weakest C—O bond in 1, 8-cineole followed by rapid dehydration step and then an dehydrogenation. Namely, a mixture of doubly unsaturated isomers can be

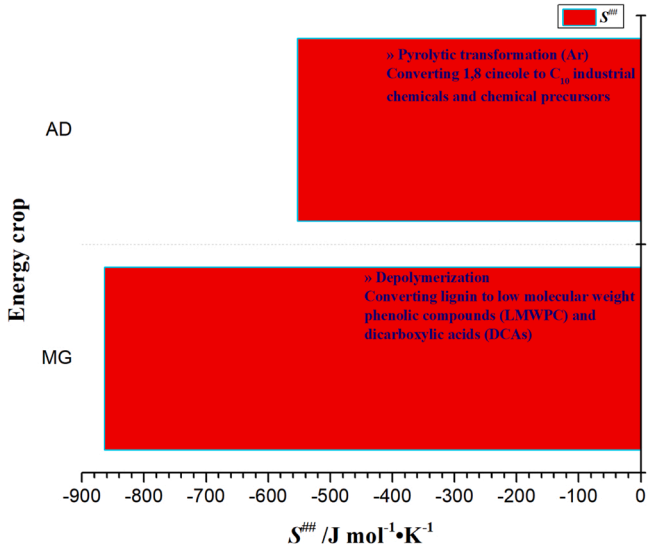

Fig. 13. Values of $S^{\#\#}$ (MG: $S^{\#\#} = -864.10$ J mol^{-1}·K^{-1}; AD: −552.70 J mol^{-1}·K^{-1}) for metal catalyst transformation of reacting molecules into value-added products: LMWPC and DCAs [*r.m. lignin*] in smaller yields, and C_{10} industrial chemicals and chemical precursors [*r.m.* 1,8-*cineole*] in higher yields (abbreviation *r.m.*: reacting molecule).

produced as a transitional state, so, dehydrogenation and rearrangement of double bonds occurs, and thus forming the last step. It should be emphasized as an important item from above discussion, that the 1, 8-cineole as targeted reactant, represents a highly value compound, that might be improved the economic viability of energy crops for their utilization in the bioenergy generation.

The degree of activation of the given reactant molecules by the catalyst among the MG and AD samples can also be estimated from the ν/ω ratio, where it should be noted, that ν/ω must me expressed by the small digits. Thus, the following ν/ω ratios were obtained: $\nu/\omega = 1.179 \approx 8{:}7$ for MG, and $\nu/\omega = 1.212 \approx 5{:}4$ for AD, respectively. Comparing these ratios, in the case of AD, the resonance energy transfer can occurs between four quanta of the catalyst system to five quanta of the reacting molecule, while in the case of MG, it is very difficult to activate the reacting molecule ($\approx$ 8:7). These results additionally confirm all the above-mentioned facts and observations.

3.9. Evaluating the most probable reaction mechanisms and verification of the obtained pyrolysis models

3.9.1. Model-based results

Since that estimated E_a value from isoconversional (model-free) methods varies with x and the conversion curve has peaks and shoulders, the investigated processes are of the complex nature, so the established E_a – conversion dependence is of a great assistance in finding an exact multi-step pyrolysis mechanism (parallel, consecutive, overlapping reactions or their combination), and the number of individual steps in multi-step process mechanism. This can be performed by using model-based method, which yield an individual kinetic triplet values for each of reaction steps (Supplementary Material, section III.). The extraordinary model-based analysis was developed by the NETZSCH Company, allowing reliable determination of the best kinetic model using multivariate nonlinear regression method, with advanced statistical analysis and prediction which are incorporated in the software. For preliminary determination of the possible presence of certain kinetic models that describe the process of interest, then the shape and slope of experimental points and isoconversional lines from Friedman's (FR) method at the start of the reaction ($x = 0.02 - 0.10$) (Supplementary Material, Fig. S2), can be used. Given the similarity of FR isoconversional plots for a given samples, it can be observed the presence of shoulders and peaks in Fig. S2 a) and d); therefore, it is important to analyze the experimental points at the start of the reaction ($x \sim 0.02 - 0.10$) and compare them with FR plots. If a) experimental points coincide with isoconversional ones, that indicates F1, F2, F*n*, R2 or R3 models (Supplementary Material, Table SIII.1), while if b) experimental points show lower slope than isoconversional ones, one is advised to consider diffusion models D1 - D4 (Table SIII.1), and if c) experimental points at the start show a steeper slope than isoconversional ones, this is a certain indication of the presence of autocatalytically activated reaction type or the Avrami-Erofeev reaction type (Moukhina, 2012). Since that in considered cases, experimental points at the start almost coincide with isoconverional ones, the reaction order or phase boundary-controlled reaction type is the most probable kinetic model. However, the number of peaks and shoulders on the FR plots indicates the number of decomposition steps. By comparing magnitudes at the peak slope (the one that is on right side of the peak) and that of isoconversional lines, the reaction type can be determined (Fig. S2). The start of the reaction in both cases is characterized by the peak with probably un-branched reaction with F*n* or R*n* reaction types (Table SIII.1), and then, an reaction profile is changes into a shoulder and peak appearances, where the peak slope is steeper than that of isoconversional lines. This indicates the presence of accelerated reaction, so that, autocatalytically reaction type or Avrami-Erofeev reaction type is to be expected to exists. In both observed cases (Fig. S2), there is one clear peak, and then surely one single-step reaction exists. For later stages of MG and AD pyrolyses, FR plots show one additional peak/shoulder so therefore, the mechanistic scheme may includes a single-step un-branched reaction path, and reaction path through at least one consecutive reaction. In a current procedure, we have attempted to make reaction models with lowest number of steps that gave an acceptable fit and that were consistent with pyrolysis mechanisms of the samples. The actual procedure was carried out in accordance with recommendations for analysis of multi-step kinetics (Vyazovkin et al., 2020).

In the context of this study, model-based approach for pyrolysis kinetics of MG and AD energy crops was carried out at various heating rates (5.1, 10.6 and 22.1 K/min), in the temperature range of $\Delta T = 130\ ^{o}C - 600\ ^{o}C$. This approach allows a simulation of pyrolysis behaviors of both MG and AD under different heating rates, as well as provides kinetic parameters and contribution of each of the thermal decomposition steps that were occurring, during the thermal breakdown of considered energy crops. Therefore, by applying statistical criteria with those calculated by isoconversional methods made, it is possible to perform multivariate nonlinear regression (MVNR) to find best fit of $f(x)$ functions (Table SIII.1) that reasonably describe the kinetic scheme of pyrolysis process. The best models were chosen taking into account of F-test and the correlation coefficient, based on the discrepancy between simulated curves and measured experimental data. The following pyrolysis reaction mechanisms were found for both samples, consisting two consecutive reaction steps and one single-step un-branched reaction, in the following form:

$$A \xrightarrow{1.1} B \xrightarrow{1.2} C \tag{6}$$

$$D \xrightarrow{2.1} E \xrightarrow{2.2} F \tag{7}$$

$$G \xrightarrow{3.1} H \tag{8}$$

where determined scheme that goes from the first to the last reaction, does not follow the sequence of changes along the entire TG-curve, considering from the left to the right side, strictly, but performs the fitting according to appropriate temperature intervals (segments). Ordinal numbers in corresponding reactions through above equations, represent previously defined reaction steps which take place during entire pyrolysis process. The proposed scheme (Eqs. (6) – (8)) is marked by *p*:, model scheme (reaction model code *p*:;) described with A*n*,F2,F*n*, A2,F*n* for the MG, and A*n*,F2,F*n*,D2,F*n* for the AD kinetics models, where *A*, *D* and *G* are the initial reactants, *B* and *E* are the intermediate products, while *C*, *F* and *H* are the final products. The two successive reactions $A \rightarrow B \rightarrow C$ in both cases (steps 1.1 and 1.2) have the following conversion functions: *n*-dimensional nucleation (Avrami-Erofeev equation), A*n*: $f(x) = n{\cdot}(1 - x)[-\ln(1 - x)]^{1-1/n}$, and second order chemical reaction, F2: $f(x) = (1 - x)^2$. For considered samples, another successive reactions $D \rightarrow E \rightarrow F$ differ in a reaction step 2.2, which is described by different kinetic models, namely: F*n*, $f(x) = (1 - x)^n$, *n*-th order chemical reaction ($n \neq 1$) (MG and AD samples, step 2.1), but two-dimensional growth of nuclei (Avrami equation), A2, $f(x) = 2{\cdot}(1 - x)[-\ln(1 - x)]^{1/2}$ (step 2.2 for MG), and two-dimensional diffusion (Valensi equation), D2, $f(x) = 1/[-\ln(1 - x)]$ (step 2.2 for AD). The single-step un-branched reaction in both cases is described by *n*-th order chemical reaction ($n \neq 1$), F*n*, $f(x) = (1 - x)^n$ (Supplementary Material, Table SIII.1). Obtained results of model-based method for pyrolysis of MG and AD samples (kinetic law equations, kinetic parameters, kinetic exponents (*i.e.*, the reaction dimension at the phase boundary) and contribution of each step to the overall process) are listed in Table 9.

A summary of the explanation of the reaction mechanisms for investigated pyrolysis processes can be presented in the following items:

a) In both cases (MG and AD pyrolysis), the successive reactions step presented by Eq. (6) occurs in two different temperature regions, which follow one to another sequentially, *viz* $A \xrightarrow{\Delta T = 250C^{o} - 325C^{o}} B$, and

Table 9
Kinetic parameters derived by MVNR approach, for pyrolysis processes of MG and AD samples, based on the most probable pyrolysis mechanism (*p*:, model scheme), in the temperature interval between 130 °C and 600 °C.

Energy crop – MG	
Step: A → B	
Reaction type: A*n*	
Equation: $d(a \rightarrow b)/dt = A_1 na[-\ln(a)]^{(n-1)/n}\exp(-E_1/RT)$	
Activation energy, E_1 /kJ mol^{-1}	378.445
logA_1, A_1 /s^{-1}	33.834
Dimension, *n*	0.307
Contribution	0.259
Step: B → C	
Reaction type: F2	
Equation: $d(b \rightarrow c)/dt = A_2 b^2\exp(-E_2/RT)$	
Activation energy, E_2 /kJ mol^{-1}	300.114
logA_2, A_2 /s^{-1}	24.029
Contribution	0.306
Step: D → E	
Reaction type: F*n*	
Equation: $d(d \rightarrow e)/dt = A_3 d^n\exp(-E_3/RT)$	
Activation energy, E_3 /kJ mol^{-1}	314.113
logA_3, A_3 /s^{-1}	33.665
Reaction order, *n*	14.160
Contribution	0.119
Step: E → F	
Reaction type: A2	
Equation: $d(e \rightarrow f)/dt = A_4 2e[-\ln(e)]^{1/2}\exp(-E_4/RT)$	
Activation energy, E_4 /kJ mol^{-1}	227.136
logA_4, A_4 /s^{-1}	16.937
Contribution	0.101
Step: G → H	
Reaction type: F*n*	
Equation: $d(g \rightarrow h)/dt = A_5 g^n\exp(-E_5/RT)$	
Activation energy, E_5 /kJ mol^{-1}	328.919
logA_5, A_5 /s^{-1}	27.461
Reaction order, *n*	20.000
Contribution	0.215
Energy crop - AD	
Step: A → B	
Reaction type: A*n*	
Equation: $d(a \rightarrow b)/dt = A_1 na[-\ln(a)]^{(n-1)/n}\exp(-E_1/RT)$	
Activation energy, E_1 /kJ mol^{-1}	339.440
logA_1, A_1 /s^{-1}	29.546
Dimension, *n*	0.317
Contribution	0.341
Step: B → C	
Reaction type: F2	
Equation: $d(b \rightarrow c)/dt = A_2 b^2\exp(-E_2/RT)$	
Activation energy, E_2 /kJ mol^{-1}	321.431
logA_2, A_2 /s^{-1}	25.437
Contribution	0.295
Step: D → E	
Reaction type: F*n*	
Equation: $d(d \rightarrow e)/dt = A_3 d^n\exp(-E_3/RT)$	
Activation energy, E_3 /kJ mol^{-1}	213.621
logA_3, A_3 /s^{-1}	21.607
Reaction order, *n*	3.126
Contribution	0.071
Step: E → F	
Reaction type: D2	
Equation: $d(e \rightarrow f)/dt = A_4(-1)/\log(e)\exp(-E_4/RT)$	
Activation energy, E_4 /kJ mol^{-1}	278.852
logA_4, A_4 /s^{-1}	21.063
Contribution	0.071
Step: G → H	
Reaction type: F*n*	
Equation: Equation: $d(g \rightarrow h)/dt = A_5 g^n\exp(-E_5/RT)$	
Activation energy, E_5 /kJ mol^{-1}	251.899
logA_5, A_5 /s^{-1}	18.979
Reaction order, *n*	8.808
Contribution	0.222

$B \xrightarrow{\Delta T=325C^o-375C^o} C$. The first step (step 1.1, Eq. (6)) corresponds to hemicelluloses (xylan) decomposition (xylan serves as a starting reaction material) where intermediate specie (*B*) which is formed from xylan pyrolysis represents an *xylose*, with the formation of other products such as H_2, H_2O, CO, CO_2, HCHO (formaldehyde), CH_3OH (methanol), C_2H_5OH (ethanol), and char (carbonaceous solid residue). This reaction scheme is generally, in very good agreement with global kinetic model for hemicelluloses pyrolysis proposed by Ranzi et al. (2008). The next step (step 1.2, Eq. (6)), can be attributed to cellulose pyrolysis indirectly implemented through the influence of xylose. Namely, with further increase in temperature, xylan decomposition resulting in a reduction of the cellulose crystallinity, which triggers its degradation. The steps 1.1 and 1.2 proceed through different kinetic models, as A*n* and F2 models, respectively. Model A*n* corresponds to random nucleation and subsequent growth which demonstrates that a new product randomly forms at reactive sites (nucleation points) in the reactant lattice, and the growth rate of nucleation may be expressed *via* the increasingly formed nuclei radius. For both samples, the growth dimension is less than unity with similar values (the quantity *n* (A*n* model for MG and AD) in Table 9) indicating an existence of growth in less than three dimensions with heterogeneous nucleation. In general, the random nucleation and subsequent growth mechanism is mathematically expressed, combining Avrami-Erofeev model, the acceleratory and the deceleratory rate constants. Considering the obtained dimension values ($n = 0.307$ (MG) and $n = 0.317$ (AD)), these cases correspond to diffusion-controlled reaction (when $n \sim 1/3$). The actual step takes place more easily in the case of AD pyrolysis than in the case of MG pyrolysis (E_1(AD) = 339.440 kJ/mol < E_2(MG) = 378.445 kJ/mol), where the contribution of this step is greater for AD thermo-chemical conversion (~ 34.1%) (Table 9). In both cases, pyrolysis mechanisms are transitioned from $A_{0.307/0.317}$ to F2, where reaction order remains unchanged. The decomposition of initial biomass feedstock starts from the nuclei sites as the growth center to initiate the thermal transormation for the step 1.1. The nuclei sites can be impure by the ash which acts as sites available for the nuclei formation, and the nucleus growth, caused by the nucleus collision (Li et al., 2020). The second order reaction mechanism (F2) is used to kinetically describes the step 1.2 (Eq. (6)). Within actual step, it is possible that the presence of H^+ ions (from present acids) at elevated temperatures may promote the cleavage of glycosidic bonds present in the xylan, liberating an xylose which stimulates decomposition of cellulose by reducing lag phase to a minimum. The stimulation is quite strong in the case of the cellulose dehydration during feedstocks pyrolysis, where the hydroxyl group on a different carbon atom reacts with H to form a water molecule and then undergoes dehydration to generate a new product (the main product is 5-HMF (5-hydroxymethylfurfural)). Based on the obtained *E* values for this step *per* both samples (*E* values ranged 300.114 kJ/mol – 321.431 kJ/mol (Table 9)), the dehydration reaction pathway which requires an energy barrier of 367.13 kJ/mol including C_4–OH + C_3–H active sites participation (3,4-dehydration) (Wang et al., 2020) is the most likely mechanism for step 1.2 in both, MG and AD pyrolyses. As another important product of the cellulose degradation within this step, glucolaldehyde can be formed, through the conversion of two carbon fragments, which requires activation energies in the range of 177.9 kJ/mol - 391.3 kJ/mol (Lu et al., 2016). The above considered successive reactions step (Eq. (6)) can be briefly summarized through the Scheme 1.

b) Another successive reactions step presented by Eq. (7) starts at lower temperatures and has the following trend: $D \xrightarrow{\Delta T=130C^o-250C^o} E \xrightarrow{\Delta T=325C^o-375C^o} F$. The first un-branched step in successive mechanism (step 2.1) occurring in $\Delta T = 130$ °C – 250 °C, can be attributed to extractives decomposition, for both samples. In general, extractives are non-structural components which include mostly wax, fat, resin, tannic acid, starch, pigment, etc (Anäs et al., 1983). The extractives decomposition may influenced on the pyrolysis process of biomass components (Wang et al., 2017). Extractives

$$Xylan \xrightarrow{\Delta} Xylose\ (+H_2, H_2O, CO, CO_2, HCHO, CH_3OH, C_2H_5OH, char) \begin{cases} \xrightarrow{\Delta, cellulose\ degradation} Dehydration_{C3-C4}: \\ \text{Products} \\ Glucolaldehyde, 5-HMF + H_2O\ [char] \end{cases}$$

Scheme 1. Brief schematic view of $A \rightarrow B \rightarrow C$ successive pyrolysis step of MG and AD with an prediction of possible products (bio-oil, syngas, chars). Scheme formed on the basis of kinetic results from *model-based* analysis.

decomposition occupies an important place in the thermo-chemical conversion of biomass because yields an additional products, resulting in different final product distribution of bio-oil, especially for extractives-rich feedstocks. It should be noted that extractive chemical species are complex and vary, depending on biomass varieties which were commonly composed of various saccharides and other carbohydrates, proteins, hydrocarbons, oils, aromatics, lipids, fats, and phenols. In that sense, it is very difficult to decouple an pyrolysis reactions of different chemical compounds, but in-depth analysis applied here may be helpful to establish a more comprehensive understanding of extractives thermal decomposition properties, during MG and AD pyrolyses. Based on the obtained kinetic parameters and kinetic model types of the step 2.1 for both samples (step: $D \rightarrow E$, Table 9), it can be noted that this process takes place with a different degree of kinetic complexity, and its contribution in the entire pyrolysis is not the same. It can be assumed that the step 2.1 belongs to the starch (stored in extractive content of both, MG and AD feedstocks, where its content is higher in C4 than in C3 energy crops (Miyake, 2016); C3 crop can have a maximum up to 4% of the starch content) pyrolysis reaction forming an intermediate product, levoglucosan (LG) (E) as the platform molecule. The higher activation energies for the step $D \rightarrow E$ in both, MG and AD (E_3 = 213.621 kJ/mol – 314.113 kJ/mol), are the consequence of existence of intermolecular hydrogen bonds in the reactant, during starch thermal decomposition. As a consequence, an steric hindrance effect caused by intermolecular hydrogen bonds leads to complicated reactions which form volatiles, except the levoglucosan; formation of these volatiles compete with the formation of levoglucosan (Yang et al., 2013). Consequently, competition affects the product distribution of the pyrolysis reaction, which leads to a more significant increase in a reaction complexity, through uprising of reaction orders values, which is larger in the case of MG ($n \sim 14.160$), than in the case of AD ($n \sim 3.126$) (Table 9). In addition, the step 2.2 ($E \rightarrow F$) takes place through various reaction mechanisms (A2 and D2 kinetic models (Table 9)) including the LG decomposition. Since that LG represents the main component released during cellulose pyrolysis (Lin et al., 2009), then, $B \rightarrow C$ and $E \rightarrow F$ steps proceed in the parallel competitive manner in both, MG and AD pyrolyses, and this is realized in the same temperature range (325 °C – 375 °C) where cellulose molecule is degraded. This finding is in excellent agreement with the results shown in the Fig. S1.

In the case of LG decomposition in cellulose pyrolytic zone of MG and AD sample, the process proceeds *via* two-dimensional growth of nuclei (A2) model and two-dimensional diffusion (Valensi) model, respectively. The A2 reaction model in LG decomposition for MG feedstock, implies the thermal decomposition of "reactant" to a new product and the gas, where a new product phase is formed at the nucleation sites of the initial "reactant". In general, the nucleation occurs especially in imperfections in solids due to displacements, defects and cracks, being regions of low activation energy also known as nucleation regions, where "solid" decomposition is favored, and the original nuclei grow into "growth nuclei" as the reaction progresses. In the actual case, the LG decomposition *via* breaking of C—O bonds is the most probable one, compared to dehydration routes which require higher activation energies (266.3 kJ/mol – 323.1 kJ/mol) (Zhang et al., 2012), and this reaction path can be described as $C_6H_{10}O_5 \rightarrow C_5H_6O_2 + CO + 2\ H_2O$ (where 4-pentene-2,3-dione ($C_5H_6O_2$) is a new formed product). Additionally, aldehydes such as acetaldehyde [AA] can be formed from C—O bond breaking decomposition, where decarbonylation reaction takes place and CO generation path is established (Guo et al., 2019).

The D2 reaction model in LG decomposition for AD feedstock (Table 9) implies that the reagent is not readily available in the solid state. Therefore, the reaction takes place at the boundary of the crystal lattice (crystallinity depends on solubility of carbohydrate fraction in a given feedstock), and for the "solid" to react with gas, the gas molecules must diffuse into "solid" structure. The reaction starts in the outer layer of the "solid" and as the reaction progresses, the reaction tends to move into "solid" particle, leaving the product layer behind. Product layer may reduces the reaction rate due to diffusion difficulty, causing an increase in the activation energy (Table 9). In the actual case, the presence of larger quantities of alkali and alkaline earth metals (AAEMs) in AD feedstock (such as K^+ and Mg^{2+}) (Table S1, Supplementary Material) takes a pivotal role in LG decomposition. Namely, AAEMs are ion-exchangeable with protons in a reversible reaction between a solution and a solid phase, considering electroneutral conditions. Namely, free AAEMs (which have not been previously 'chemically' removed) may promote fragmentation reactions to small molecules at the expense of LG, without increasing the carbonaceous residue yield (char). A certain study showed that released AAEMs and bounded AAEMs participate in volatile-volatile and volatile-char interactions (Hu et al., 2015). The present AAEMs may change the structure of biomass carbohydrates by interacting with oxygen and impacting the stereochemistry of molecules during pyrolysis (Mayes et al., 2015). This interaction promotes rearrangement possibilities and dehydration reactions followed by the fragmentation reaction. Consequently, in our considered case, the established kinetic model is attached to the rate of diffusion (in two dimension) of 'dissolved'AAEM ions, where the rate of diffusion is mainly controlled by the concentration of minerals which are not bonded to the organic structure. These AAEMs can affect the LG decomposition products during AD pyrolysis. In that sense, considering AD feedstock, excess of metal catalysts shift LG decomposition mechanism towards fragmentation. Namely, it should be expected that LG enters into deoxygenation reaction pathway, including dehydration to form furans (product F for AD), but further transformation to aromatic compounds *via* decarboxylation is less expected (the energy required for this reaction exceeds 300 kJ/mol (Guo et al., 2019)) since that LG is poorly produced from the previous reaction step in AD pyrolysis (step 2.1, $D \rightarrow E$, contribution ~ 7.1% (Table 9)). The activation energy for dehydration of LG-to-furan route is approximately 273.07 kJ/mol (Osatiashtiani et al., 2022), which is in good agreement with the activation energy value obtained in our study (Table 9). The considered successive reactions step (Eq. (7)) for MG and AD feedstocks can be briefly summarized through Schemes 2 and 3.

c) The single un-branched reaction step (step 3.1, $G \rightarrow H$, Eq. (8)) can be attributed to lignin pyrolysis in both samples. The actual reaction step takes place at temperatures higher than 375 °C ($T > 375$ °C).

MG (C4 crop):

$$Starch\ (extractives) \xrightarrow{\Delta\,[+gases,H_2O,(char)]} LG \xrightarrow{\{C-O\ bond\ breaking\}} C_5H_5O_2 + CO + H_2O + \{[C_2H_4O] + CO_{ad}\uparrow\}.$$

Scheme 2. Brief schematic view of $D \rightarrow E \rightarrow F$ successive pyrolysis step of MG feedstock, with an prediction of possible products (primarily bio-oils and gases (CO), where *ad* means additional). Scheme formed on the basis of kinetic results from *model-based* analysis.

AD (C3 crop):

$$Starch\ (extractives) \xrightarrow{\Delta\,[+gases,H_2O,(char)]} LG \xrightarrow{AAEMs\ \{dehydration\ [-H_2O]\}} Furans\ [+\ viscous\ bio-oils].$$

Scheme 3. Brief schematic view of $D \rightarrow E \rightarrow F$ successive pyrolysis step of AD feedstock, with an prediction of possible products (primarily bio-oils). Scheme formed on the basis of kinetic results from *model-based* analysis.

Considering the reaction order values obtained for F*n* model as well as the range of activation energies (Table 9), it is obvious that this pyrolytic stage related to lignin decomposition in MG and AD samples, has different kinetic characteristics. Consequently, as an important structure factor represents the cleavage of β-O-4 bonds in the lignin depolymerization (Reiter et al., 2013). Lignin depolymerization during energy crops pyrolysis is very significant, considering its potential for industrial applications. The primary pyrolysis of lignin takes place in the temperature range between 200 °C and 400 °C. In the current *T*-range, ether cleavage, especially β-O-4 bond accounts for most of the reactions. When the temperature exceeds 400 °C, radical reactions can be dominant, and as a result, an extensive rearrangement of lignin structure may occurs. It can be assumed that in the case of MG pyrolysis, the lignin depolymerization proceeds through one-pot thermal rupturing of C—C linkages as one of the lignin interunit. Namely, the C—C bonds have much higher dissociation energy (span 226–494 kJ/mol) than C—O bonds in the lignin (Rinaldi et al., 2016). This pyrolysis route which was linked to presented kinetic results for MG (Table 9) is thermodynamically unfavorable, which was previously proven (see results and accompanying discussion in sub-Section *3.8.1.*). The reaction step is characterized by high E_5 value (~ 328.919 kJ/mol) and extremely high reaction order ($n \sim 20.000$) (Table 9). As presented previously, the influence of metal catalysts in this case is minor (probably blocked). So, in the considered case, the pure thermal depolymerization reaction route with a strong intensification of system heating has the primary influence. Therefore, the yield of MG lignin monomers is limited because of the presence of stable C–C bonds, which require a high energy input for their rupturing. The presumable absence of catalytic cleavage of C–C bonds of the MG lignin, minimizes lignin monomer production in the pyrolysis. So, the presence of native catalysts (minerals) in the MG feedstock have poor activity in a cleaving of C—C bonds in the MG lignin. On the other hand, the lignin depolymerization in the case of AD pyrolysis proceeds through the same kinetic model of *n*-th order reaction, but with much lower values of activation energy and reaction order ($E_5 \sim$ 251.899 kJ/mol, $n \sim 8.808$), which means that the process loses its original complexity. In this case, we can expect the active participation of metal catalysts (Zhou et al., 2022), which facilitate the rupturing of C—O linkages in the AD lignin, which would lead to the maximization of lignin monomer production and what is highly desirable. Increased participation of catalysts prevents undesirable condensation of lignin by hydrogenation of reactive intermediates resulting from solvolytic depolymerization (Van den Bosch et al., 2017). The presence of catalysts such as alkali earths (Mg, Ca) or transition metal catalyst (Fe in combination with Mn) may supports C-C bonds cleavage among monocyclic arenes, which causes the attainment of very high yields of aromatic hydrocarbons. Therefore, for AD lignin pyrolysis, we can consider with high probability, that a combination of thermal and chemical depolymerization route exists.

A brief overview of lignin depolymerization pathways in MG and AD pyrolyses is shown in Schemes 4 and 5.

The competitive reaction steps among MG and AD feedstock pyrolyses represent $E \rightarrow F$ step, that proceeds with different reaction mechanisms (as A2 and D2 kinetic models), *i.e.*, between the production of value-added chemicals and gases (CO), and the viscous bio-oils. This process can be strictly regulated by heating rate (β) variation. The reduction of the heating rate lowers the reaction temperature by a forcing more the $E \rightarrow F$ step for the MG towards greater high-value chemicals and gas productions. Increase in the heating rate, pushes the $E \rightarrow F$ step for the AD towards greater bio-oils production. This is in very good agreement with the results discussed in a sub-Section *3.3* (see above). In order to verify the established *p*:, model scheme (Table 9) for the MG and AD pyrolysis processes, the corresponding numerical calculations (the application of MVNR method) from the model-based results are compared to the experimental TG-curves at various heating rates ($\beta = 5.1$, 10.6 and 22.1 K/min) (Fig. 14 a) – b)). In Fig. 14, an each individual reaction step in the process mechanistic schemes is highlighted, together with the given physical-geometrical model.

It is evident that fit of theoretical curves to experimental ones follows *p*:, model scheme, with very high values of R^2, so the established pyrolysis mechanisms are fully verified (Fig. 14 a) – b)). Based on the statistical evaluation (Supplementary Material, section IV.), the different kinetic models/methods were compared statistically and the results of this analysis are listed in Table S5 (Supplementary Material). According to these results, based on the statistical assessment of the quality of the fits, it is possible, approximately ranked applied methods/models as followed: Numerical > FR > VY > *p*:, model (Table S5). Other methods such as OFW and KAS give poorer fitting qualities. Summarizing the obtained results based on this analysis, there is a good agreement between the derived kinetic parameters and the mechanisms assumed in model-free (isoconversional) approach (especially for FR and VY methods, confirmed by numerical optimization of the pyrolysis process) and the verified kinetic quantities and reaction models in model-based approach (see above results).

This study provides a detailed insight into the possibilities of maximum utilization of C3 and C4 energy crops for their thermochemical conversion (slow pyrolysis process) into high value biochemicals, commodity chemicals, drop-in fuels and syngas constituents, using in-depth coupled kinetic and thermodynamic analyses of possible reaction pathways up to desired products. For the first time, in this

MG (C4 crop) (contribution to entire pyrolysis ~ 21.5 %):

$$Lignin \xrightarrow{\Delta\uparrow\,(thermal\ depolymerization)} Aromatic\ hydrocarbons\ (low\ yield\ \downarrow)$$

Scheme 4. Brief schematic view of the un-branched single-step lignin conversion during the MG pyrolysis process (step 3.1, $G \rightarrow H$) ($\Delta\uparrow$ indicates *T* (heating) intensification, while ↓ indicates *declines*). Scheme formed on the basis of kinetic results from *model-based* analysis.

AD (C3 crop) (contribution to entire pyrolysis ~ 22.2 %)

$$Lignin \xrightarrow{\Delta\,(Thermo-chemical\ depolymerization)\{Mg,Ca,Fe/Mn-activity\}} Aromatic\ hydrocarbons\ (high\ yield\ \uparrow)$$

Scheme 5. Brief schematic view of the un-branched single-step lignin conversion during the AD pyrolysis process (step 3.1, $G \rightarrow H$) (↑ indicates *rise*; *drop-in* fuels production). Scheme formed on the basis of kinetic results from *model-based* analysis.

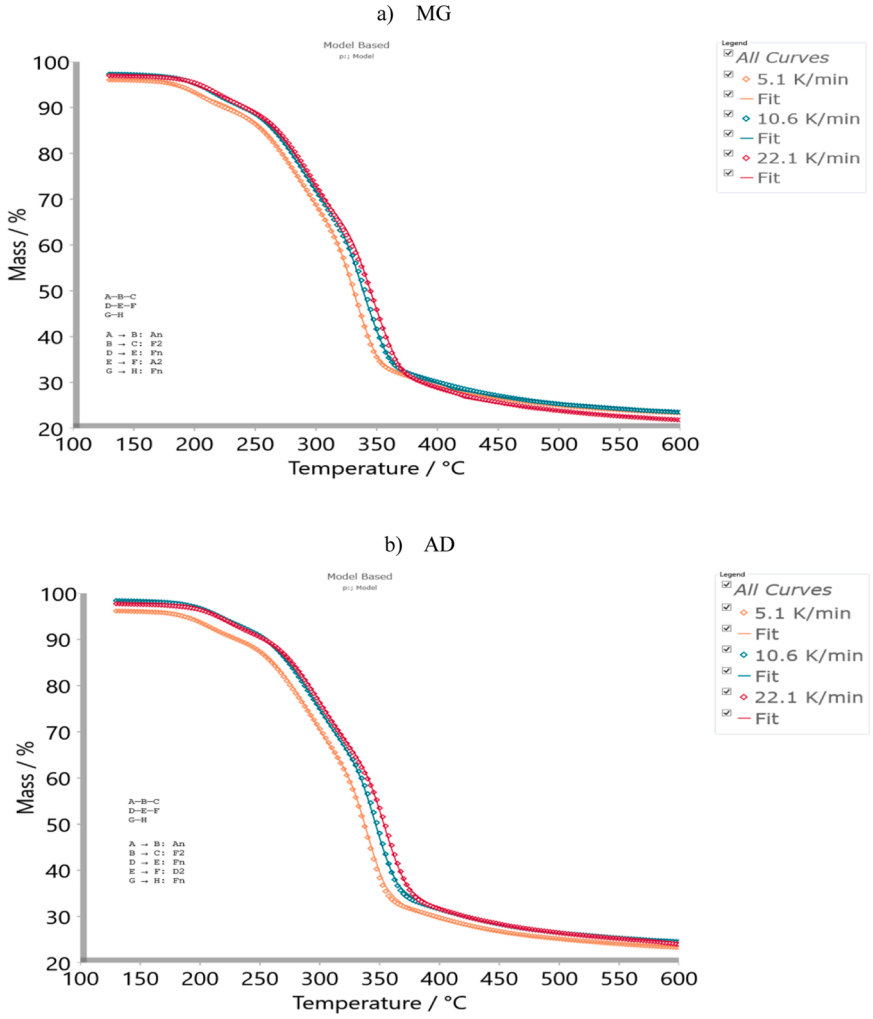

Fig. 14. Results of model-based analysis (*p*:; model scheme) compared with experimental TG-curves at various heating rates (5.1, 10.6, and 22.1 K/min) (experimental data: colored symbols, theoretical fits: full colored lines) (a) MG: $R^2 = 0.99995$; b) AD: $R^2 = 0.99995$).

research, the confirmation of existence of chemical compensation effect *viz* thermodynamic compensation (enthalpy-entropy compensation) was used to explain the real structural conformations inside the lignocellulosic molecular structure, guided by the entropy term, for identification and the production of some industrial chemicals from renewable resources. For that purpose, in this study, it was applied for the first time, the SET (selective energy transfer) model, for catalysts activity in the slow pyrolysis of C3 (*Arundo donax* L.) and C4 (*Miscanthus* × *giganteus*) energy crops. These results are confirmed with the proposed schemes of pyrolytic conversion mechanisms *via* model-free and model-based kinetics modeling, correlated with the extent of native catalysts activity, present in feedstocks as the mineral fraction. This work provides the background, the principal theoretical concept, and actual development status of C3 (*Arundo donax* L.) and C4 (*Miscanthus* × *giganteus*) energy crops for their efficient use for obtaining industrial chemicals *via* pyrolysis, with maximum heat utilization of the process, through the evaluation of kinetic and thermodynamic data. The findings presented in this work have the potential for worldwide application in large scale, since any kind of dry biomass can be used as feedstock. In addition, "*bio-liquid production*" described in actual research under development of kinetic and thermodynamic compensation phenomena can be considered as the backbone of a large future thermo-chemical biorefinery. Likewise, the approach shown here can be used for significant contribution to a sustainable future energy supply, which provides its achievement.

4. Conclusion

The main aim of the present study was to provide a detailed thermodynamic and kinetic explanation of reaction pathways in slow pyrolysis of C3 (*Arundo donax* L. (AD)) and C4 (*Miscanthus* × *giganteus* (MG)) energy crops which enable obtaining high-value chemicals, platform chemicals, bio-fuels, and important gaseous products. This work was focused on the use of kinetic compensation effect (KCE) and

enthalpy-entropy compensation (EEC) in the interpretation of energetically (thermodynamically) 'favorable' and 'unfavorable' reaction paths to obtain bio-oils in high and low yields (depending on the purpose), respectively. The approach presented in this study was implemented for the first time for C3 and C4 energy crops slow pyrolysis, using thermal analysis laboratory measurements. A special part of this research was devoted to the impact of host catalysts (present in the form of alkaline/alkaline earth and transition metals in tested feedstocks) on the production extent of value-added products from pyrolysis processes. In that sense, it was applied an SET (selective energy transfer) model for the identification and assessment of the activity of certain catalysts by the direct use of the results from EEC. The results and conclusions of this analysis were confirmed in the second part of the paper, where detailed kinetic investigations based on reaction models (model-based approach) are performed. It was shown that both pyrolytic processes can be described by two consecutive reaction steps and one single-step unbranched reaction. The difference in the conversion paths of these two energy crops occurs in consecutive reactions step, which encompasses levoglucosan (LG) (platform molecule) pyrolysis into ketones and gases (predominatly CO), and furans (heterocyclic compounds), for MG and AD, respectively. Changes in reaction mechanisms of LG degradation in MG and AD pyrolysis, are reflected *via* different kinetic models which mechanistically explain this transformation: two-dimensional growth of nuclei (A2) (Avrami) (MG) and two-dimensional diffusion (Valensi) (AD) models. The mechanisms are explained through C—O bonds breaking and decarbonylation (case: MG), as well as through LG dehydration with significant participation of AAEMs (alkali and alkaline earth metals) (case: AD). From LG conversion pathways in C3 and C4 energy crops, it was concluded that LG degradation trail is preferable for production of high-value chemicals and syngas constituents (towards CO formation) into MG feedstock, while the LG degradation trail is preferable for bio-oils production (furans) into AD feedstock. It was found that yields of these products depend to a significant extent on the heating rate of the system. From the aspect of pyrolytic performance, as well as regulation of the yield of given conversion products, it was determined that low heating rates are desirable for effective production of chemicals from MG, while high heating rates are recommended for obtaining high yield bio-oils from AD. From a thermodynamic point of view, C3 crop (*Arundo donax* L.) is more convenient in regards to C4 crop (*Miscanthus* × *giganteus*), considering lower transformation energy requirement, higher reactivity, as well as much faster accumulation of products. This is particularly important for valorization of these biomasses for the production of higher-value-added fuels and chemicals.

CRediT authorship contribution statement

Bojan Janković: Conceptualization, Methodology, Software, Validation, Formal analysis, Data curation, Writing – original draft, Writing – review & editing, Visualization, Supervision, Project administration. **Nebojša Manić:** Methodology, Software, Validation, Formal analysis, Investigation, Writing – review & editing, Supervision. **Mina Popović:** Validation, Investigation, Writing – review & editing, Supervision. **Slobodan Cvetković:** Validation, Investigation, Writing – review & editing, Supervision. **Željko Dželetović:** Validation, Investigation, Resources, Writing – review & editing, Supervision. **Dragoslava Stojiljković:** Validation, Investigation, Writing – review & editing, Supervision.

Declaration of Competing Interest

The authors declare that they have no known competing financial interests or personal relationships that could have appeared to influence the work reported in this paper.

Data availability

Data will be made available on request.

Acknowledgments

Authors would like to acknowledge financial support of Ministry of Education, Science and Technological Development of the Republic of Serbia, under Contract numbers: 451–03-68/2022–14/200017 (B. Janković), 451–03-68/2022–14/200105 (N. Manić), 451–03-68/2022–14/200026 (M. Popović and S. Cvetković), and 451–03-68/2022–14/200019 (Ž. Dželetović).

Appendix A. Supporting information

Supplementary data associated with this article can be found in the online version at doi:10.1016/j.indcrop.2023.116275.

References

Abreu, M., Silva, L., Ribeiro, B., Ferreira, A., Alves, L., Paixão, S.M., Gouveia, L., Moura, P., Carvalheiro, F., Duarte, L.C., Fernando, A.L., Reis, A., Gírio, F., 2022. Low indirect land use change (ILUC) energy crops to bioenergy and biofuels - A review. Energies 15, 4348. https://doi.org/10.3390/en15124348.

Agarwal, U.P., 1999. An overview of Raman spectroscopy as applied to lignocellulosic materials. In: Argyropoulos, D.S. (Ed.), Advances in Lignocellulosics Characterization, Ch. 9. TAPPI Press, Atlanta, GA, pp. 201–225.

Al-Snafi, A.E., 2015. The constituents and biological effects of Arundo donax - A review. Int. J. Phytophar. Res. 6 (1), 34–40 (⟨www.phytopharmacyresearch.com⟩), e - ISSN 2249-7544, Print ISSN 2229-7464.

Anäs, R., Ekman, B., Holmbom, B., 1983. Composition of nonpolar extractives in bark of Norway spruce and Scots pine. J. Wood Chem. Technol. 3 (2), 119–130.

Anca-Couce, A., Mehrabian, R., Scharler, R., Obernberger, I., 2014. Kinetic scheme of biomass pyrolysis considering secondary charring reactions. Energy Convers. Manag. 87, 687–696.

Anca-Couce, A., Tsekos, T., Retschitzegger, S., Zimbardi, F., Funke, A., Banks, S., Kraia, T., Marques, P., Scharler, R., de Jong, W., Kienzl, N., 2020. Biomass pyrolysis TGA assessment with an international round robin. Fuel 276, 118002. https://doi.org/10.1016/j.fuel.2020.118002.

Angelini, L.G., Ceccarini, L., Nassi o Di Nasso, N., Bonari, E., 2009. Comparison of Arundo donax L. and Miscanthus x giganteus in a long-term field experiment in Central Italy: Analysis of productive characteristics and energy balance. Biomass Bioenergy 33, 635–643.

Aparicio, S., Alcalde, R., Dávila, M.J., García, B., Leal, J.M., 2007. Properties of 1,8-cineole: A thermophysical and theoretical study. J. Phys. Chem. B 111 (12), 3167–3177. https://doi.org/10.1021/jp067405b.

Arellano, O., Flores, M., Guerra, J., Hidalgo, A., Rojas, D., Strubinger, A., 2016. Hydrothermal carbonization of corncob and characterization of the obtained hydrochar. Chem. Eng. Trans. 50, 235–240.

ArundoBioEnergy, Plant Arundo, Harvest Energy, ACF-ArundoCellulózFarmingu, 2022. Available at: ⟨https://arundobioenergy.com/⟩.

ASTM E1755-01, 2001. Standard Test Method for Ash in Biomass. updated 2010. American Society for Testing and Materials, ASTM International,, West Conshohocken, PA 19428-2959, US.

ASTM E1756-08, 2008. Standard Test Method for Determination of Total Solids in Biomass. updated 2015. American Society for Testing and Materials, ASTM International,, West Conshohocken, PA 19428-2959, US.

ASTM E872-82, 1998. Standard Test Method for Volatile Matter in the Analysis of Particulate Wood Fuels. updated 2019. American Society for Testing and Materials, ASTM International,, West Conshohocken, PA 19428-2959, US.

Ba, Y., Liu, F., Wang, X., Yang, J., 2020. Pyrolysis of C3 energy plant (Arundo donax): Thermogravimetry, mechanism, and potential evaluation. Ind. Crops Prod. 149, 112337 https://doi.org/10.1016/j.indcrop.2020.112337.

Bajpai, P., 2016. Structure of lignocellulosic biomass. Pretreatment of Lignocellulosic Biomass for Biofuel Production. Springer Briefs in Molecular Science (book series GREENCHEMIST). Springer,, Singapore, pp. 7–12. https://doi.org/10.1007/978-981-10-0687-6_2. ISBN: 978-981-10-0686-9.

Barrie, P.J., 2012. The mathematical origins of the kinetic compensation effect: 1. The effect of random experimental errors. Phys. Chem. Chem. Phys. 14, 318–326.

Biagini, E., Barontini, F., Tognotti, L., 2006. Devolatilization of biomass fuels and biomasscomponents studied by TG/FTIR technique. Ind. Eng. Chem. Res. 45, 4486–4493.

Brosse, N., Dufour, A., Meng, X., Sun, Q., Ragauskas, A., 2012. Miscanthus: A fast-growing crop for biofuels and chemicals production. Biofuels Bioprod. Bioref. 6 (5), 580–598.

Carrier, M., Loppinet-Serani, A., Denux, D., Lasnier, J.M., Ham-Pichavant, F., Cansell, F., Aymonier, C., 2011. Thermogravimetric analysis as a new method to determine the lignocellulosic composition of biomass. Biomass Bioenergy 35, 298–307.

Casillo, A., Lanzetta, R., Parrilli, M., Corsaro, M.M., 2018. Exopolysaccharides from marine and marine extremophilic bacteria: Structures, properties, ecological roles and applications. Mar. Drugs 16 (2), 69. https://doi.org/10.3390/md16020069.
Chandraratne, M.R., Daful, A.G., 2021. Recent advances in thermochemical conversion of biomass. In: Bartoli, M., Giorcelli, M. (Eds.), Recent Perspectives in Pyrolysis Research. Ch. 8.,IntechOpen, London, Greater London, United Kingdom. https://doi.org/10.5772/intechopen.100060.
Chen, B., Wang, X., Leng, W., Kan, Y., Mei, C., Zhai, S., 2019. Spectroscopic/microscopic elucidation for chemical changes during acid pretreatment on Arundo donax. J. Bioresour. Bioprod. 4, 192–199.
Collura, S., Azambre, B., Weber, J.V., 2005. Thermal behavior of Miscanthus grasses, an alternative biological fuel. Environ. Chem. Lett. 3, 95–99.
Corno, L., Pilu, R., Adani, F., 2014. Arundodonax L.: A non-food crop for bioenergy and bio-compound production. Biotechnol. Adv. 32, 1535–1549.
Curtis, W.M., Conner, J.R., 1982. A general explanation for the compensation effect: The relationship between ΔS and activation energy. J. Catal. 78, 238–246.
deCarvalho, A.V., 2017, Effects of Potassium and Calcium on the Combustion Behaviour of Biomass. Master of Science Degree Thesis in Mechanical Engineering, TécnicoLisboa, University of Lisbon, Portugal, July 2017, pp. 7–8.
Demirbas, A., Arin, G., 2002. An overview of biomass pyrolysis. Energy Sour. 24 (5), 471–482. https://doi.org/10.1080/00908310252889979.
Dražić, G., Milovanović, J., Ikanović, J., Glamočlija, Đ., 2010. Impacts of agroecological factors on the biomass production of gigantmiscanthus (Miscanthusgiganteus). J. Sci. Agric. Res. 71, 81–85.
Dželetović, Ž., Dražić, G., Glamočlija, Đ., Mihailović, N., 2007. *Miscanthus* – European experience with a new energy crop. 173 PTEP – J. Process Eng. Energy Agric. 11 (1–2), 66–70.
Dželetović, Ž., Mihailović, N., Živanović, I., 2013. Prospects of using bioenergy crop Miscanthus × giganteus in Serbia. In: Méndez-Vilas, A. (Ed.), Materials and Processes for Energy: Communicating Current Research and Technological Developments. Formatex Research Center, Badajoz, Spain, pp. 360–370.
Dželetović, Ž., Maksimović, J., Živanović, I., 2014. Yield of Miscanthus × giganteus during crop establishment at two locations in Serbia. J. Process. Energy Agric. 18 (2), 62–64.
Escalante, J., Chen, W.-H., Tabatabaei, M., Hoang, A.T., Kwon, E.E., Andrew Lin, K.-Y., Saravanakumar, A., 2022. Pyrolysis of lignocellulosic, algal, plastic, and other biomass wastes for biofuel production and circular bioeconomy: A review of thermogravimetric analysis (TGA) approach. Renew. Sustain. Energy Rev. 169, 112914 https://doi.org/10.1016/j.rser.2022.112914.
Felten, D., Fröba, N., Fries, J., Emmerling, C., 2013. Energy balances and greenhouse gas-mitigation potentials of bioenergy cropping systems (Miscanthus, rapeseed, and maize) based on farming conditions in Western Germany. Renew. Energy 55, 160–174.
Figala, J., Vranová, V., Rejšek, K., Formánek, P., 2015. Giant miscanthus (Miscanthus × giganteus Greef Et Deu.) – A promising plant for soil remediation: A mini review. Acta Univer. Agric. etSilvicult. Mendel. Brunen. 63, 2241–2246.
Fonseca, F.G., Anca-Couce, A., Funke, A., Dahmen, N., 2022. Challenges in kinetic parameter determination for wheat straw pyrolysis. Energies 15, 7240. https://doi.org/10.3390/en15197240.
Fournel, S., Palacios, J.H., Morissette, R., Villeneuve, J., Godbout, S., Heitz, M., Savoie, P., 2015. Influence of biomass properties on technical and environmental performance of a multi-fuel boiler during on-farm combustion of energy crops. Appl. Energy 141, 247–259.
Friendly, M., Monette, G., Fox, J., 2013. Elliptical insights: Understanding statistical methods through elliptical geometry. Stat. Sci. 28 (1), 1–39. https://doi.org/10.1214/12-STS402.
Galletti, A.M.R., D'Alessio, A., Licursi, D., Antonetti, C., Valentini, G., Galia, A., Nassio Di Nasso, N., 2015. Midinfrared FT-IR as a tool for monitoring herbaceous biomass composition and its conversion to furfural. J. Spectr. 2015, 12. Article ID 719042. ⟨https://doi.org/10.1155/2015/719042⟩.
Ge, X., Xu, F., Vasco-Correa, J., Li, Y., 2016. Giant reed: A competitive energy crop in comparison with miscanthus. Renew. Sustain. Energy Rev. 54, 350–362. https://doi.org/10.1016/j.rser.2015.10.010.
Girotto, L., Franco, A.C., Nunez, C.V., Oliveira, S.C.C., Scheffer de Souza, M.C., Fachin-Espinar, M.T., Ferreira, C.S., 2021. Phytotoxicity and allelopathic potential of extracts from rhizomes and leaves of Arundodonax, an invasive grass in neotropical savannas. Not. Bot. Horti Agrobot. Cluj. -Nap. 49 (3), 12440. https://doi.org/10.15835/nbha49312440.
Goussougli, M., Sirjean, B., Glaude, P.-A., Fournet, R., 2021. Theoretical study of the pyrolysis of β-1,4-xylan: A detailed investigation on unimolecular concerted reactions. Phys. Chem. Chem. Phys. 23 (4), 2605–2621.
Gray, K.A., Zhao, L.S., Emptage, M., 2006. Bioethanol. Curr. Opin. Chem. Biol. 10, 141–146.
Guo, S., Liang, H., Che, D., Liu, H., Sun, B., 2019. Quantitative study of the pyrolysis of levoglucosan to generate small molecular gases. RSC Adv. 9, 18791–18802. https://doi.org/10.1039/c9ra03138c.
Gupta, R.B., Demirbas, A., 2010. Gasoline, Diesel and Ethanol Biofuels from Grasses and Plants. Cambridge University Press,, New York, NY, USA.
Haykiri-Acma, H., Yaman, S., Kucukbayrak, S., 2006. Effect of heating rate on the pyrolysis yields of rapeseed. Renew. Energy 31 (6), 803–810.
Horikawa, Y., Hirano, S., Mihashi, A., Kobayashi, Y., Zhai, S., Sugiyama, J., 2019. Prediction of lignin contents from infrared spectroscopy: Chemical digestion and lignin/biomass ratios of Cryptomeria japonica. Appl. Biochem. Biotechnol. 188, 1066–1076.
Hu, S., Jiang, L., Wang, Y., Su, S., Sun, L., Xu, B., He, L., Xiang, J., 2015. Effects of inherent alkali and alkaline earth metallic species on biomass pyrolysis at different temperatures. Bioresour. Technol. 192, 23–30.
Ibarz, R., Garvín, A., Ibarz, A., 2017. Kinetic and thermodynamic study of the photochemical degradation of patulin. Food Res. Int. 99, 348–354.
ISO 18125:2017, 2017, Solid biofuels - Determination of calorific value. ISO (the International Organization for Standardization), Release date: 26/06/2017.
ISO 5351:2004, 2004, Pulps - Determination of limiting viscosity number in cupri-ethylenediamine (CED) solution. This standard has been revised by ISO 5351:2010, International Organization for Standardization.
Janković, B., Manić, N., Dodevski, V., 2021. Pyrolysis kinetics of Poplar fluff bio-char produced at high carbonization temperature: A mechanistic study and isothermal life-time prediction. Fuel 296, 120637. https://doi.org/10.1016/j.fuel.2021.120637.
Jensen, A., Dam-Johansen, K., 1998. TG-FTIR study of the influence of potassium chloride on wheat straw pyrolysis. Energy Fuels 12, 929–938.
Johansen, J.M., Jakobsen, J.G., Frandsen, F.J., Glarborg, P., 2011. Release of K, Cl, and S during pyrolysis and combustion of high-chlorine biomass. Energy Fuels 25, 4961–4971.
Kalembkiewicz, J., Galas, D., Sitarz-Palczak, E., 2018. The physicochemical properties and composition of biomass ash and evaluating directions of its applications. Pol. J. Environ. Stud. 27 (6), 1–11.
Kenkyu, T.N., 1997. The assignment of IR absorption bands due to free hydroxyl groups in cellulose. Cellulose 4, 281–292.
Khawam, A., Flanagan, D.R., 2006. Solid-state kinetic models: Basics and mathematical fundamentals. J. Phys. Chem. B 110 (35), 17315–17328.
Kirti, N., Tekade, S.P., Tagade, A., Sawarkar, A.N., 2022. Pyrolysis of pigeon pea (*Cajanus cajan*) stalk: Kinetics and thermodynamic analysis of degradation stages via isoconversional and master plot methods. Bioresour. Technol. 347, 126440 https://doi.org/10.1016/j.biortech.2021.126440.
Knudsen, J.N., Jensen, P.A., Dam-Johansen, K., 2004. Transformation and release to the gas phase of Cl, K, and S during combustion of annual biomass. Energy Fuels 18, 1385–1399.
Koudriavtsev, A.B., Jameson, R.F., Linert, W., 2001. The Law of Mass Action, 1st ed..,. Springer-Verlag,, Berlin Heidelberg. ISBN 978-3-642-62494-0, DOI 10.1007 /978-3-642-56770-4.
Kowalczyk-Juśko, A., Mazur, A., Pochwatka, P., Janczak, D., Dach, J., 2022. Evaluation of the effects of using the giant Miscanthus (Miscanthus × Giganteus) biomass in various energy conversion processes. Energies 15, 3486. https://doi.org/10.3390/en15103486.
Krička, T., Matin, A., Bilandžija, N., Jurišić, V., Antonović, A., Voća, N., Grubor, M., 2017. Biomass valorisation of Arundodonax L., Miscanthus × giganteus andSidahermaphrodita for biofuel production. Int. Agrophys 31, 575–581.
Krug, R.R., Hunter, W.G., Grieger, R.A., 1976. Enthalpy-entropy compensation. 1. Some fundamental statistical problems associated with the analysis of Van't Hoff and Arrhenius data. J. Phys. Chem. 80 (21), 2335–2341.
Kumar, A., Monika, Kumar, Mishra, R., Jaglan, S., 2022. Pyrolysis of low-value waste miscanthus grass: Physicochemical characterization, pyrolysis kinetics, and characterization of pyrolytic end products. Process Saf. Environ. Prot. 163, 68–81.
Kumar, P., Singh, V.P., Tagade, A., Sawarkar, A.N., 2023. Thermochemical characterization of post-phytoremediated vetiver (*Vetiveria zizanioides* (L.) Nash) root and shoot for their prospective bioenergy potential. Ind. Crop. Prod. 191 (Part A), 115964. https://doi.org/10.1016/j.indcrop.2022.115964.
Kumar, R., Chandrashekar, N., Prasad, N.R.R., Tailor, R., 2020. Effect of extractive content on fuelwood characteristics of certain woody and non-woody biomass. Curr. Sci. 118 (6), 966–969.
Larsen, K.L., Barsberg, S., 2010. Theoretical and Raman spectroscopic studies of phenolic lignin model monomers. J. Phys. Chem. B 114, 8009–8021.
Lathière, J., Hauglustaine, D.A., Friend, A.D., De Noblet-Ducoudré, N., Viovy, N., Folberth, G.A., 2006. Impact of climate variability and land use changes on global biogenic volatile organic compound emissions. Atmos. Chem. Phys. 6, 2129–2146.
Leita, B.A., Warden, A.C., Burke, N., O'Shea, M.S., Trimm, D., 2010. Production of p-cymene and hydrogen from a bio-renewable feedstock–1,8-cineole (eucalyptus oil). Green. Chem. 12, 70–76.
Lewandowski, I., Kicherer, A., Vonier, P., 1995. CO_2-balance for the cultivation and combustion of Miscanthus. Biomass Bioenergy 8, 81–90.
Lewandowski, I., Clifton-Brown, J.C., Scurlock, J.M.O., Huisman, W., 2000. Miscanthus: European experience with a novel energy crop. Biomass Bioenergy 19, 209–227.
Li, T., Song, F., Zhang, J., Liu, S., Xing, B., Bai, Y., 2020. Pyrolysis characteristics of soil humic substances using TG-FTIR-MS combined with kinetic models. Sci. Total Environ. 698, 134237 https://doi.org/10.1016/j.scitotenv.2019.134237.
Lin, Y.-C., Cho, J., Tompsett, G.A., Westmoreland, P.R., Huber, G.W., 2009. Kinetics and mechanism of cellulose pyrolysis. J. Phys. Chem. C. 113, 20097–20107.
van Lith, S.C., Jensen, P.A., Frandsen, F.J., Glarborg, P., 2008. Release to the gas phase of inorganic elements during wood combustion. Part 2: Influence of fuel composition. Energy Fuels 22, 1598–1609.
Liu, L., Guo, Q.-X., 2001. Isokinetic relationship, isoequilibrium relationship, and enthalpy-entropy compensation. Chem. Rev. 101, 673–696.
Liu, X., Tan, H., Wang, X., Wang, Z., Xiong, X., 2020. Oxidation reactivity and kinetic analysis of bituminous coal char from high-temperature pyrolysis: Effect of heating rate and pyrolysis temperature. Thermochim. Acta 690, 178660. https://doi.org/10.1016/j.tca.2020.178660.
Lu, Q., Tian, H.-Y., Hu, B., Jiang, X.-Y., Dong, C.-Q., Yang, Y.-P., 2016. Pyrolysis mechanism of holocellulose-based monosaccharides: The formation of hydroxyacetaldehyde. J. Anal. Appl. Pyrol. 120, 15–26.

Lupoi, J.S., Gjersing, E., Davis, M.F., 2015. Evaluating lignocellulosic biomass, its derivatives, and downstream products with Raman spectroscopy. Front. Bioeng. Biotechnol. 3, 50. https://doi.org/10.3389/fbioe.2015.00050.
Mani, T., Murugan, P., Abedi, J., Mahinpey, N., 2010. Pyrolysis of wheat straw in a thermogravimetric analyzer: effect of particle size and heating rate on devolatilization and estimation of global kinetics. Chem. Eng. Res. Des. 88 (8), 952–958.
Manimekalai, K., Jayaprakash, P., 2021. Influence of potassium chloride doping on the properties of potassium dihydrogen phosphate crystal for nonlinear optical applications. J. Mater. Sci. Mater. Electron 32, 8033–8042.
Mann, J.J., Barney, J.N., Kyser, G.B., Di Tomaso, J.M., 2013. Miscanthus × giganteus and Arundodonax shoot and rhizome tolerance of extreme moisture stress. GCB Bioenergy Bioprod. Sustain. Bioecon 5 (6), 693–700.
Martín, M.T., Aguirre, J.L., Baena-González, J., González, S., Pérez-Aparicio, R., Saiz-Rodríguez, L., 2022. Influence of specific power on the solid and liquid products obtained in the microwave-assisted pyrolysis of end-of-life tires. Energies 15, 2128. https://doi.org/10.3390/en15062128.
Matusiak, M., Ślęzak, R., Ledakowicz, S., 2020. Thermogravimetric kinetics of selected energy crops pyrolysis. Energies 13, 3977. https://doi.org/10.3390/en13153977.
Mayes, H.B., Nolte, M.W., Beckham, G.T., Shanks, B.H., Broadbelt, L.J., 2015. The alpha-bet(a) of salty glucose pyrolysis: Computational investigations reveal carbohydrate pyrolysis catalytic action by sodium ions. ACS Catal. 5 (1), 192–202. https://doi.org/10.1021/cs501125n.
Miyake, H., 2016. Starch accumulation in the bundle sheaths of C3 plants: A possible pre-condition for C4 photosynthesis. Plant Cell Physiol. 57 (5), pcw046. DOI:10.1093/pcp/pcw046.
Mosiewicki, M.A., Marcovich, N.E., Aranguren, M.I., 2011. Characterization of Fiber Surface Treatments in Natural Fiber Composites by Infrared and Raman Spectroscopy. In: Zafeiropoulos, N.E. (Ed.), Interface Engineering of Natural Fibre Composites For Maximum Performance. Woodhead Publishing, Cambridge, UK, pp. 117–145.
Mou, H.Y., Orblin, E., Kruus, K., Fardim, P., 2013. Topochemical pretreatment of wood biomass to enhance enzymatic hydrolysis of polysaccharides to sugars. Bioresour. Technol. 142, 540–545.
Moukhina, E., 2012. Determination of kinetic mechanisms for reactions measured with thermoanalytical instruments. J. Therm. Anal. Calor. 109, 1203–1214.
Moulik, S.P., Naskar, B., Kumar Rakshit, A., 2019. Current status of enthalpy-entropy compensation phenomenon. Curr. Sci. 117 (8), 1286–1291.
Munir, S., Daood, S.S., Nimmo, W., Cunliffe, A.M., Gibbs, B.M., 2009. Thermal analysis and devolatilization kinetics of cotton stalk, sugar cane bagasse and shea meal under nitrogen and air atmospheres. Bioresour. Technol. 100, 1413–1418.
Nawaz, A., Kumar, P., 2022. Elucidating the bioenergy potential of raw, hydrothermally carbonized and torrefied waste Arundo donax biomass in terms of physicochemical characterization, kinetic and thermodynamic parameters. Renew. Energy 187, 844–856.
Ng, H.M., Saidi, N.M., Omar, F.S., Ramesh, K., Ramesh, S., Bashir, S., 2018. Thermogravimetric Analysis of Polymers. Encycl. Polym. Sci. Technol. 1–29. https://doi.org/10.1002/0471440264.pst667.
Oginni, O., Singh, K., 2019. Pyrolysis characteristics of Arundo donax harvested from a reclaimed mine land. Ind. Crop. Prod. 133, 44–53.
Oh, S.Y., Yoo, D.I., Shin, Y., Seo, G., 2005. FTIR analysis of cellulose treated with sodium hydroxide and carbon dioxide. Carbohydr. Res. 340, 417–428.
Osatiashtiani, A., Zhang, J., Stefanidis, S.D., Zhang, X., Bridgwater, A.V., 2022. The mechanism for catalytic fast pyrolysis of levoglucosan, furfural and furan over HZSM-5: An experimental and theoretical investigation. Fuel 328, 125279. https://doi.org/10.1016/j.fuel.2022.125279.
Osman, A.I., Abdelkader, A., Johnston, C.R., Morgan, K., Rooney, D.W., 2017. Thermal investigation and kinetic modeling of lignocellulosic biomass combustion for energy production and other applications. Ind. Eng. Chem. Res. 56, 12119–12130.
Oyedun, A.O., Gebreegziabher, T., Hui, C.W., 2013. Mechanism and modelling of bamboo pyrolysis. Fuel Process. Technol. 106, 595–604.
Paniagua, S., Escudero, L., Coimbra, R.N., Escapa, C., Otero, M., Calvo, L.F., 2018. Effect of applying organic amendments on the pyrolytic behavior of a poplar energy crop. Waste Biomass-.-. Valor 9, 1435–1449.
Perić, M., Komatina, M., Antonijević, D., Bugarski, B., Dželetović, Ž., 2018. Life cycle impact assessment of Miscanthuscrop for sustainable household heating in Serbia. Forests 9 (10), 654. https://doi.org/10.3390/f9100654.
Pulighe, G., Bonati, G., Colangeli, M., Morese, M.M., Traverso, L., Lupia, F., Khawaja, C., Janssen, R., Fava, F., 2019. Ongoing and emerging issues for sustainable bioenergy production on marginal lands in the Mediterranean regions. Renew. Sustain. Energy Rev. 103, 58–70.
Putro, J.N., Soetaredjo, F.E., Lin, S.-Y., Ju, Y.-H., Ismadji, S., 2016. Pretreatment and conversion of lignocellulose biomass into valuable chemicals. RSC Adv. 6, 46834–46852.
Rajpoot, L., Tagade, A., Deshpande, G., Verma, K., Geed, S.R., Patle, D.S., Sawarkar, A.N., 2022. An overview of pyrolysis of de-oiled cakes for the production of biochar, bio-oil, and pyro-gas: Current status, challenges, and future perspective. Bioresour. Technol. Rep. 19, 101205 https://doi.org/10.1016/j.biteb.2022.101205.
Ranzi, E., Cuoci, A., Faravelli, T., Frassoldati, A., Migliavacca, G., Pierucci, S., Sommariva, S., 2008. Chemical kinetics of biomass pyrolysis. Energy Fuels 22, 4292–4300.
Raza, N., Ahsan, M., Taqi Mehran, M., Raza Naqvi, S., Ahmad, I., 2021. Computational analysis of the hydrodynamic behavior for different air distributor designs of fluidized bed gasifier. Front. Energy Res. 9, 692066 https://doi.org/10.3389/fenrg.2021.692066.
Raza Naqvi, S., Uemura, Y., Yusup, S., Sugiur, Y., Nishiyama, N., Naqvi, M., 2015. The role of zeolite structure and acidity in catalytic deoxygenation of biomass pyrolysis vapors. Energy Proc. 75, 793–800. https://doi.org/10.1016/j.egypro.2015.07.126.
Raza Naqvi, S., Tariq, R., Shahbaz, M., Naqvi, M., Aslam, M., Khan, Z., Mackey, H., Mckay, G., Al-Ansari, T., 2021. Recent developments on sewage sludge pyrolysis and its kinetics: Resources recovery, thermogravimetric platforms, and innovative prospects. Comput. Chem. Eng. 150, 107325 https://doi.org/10.1016/j.compchemeng.2021.107325.
Reiter, J., Strittmatter, H., Wiemann, L.O., Schieder, D., Sieber, V., 2013. Enzymatic cleavage of lignin β-O-4 aryl ether bonds vianet internal hydrogen transfer. Green. Chem. 15, 1373–1381. https://doi.org/10.1039/c3gc40295a.
Rinaldi, R., Jastrzebski, R., Clough, M.T., Ralph, J., Kennema, M., Bruijnincx, P.C.A., Weckhuysen, B.M., 2016. Paving the way for lignin valorisation: Recent advances in bioengineering, biorefining and catalysis. Angew. Chem. Int. Ed. 55 (29), 8164–8215. https://doi.org/10.1002/anie.201510351.
Rogaume, T., 2019. Thermal decomposition and pyrolysis of solid fuels: Objectives, challenges and modelling. Fire Saf. J. 106, 177–188.
Runge, T.M., Zhang, C., Mueller, J., Wipperfurth, P., 2013. Economic and Environmental Impact of Biomass Types for Bioenergy Power Plants. Environ. Econ. Res. Dev. Program Wisconsin's Focus Energy Final Rep. 1–41 (Available at). ⟨https://www.focusonenergy.com/sites/default/files/research/1010RungeFinalReportx.pdf⟩.
Schimmelpfennig, S., Glaser, B., 2012. One step forward toward characterization: Some important material properties to distinguish biochars. J. Environ. Qual. 41 (4), 1001–1013.
Schulz, H., Baranska, M., 2007. Identification and quantification of valuable plant substances by IR and Raman spectroscopy. Vib. Spectrosc. 43, 13–25.
Singh, A., Nanda, S., Guayaquil-Sosa, J.F., Berruti, F., 2021. Pyrolysis of Miscanthus and characterization of value-added bio-oil and biochar products. Can. J. Chem. Eng. 99, S55–S68.
Slezak, R., Krzystek, L., Ledakowicz, S., 2018. Thermogravimetric analysis coupled with mass spectrometry of spent mushroom substrate and its fractions. J. Anal. Appl. Pyrol. 133, 1–8. https://doi.org/10.1016/j.jaap.2018.05.010.
Strömberg, B., Zintl, F., 2008. Release of chlorine from biomass and model compounds at pyrolysis and gasification conditions. In: Bridgwater, A.V. (Ed.), Progress in Thermochemical Biomass Conversion, Vol. 1. Blackwell Science Ltd, London, UK, pp. 1234–1246.
Tauler, M., Baraza, E., 2015. Improving the acclimatization and establishment of Arundodonax L. plantlets, a promising energy crop, using a mycorrhiza-based biofertilizer. Ind. Crop. Prod. 66, 299–304.
Technical Bulletin No. 0685., 1994, Alternatives for Management of Pulp and Paper Industry Solid Wastes: Production of Ethanol. October 1994, Dr. Isaiah Gellman, President at National Council of the Paper Industry for Air and Stream Improvement, Inc., 260 Madison Ave, new York, NY, USA, pp. 19–21.
Thakur, L.S., Kumar Varma, A., Mondal, P., 2018. Analysis of thermal behavior and pyrolytic characteristics of vetiver grass after phytoremediation through thermogravimetric analysis. J. Therm. Anal. Calor. 131, 3053–3064. https://doi.org/10.1007/s10973-017-6788-0.
Titiloye, J.O., Abu Bakar, M.S., Odetoye, T.E., 2013. Thermochemical characterisation of agricultural wastes from West Africa. Ind. Crop. Prod. 47, 199–203.
Trendewicz, A., Evans, R., Dutta, A., Sykes, R., Carpenter, D., Braun, R., 2015. Evaluating the effect of potassium on cellulose pyrolysis reaction kinetics. Biomass Bioenergy 74, 15–25. https://doi.org/10.1016/j.biombioe.2015.01.001.
Van den Bosch, S., Renders, T., Kennis, S., Koelewijn, S.-F., Van den Bossche, G., Vangeel, T., Deneyer, A., Depuydt, D., Courtin, C.M., Thevelein, J.M., Schutyser, W., Sels, B.F., 2017. Integrating lignin valorization and bio-ethanol production: On the role of Ni-Al_2O_3 catalyst pellets during lignin-first fractionation. Green. Chem. 19 (14), 3313–3326. https://doi.org/10.1039/C7GC01324H.
Verma, K., Gajera, Z.R., Sawarkar, A.N., 2022. Kinetics of gasification and co-gasification of petcoke and coal. J. Inst. Eng. (India): Ser. E 103, 31–39. https://doi.org/10.1007/s40034-020-00178-x.
Villaverde, J.J., Domingues, R.M.A., Freire, C.S.R., Silvestre, A.J.D., Neto, C.P., Ligero, P., de Vega, A., 2009. Miscanthus x giganteus extractives: A source of valuable phenolic compounds and sterols. J. Agric. Food Chem. 57 (9), 3626–3631.
Visconti, D., Fiorentino, N., Cozzolino, E., Di Mola, I., Ottaiano, L., Mori, M., Cenvinzo, V., Fagnano, M., 2020. Use of giant reed (Arundodonax L.) to control soil erosion and improve soil quality in a marginal degraded area. Ital. J. Agron. 15–1764 (4), 333–338.
Vyazovkin, S., Linert, W., 1995. The application of isoconversional methods for analyzing isokinetic relationships occurring at thermal decomposition of solids. J. Solid State Chem. 114 (2), 392–398.
Vyazovkin, S., Burnham, A.K., Criado, J.M., Pérez-Maqueda, L.A., Popescu, C., Sbirrazzuoli, N., 2011. ICTAC Kinetics Committee recommendations for performing kinetic computations on thermal analysis data. Thermochim. Acta 520 (1), 1–19.
Vyazovkin, S., Burnham, A.K., Favergeon, L., Koga, N., Moukhina, E., Pérez-Maqueda, L. A., Sbirrazzuoli, N., 2020. ICTAC Kinetics Committee recommendations for analysis of multi-step kinetics. Thermochim. Acta 689, 178597. https://doi.org/10.1016/j.tca.2020.178597.
Wan, S., Zheng, N., Zhang, J., Wang, J., 2019. Role of neutral extractives and inherent active minerals in pyrolysis of agricultural crop residues and bio-oil formations. Biomass Bioenergy 122, 53–62.
Wang, Q., Song, H., Pan, S., Dong, N., Wang, X., Sun, S., 2020. Initial pyrolysis mechanism and product formation of cellulose: An experimental and density functional theory (DFT) study. Sci. Rep. 10, 3626. https://doi.org/10.1038/s41598-020-60095-2.
Wang, S.R., Dai, G.X., Yang, H.P., Luo, Z.Y., 2017. Lignocellulosic biomass pyrolysis mechanism: A state-of-the-art review. Prog. Energy Combust. Sci. 62, 33–86.

Wang, Y., Wu, H., Sárossy, Z., Dong, C., Glarborg, P., 2017. Release and transformation of chlorine and potassium during pyrolysis of KCl doped biomass. Fuel 197, 422–432.
Wróblewska, H., Komorowicz, M., Pawłowski, J., Cichy, W., 2009. Chemical and energetical properties of selected lignocellulosic raw materials. Folia . Pol. Ser. B 40, 67–78.
Xu, D., Chai, M., Dong, Z., Rahman, M.M., Yu, X., Cai, J., 2018. Kinetic compensation effect in logistic distributed activation energy model for lignocellulosic biomass pyrolysis. Bioresour. Technol. 265, 139–145.
Xu, Y., Chen, B., 2013. Investigation of thermodynamic parameters in the pyrolysis conversion of biomass and manure to biochars usingthermogravimetric analysis. Bioresour. Technol. 146, 485–493.
Yang, J., Wang, X., Shen, B., Hu, Z., Xu, L., Yang, S., 2020. Lignin from energy plant (Arundo donax): Pyrolysis kinetics, mechanism and pathway evaluation. Renew. Energy 161, 963–971.
Yang, Z., Liu, X., Yang, Z., Zhuang, G., Bai, Z., Zhang, H., Guo, Y., 2013. Preparation and formation mechanism of levoglucosan from starch using a tubular furnace pyrolysis reactor. J. Anal. Appl. Pyrol. 102, 83–88. https://doi.org/10.1016/j.jaap.2013.03.012.
Zabel, Y.G., 2018, Thermal Decomposition Characteristics of Miscanthus and Ulva during Pyrolysis. Master of Science in Sustainable Process and Energy Technology, Faculty of Mechanical Engineering Delft University of Technology, Netherlands, pp, 1–77. Available at: ⟨https://repository.tudelft.nl⟩.
Zhang, J., Chen, T., Wu, J., Wu, J., 2014. A novel Gaussian-DAEM-reaction model for the pyrolysis of cellulose, hemicellulose and lignin. RSC Adv. 4, 17513–17520.
Zhang, X., Yang, W., Blasiak, W., 2012. Thermal decomposition mechanism of levoglucosan during cellulose pyrolysis. J. Anal. Appl. Pyrol 96, 110–119.
Zhang, Z., Duan, H., Zhang, Y., Guo, X., Yu, X., Zhang, X., Rahman, M.M., Cai, J., 2020. Investigation of kinetic compensation effect in lignocellulosic biomass torrefaction: Kinetic and thermodynamic analyses. Energy 207, 118290. https://doi.org/10.1016/j.energy.2020.118290.
Zhou, N., Wass Thilakarathna, W.P.D., He, Q.S., Vasantha Rupasinghe, H.P., 2022. A review: Depolymerization of lignin to generate high-value bio-products: Opportunities, challenges, and prospects. Front. Energy Res. 9, 758744 https://doi.org/10.3389/fenrg.2021.758744.